Yiyang LUO
Vladyslav LUTSENKO
Serhiy SHULGA

SYNTHESIS OF TWO-DIMENSIONAL NON-EQUIDASTANT ANTENNA ARRAYS USING SPECIAL MATRICES

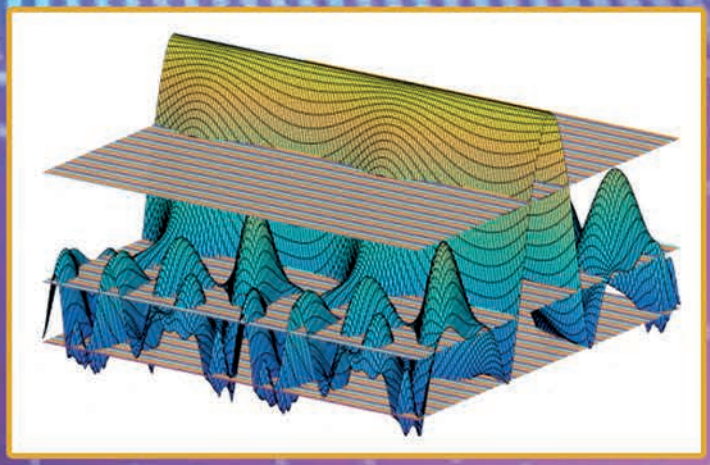

NATIONAL ACADEMY
OF SCIENCES OF UKRAINE
O.Ya. USIKOV INSTITUTE
FOR RADIOPHYSICS AND ELECTRONICS
OF THE NAS OF UKRAINE

НАЦІОНАЛЬНА
АКАДЕМІЯ НАУК УКРАЇНИ
ІНСТИТУТ РАДІОФІЗИКИ ТА ЕЛЕКТРОНІКИ
ім. О.Я. УСИКОВА НАН УКРАЇНИ

Іян ЛО
Владислав ЛУЦЕНКО
Сергій ШУЛЬГА

СИНТЕЗ ДВОМІРНИХ НЕЕКВІДИСТАНТНИХ АНТЕННИХ РЕШІТОК З ВИКОРИСТАННЯМ СПЕЦІАЛЬНИХ МАТРИЦЬ

ПРОЄКТ
«УКРАЇНСЬКА НАУКОВА КНИГА
ІНОЗЕМНОЮ МОВОЮ»

КИЇВ
АКАДЕМПЕРІОДИКА
2025

Yiyang LUO
Vladyslav LUTSENKO
Serhiy SHULGA

SYNTHESIS OF TWO-DIMENSIONAL NON-EQUIDASTANT ANTENNA ARRAYS USING SPECIAL MATRICES

PROJECT
«UKRAINIAN SCIENTIFIC BOOK
IN A FOREIGN LANGUAGE»

KYIV
AKADEMPERIODYKA
2025

https://doi.org/10.15407/akademperiodyka.554.128
UDC 537.86 + 621.371; 621.396
L97

Reviewers:

Yu.F. LOHVINOV, Acting Director of the O. Ya. Usikov Institute for Radiophysics and Electronics of the NAS of Ukraine, Doctor of Physical and Mathematical Sciences, Senior Staff Scientist, Corresponding Member of the NAS of Ukraine

V.V. ZAKHARENKO, Director of the Institute of Radio Astronomy of the NAS of Ukraine, Doctor of Physical and Mathematical Sciences, Senior Staff Scientist, Senior Researcher, Corresponding Member of the NAS of Ukraine

M.M. HOROBETS, Head of the Department of Applied Electrodynamics, Faculty of Radiophysics, Biomedical Electronics and Computer Systems of V.N. Karazin Kharkiv National University, Doctor of Physical and Mathematical Sciences, Professor

Approved for publication by the O.Ya. Usikov Institute for Radiophysics and Electronics of the National Academy of Sciences of Ukraine (29.06.2023, Protocol No. 5)

The publication was funded within the framework of the Targeted Complex Program of the NAS of Ukraine "Scientific Bases of Functioning and Providing for Conditions for the Development of the Scientific and Publishing Complex of the NAS of Ukraine"

Luo Yiyang

L97 Synthesis of Two-Dimensional Non-Equidistant Antenna Arrays Using Special Matrices / Yiyang Luo, Vladislav Lutsenko, Serhiy Shulga; O.Ya. Usikov Institute for Radiophysics and Electronics of the NAS of Ukraine. — Kyiv: Akademperiodyka, 2025. — 128 p.

ISBN 978-966-360-554-8

The monograph is devoted to the development of new methods of constructing two-dimensional non-equidistant antenna arrays (AAs), which can be used for multiple functions, especially for radiotelescopes (8—80 MHz). A series of direct and simple methods for designing such a two-dimensional non-equidistant AA was proposed. Non-equidistant AAs constructed on the structure of Latin Squares and their Triangular matrix are the most satisfactory results currently available. A method for their construction, different from the previous one, is proposed. The properties of this type of AA, which ensure entire coverage of spatial frequencies at a high degree of rarefaction with a sufficiently small lateral radiation, are thoroughly examined.

UDC 537.86 + 621.371; 621.396

ISBN 978-966-360-554-8

CONTENTS

FOREWORD

Recently, the design of two-dimensional non-traditional antenna arrays (AAs) has gained popularity due to their advantages not found in conventional equidistant arrays. Sparse AAs, created by reducing elements in equidistant AAs, maintain system quality while reducing weight, energy consumption, and costs.

Common methods for element reduction include genetic algorithms, biogeography-based optimization, almost difference sets, particle swarm methods, Ant algorithms, iterative Fourier transform algorithms, and hybrid approaches. However, these methods rely on complex optimization techniques, making direct sparse AA design challenging. Traditional approaches treat AA design as a multidimensional, nonlinear local optimization problem, often leading to unsatisfactory results despite significant effort. Therefore, there is an urgent need for a straightforward, effective method for designing sparse AAs.

The object of this work is the methods of designing two-dimensional non-equidistant AAs based on special matrices for use in radio astronomy and radar.

The subject of the study is the determination and optimization of the parameters of non-equidistant AAs, including the pattern, filling factor, and redundancy of the designed AAs in the decameter wave range.

The scientific novelty of the obtained results includes:

1) Several unconventional, direct, and simple methods for generating planar sparse antenna arrays using special matrices, such as magic and Latin squares and triangular matrices, are proposed.

2) A solution for further optimization of the existing multidevice and antenna ground surveillance system, aiming at improving performance and reducing power consumption, is proposed.

3) A method is created, and an algorithm is developed to supplement the AA with elements to ensure comprehensive spatial frequency coverage.

4) The characteristics of antenna arrays formed using special matrices are evaluated, showing that some arrays, especially those obtained using Latin squares and their triangular matrices, exhibit significantly better characteristics in terms of the number of elements, redundancy factor, and filling factor.

The structure and scope of the monography. The book consists of an introduction, 5 chapters, conclusions and references. The list of references contains 168 sources. The outline of the main content of the book is as follows:

In *Chapter 1*, the research history of radiowave propagation, antenna theory, linear AA, and planar AA was reviewed. Some parameters used in this book (including radiation pattern, main beam width, average side lobe level, filling factor, redundancy, spatial frequency, etc.) are explained. And the traditional matrix-based method of constructing antenna arrays is also explained.

In *Chapter 2*, the feasibility of constructing non-equidistant AA based on Latin squares is explored. The algorithm used for computing the coordinates of the AA, based on "Latin" squares, mirrors the approach employed in AA constructed from "Magic" squares. This algorithm is grounded in using the matrix element values that generate (or form the square) as the basis for the interferometer created by adjacent elements. While the resulting AA provides complete coverage of the spatial frequency in the AA element placement area, it exhibits a substantial redundancy coefficient. Radiation patterns of the generated AA are studied, and side lobe levels of the obtained non-equidistant AA are assessed. Mitigating redundancy in AA based on Latin squares has a minimal impact on the main lobe width. However, it significantly reduces fill and redundancy coefficients while notably increasing the average side lobe levels. The possibility of synthesizing large AA based on component squares using embedded Latin squares is demonstrated. Characteristics of the obtained grids are examined under additive and multiplicative shifts, as well as rotation (transposition). It is shown that employing mutual rotations of individual layers within the synthesized grid can enhance its characteristics. The study establishes that AAs with the most favorable characteristics are those obtained by embedding a magic square through additive shifts of elements in a Latin square, resulting in the formation of a new Latin square. This remains true even when employing rotation operations (transposition). The results open new possibilities for creating non-uniform antenna grids with low fill and redundancy coefficients and acceptable side lobe levels, surpassing the characteristics of previously utilized non-equidistant planer AA based on cyclic-difference sets (CDS). New avenues are proposed in the presented approach and methodology, including the use of Greco-Latin (Eulerian) orthogonal squares as starting elements, offering promising possibilities for further exploration.

In *Chapter 3*, the construction of non-equidistant Antenna Arrays (AAs) based on Latin squares with CDS as elements, employing the traditional algorithm presented in *Chapter 1*. The resulting AAs demonstrate nearly complete

spatial frequency coverage with a minimal redundancy factor. Notably, AAs based on Latin squares utilizing CDS as elements outperform other configurations, offering new possibilities for AAs with reduced filling and redundancy coefficients. The synthesis of large AAs using Latin squares with CDS as element were also explored, highlighting performance improvements and increased flexibility in design parameter adjustments. The proposed synthesis approaches hold potential applications in designing low-frequency radio telescopes, radar complexes, and systems monitoring seismic and atmospheric activity.

In *Chapter 4*, a novel AA synthesis method, based on the Latin square and its triangular matrix, was proposed and has been demonstrated as a direct and efficient approach for sparse AA synthesis. This method ensures full spatial frequency coverage, reduces array compactness and the overall number of arrays, while maintaining effective control over side lobes. The synthesized array exhibits a narrow main lobe and low side lobe levels, making it versatile for various applications, including radar, communications, radio astronomy, radiotherapy, remote sensing, automotive, medical imaging, navigation, and more. Despite the large number of AA elements synthesized using this method, the array maintains a fixed geometry, displaying consistent characteristics when rotated on a plane.

In *Chapter 5*, a comparative analysis was conducted using the example of an antenna element designed for a 25 MHz radio astronomical telescope. The novel approaches to constructing non-equidistant planar sparse AAs utilizing mathematical constructions such as Magic squares, Latin squares (including elements in the form of CDS), were proven to offer several unique properties. Firstly, the methodology is characterized by simplicity and efficiency, steering clear of the intricate nonlinearity associated with traditional sparse AA design. Instead, it employs straightforward mathematical concepts like matrix multiplication, nesting, and element generation, resulting in a straightforward and effective AA design process. Secondly, the methodology exhibits regularity and scalability, as the mathematical concepts employed can be expanded with increasing order, allowing for the synthesis of large AAs. Thirdly, it combines nonlinearity and multidimensionality, representing a nonlinear approach using linear forms (matrices) for AA design. The method's multidimensional nature enables the generation of coordinate matrices of varying sizes, making it adaptable to multidimensional constraints. Finally, this innovative approach holds significant future potential, providing a new paradigm for AA design with clear foundations, transparency, and the prospect for further development. It opens the door to a comprehensive AA optimization design system, accommodating additional mathematical concepts, modifications, and replacements. With a sufficient number of projected AAs and a high matrix order, it can facilitate the creation of knowledge bases for AA classification, systematic studies on the characteristics of sparse AAs, and the geometric distribution of their elements.

In the *Conclusions*, a comprehensive review of the entire book is presented. The book introduces a set of novel direct design methods for 2D non-equidistant AAs based on special matrices, highlighting their numerous advantages (especially, low cost, low side lobe level, low redundancy while ensuring complete spatial frequency coverage) and versatile applications (especially in the field of radio astronomy and monitoring for the atmosphere and Geospace). The prospects for applying these methods are discussed, emphasizing their potential benefits in various scenarios. However, critical shortcomings in current research are also discussed, including: 1) the absence of specific measurements in real-world situations, 2) a lack of in-depth understanding of specific application scenarios and constraints, 3) the need for further development of the mathematical nature of generating sparse AAs based on special matrices, the necessity for comparative analyses of arrays using different types of antennas as antenna units, and 4) the requirement for in-depth analysis and consideration of signal processing systems (such as phase shifters and signal amplifiers) in the integration of sparse AA designs. These identified areas for improvement serve as valuable directions for future research and development in the field.

Founding Information and Acknowledgments. The work was carried out at the Department of Theoretical Radiophysics of V.N. Karazin Kharkiv National University (KhNU) and the laboratory of environmental monitoring and spectroscopy of O.Ya. Usikov Institute for Radiophysics and Electronics (IRE) of the National Academy of Sciences of Ukraine (NASU) within a cooperative contract framework and state-budget research topics:

1) The scientific research project (SRP) of the National Research Fund of Ukraine 2020.02/0015: "Theoretical and experimental studies of global disturbances of natural and man-made origin in the system Earth-atmosphere-ionosphere" (KhNU, realizer, 2020, 2021, 2023);

2) SRP "Aureole", state registration number 0111U010479: "Development of methods and means of optics and quasi-optics for the study of regularities and features of the interaction of terahertz radiation with physical and biological objects" (4 books) — Book No. 2 "Methods of forming and processing images in the terahertz region of the electromagnetic spectrum" (IRE NASU, realizer, 2016);

3) SRP "Horizon", state registration No. 0113U000048: "Spatio-temporal non-stationary electromagnetic and acoustic interactions in the atmosphere-sea-substance system; the influence of the state of the environment and complex reflectors on remote diagnostics during location and relay sounding and on meteor radio communication" (IRE NASU, realizer/May 23, 2012 Protocol No. 5 of the Resolution of the Bureau of the Department of Physics and Astronomy (DPA) of the IRE NASU, 2015, 2016, 2017);

4) SRP "Horizon-2", state registration number 0118U003034: "Interactions of electromagnetic and acoustic waves in the environment-matter system and

their use for solving the problems of radar, energy, ecology, medicine and communication" (IRE NASU, realizer/June 6, 2017, Minutes No. 4 of the Resolution of DPA IRE NASU, 2018, 2019, 2020, 2021, 2022).

The authors of the monography express their gratitude to all the co-authors of the works that formed the basis of the monography, as well as to the employees of the Department of Space Radiophysics of KhNU, the Department of Theoretical Radiophysics of KhNU, and the Laboratory of "Monitoring and Spectroscopy" of the IRE NASU, who made a significant contribution to the results of the research presented in the monography.

Separately, the author would like to note the special contribution and express their sincere gratitude to: Mykyta Shevelev and Vladyslav Khrychov for benefit and inspiring discussion, Oleksandr Sobolyak for consultations and explanations of some computer methods and algorithms, Iryna Lutsenko for mastering basic data processing methods, Ihor Popov for providing computer data processing tools and detailed instructions for their use, Anh Nguyen, Qiang Guo, Yu Zheng for useful recommendations on the application of basic methods of parameter calculation in specialized computer mathematics packages, Professor Chornogor Leonid Feoktystovych and Masalov Serhii Oleksandrovych for their useful recommendations and fruitful discussions of the monograph materials.

The authors also sincerely thank the reviewers, NASU corresponding member Yurii. F. Lohvinov, NASU corresponding member Vyacheslav V. Zakharenko, and Professor Mykola M. Horobets for their valuable comments and recommendations that contributed to the improvement of the manuscript.

INTRODUCTION

Two-dimentional non-equidistant antenna arrays (AAs), including sparse linear AAs and sparse planar AAs, help reduce the number of antenna elements while maintaining high fidelity and reducing side lobes.

The work is aimed at the development of new methods of constructing non-equidistant AAs using a set of special matrices. New two-dimentional non-equidistant AAs were created using magic/Latin square matrices, their nested matrix, a Latin square matrix using cyclic difference sets (CDS) as an element, and a triangular Latin square matrix. From a methodological point of view, a special mathematical concept was used to construct the AA. This is an interesting, unusual approach that creates the prerequisites for an innovative breakthrough in the development of radio telescopes, radars and antenna systems, and is relevant today.

Urgency of the research. In recent years, the construction of non-traditional two-dimentional non-equidistant AAs has become a trend with many advantages that are not found in conventional equidistant AAs [1]. Since the expediency of using rarefied lattices was obvious, appropriate methods began to be developed, but their full theoretical justification [2] is still missing. A rarefied AA can be considered as a result of thinning an equidistant AA, the total number of active elements of which is reduced, without a significant deterioration in the quality of the system [3]. Still, in many cases, sparse AAs are designed by first designing equidistant AAs, and then using a series of methods to reduce elements (lattice thinning), such as: genetic algorithm (GA) [3—6], optimization using a biogeography model [7], approach based on almost difference sets [8], the particle swarm method (PSM) [9], the ant algorithm [10], the iterative Fourier transform algorithm [11—13], and even a hybrid method based on the iterative Fourier transform and differential evolution [14]. Some of them have already been put into operation and

have made it possible to achieve good results: effectively reduce weight, energy consumption, heat generation, and economic costs of AA.

However, these approaches are based on the application of optimization methods belonging to fitting methods, and this, in fact, makes it impossible to design sparse AAs directly. The traditional method of direct lattice design considers the AA design problem as a multidimensional nonlinear local optimization [15—19]. Despite the amount of time, energy, and resources spent conducting multiple iterations, the results are still unsatisfactory [20—37]. In view of this, there is currently an urgent need to develop a formal, simple, and effective method.

The purpose and tasks of the research. The purpose of the work is to develop methods for creating and optimizing two-dimensional non-equidistant AAs based on matrices of a special form for full coverage of spatial frequencies at low values of the filling factor and redundancy, which could be used in low-frequency radio telescopes and decameter radars. To achieve this goal, the following research tasks were set and fulfilled:

1. To analyze the current state of the problem of modeling two-dimensional non-equidistant antenna arrays for low-frequency radio telescopes and radars;

2. To create methods that allow transforming the values of matrices of a special form into the coordinates of the elements of the AA and a computer program for calculating the characteristics of the obtained AA, such as:

a) To calculate the radiation pattern (RP), its width, and the average level of the side petals;

b) To determine the covering spatial frequencies and create a methodology for their addition to full coverage;

c) To estimate the coefficients of filling and redundancy.

3. To model AAs based on matrices of a special form (Latin squares, magic squares, triangular matrices) and compare the characteristics of the obtained AAs with those obtained earlier using CDSs.

4. To compare the characteristics of AAs obtained using the proposed approach based on special matrices with the characteristics of previously known non-equidistant AAs.

5. To consider the possibility and potential application of using two-dimensional non-equidistant AAs based on special matrices.

Research methods. The methods of modern radio physics, computational electrodynamics, and mathematical physics were used in the work to solve the tasks:

• statistical methods for analyzing the characteristics obtained during the design of two-dimensional non-equidistant AAs;

• "greedy" algorithm (for addition and deletion of AA coordinates);

• matrix operations (transformation, rotation, expansion, nesting) (using a special matrix to generate a coordinate AA);

• a technique for analyzing the convolution distribution and histogram (for determining and analyzing the spatial frequency distribution of AA).

Practical significance of the obtained results. The mentioned new approaches to the construction of two-dimentional non-equidistant AAs based on mathematical constructions, such as magic squares, Latin squares, and CDS, have numerous advantages and unique properties that make them attractive for research and use in the field of antenna technologies. The main aspects of these approaches can be justified as follows:

• *Simplicity and efficiency.* The proposed methods use simple mathematical concepts such as matrix multiplication, matrix nesting, and matrix element generation. It avoids complex nonlinear optimization in the design of sparse AAs, while ensuring efficiency in the synthesis process.

• *Regularity and scalability.* Using mathematical concepts such as magic squares and Latin squares makes it easy to scale the size of the AA according to certain laws. It makes them scalable and suitable for use in various fields of application.

• *Nonlinearity and multidimensionality.* The synthesis of AAs using the proposed methods is a non-linear problem; however, the use of matrices for the generation of coordinate matrices of different sizes allows bypassing multidimensional limitations and solving the corresponding problems.

• *Perspective.* This approach is new and different from traditional methods. It forms a new thinking system for designing AAs, which has potentially broad prospects in the field of antenna technology. Its simplicity, efficiency, and extensibility create prerequisites for further research and development.

These methods open up new opportunities for creating AAs with unique characteristics that can be applied in modern communication and radio engineering systems. Their potential value lies in their ability to meet the requirements of a wide range of purposes.

The material presented in the monograph will be useful for scientists and specialists involved in the development of methods and technologies of remote sensing of the environment using the radiation of existing terrestrial and space radio engineering systems.

CHAPTER 1

THE CURRENT RESEARCH STATE OF DESIGN AND OPTIMIZATION OF AN ANTENNA ARRAY

Antenna arrays (AAs) play a critical role in a variety of applications, including mobile communications [38], synthetic aperture radars [39—44], medicine [45—47], sensing [48], imaging [49], and radio astronomy [49, 50], ensuring fast and accurate beam formation. Although some systems operate in the near field [45, 51—53], studies of far-field emission/radiation characteristics and beamforming often use the far-field approximation to obtain accurate results. In the far zone [54, 55], the effect of coupling between array elements is considered insignificant due to the significant distance between them and low radiation in the direction of neighboring antennas. The main focus of the research is on the optimization of parameters and the development of AAs in the far-field approximation to improve their performance in beamforming applications.

This monograph considers and investigates AAs created using magic/Latin square matrices, their nested matrices, Latin square matrices using cyclic difference sets (CDS) as an element, and triangular Latin square matrices.

From a methodological point of view, a special mathematical concept (matrix/square) was used to construct AAs. The algorithm proposed in this monograph is a simple and direct mathematical method of designing an AA based on matrix calculation, which has wide application and substantial economy.

1.1. Literature review in the field of mathematics, physics, antennas, and radio wave propagation

The field of propagation of radio waves is large and covers a wide range of phenomena. Even before Marconi's pioneering transatlantic radio experiment in 1901, scientists struggled with the complexity of the means of transmission. Early theories, such as the surface wave models of Zenneck (1907) and the airless dif-

fraction models of Watson (1918), were quickly superseded by subsequent developments. The evolution of this field has witnessed a dynamic interaction between experimenters and theoreticians, leading to the creation of new physical concepts. The foundation of modern plasma physics can be traced back to the pioneering work (1920—1938) of Luxmore, Appleton, Ratcliffe, Booker, and Budden on magneto-ion theory, particularly its application to the description of the phenomena of electromagnetic waves reflecting off the ionosphere. The advent of microwave radar during World War II expanded our understanding of the influence of the non-ionized troposphere, albeit in a qualitative sense [56].

Electromagnetic energy emitted by a source, such as an antenna, at nearly the speed of light is attenuated and affected by the medium through which it passes. In radio communications, this process involves transmitting radio frequency energy into the propagation medium, detecting it remotely, and extracting information while "mitigating" noise and other transmission-related factors. A complete understanding of radio wave propagation is critical to the planning and operation of radio communication systems, achieving a balance between communication costs and availability. Fraidoon Mazda's research on the propagation of radio waves covers a wide range of frequencies, from very low frequencies (VLF) (10 kHz) to the millimeter range (up to 100 GHz). The influence of the Earth, the atmosphere, and the ionosphere on transmission, taking into account propagation, was studied in the far field [57]. Fraidoon Mazda studied the influence of the Earth, atmosphere, and ionosphere on such transmissions. Analysis assumes distribution in the far field, where the electric and magnetic components of the wavefront are perpendicular and perpendicular to the direction of propagation, which occurs several wavelengths from the antenna. Radio waves propagate in five modes, depending on the medium through which they pass:

1) propagation in free space: the Earth or its atmosphere does not affect radio waves;

2) ground wave propagation: radio waves follow the Earth's surface;

3) propagation in the ionosphere (space waves): radio waves are refracted due to the ionized layers of the atmosphere;

4) propagation in the troposphere: transmission occurs in "line-of-sight" with some atmospheric refraction;

5) scattering: natural phenomena such as tropospheric turbulence or ionized meteor trails are used to scatter radio waves.

Antennas play an important role in wireless systems for efficient transmission and reception of electromagnetic signals in a specified spectrum, direction, and polarization range [58—60]. Advances in antenna technology have profoundly affected all aspects of daily life, including communications, entertainment, scientific research, and many other applications. The field of antennas remains very active, as evidenced by annual journal publications, conference

proceedings, and undergraduate and graduate courses. Radio waves are radiated most efficiently by metal antennas that are a fraction of a wavelength long (such as half a wave), and reception of radio waves is best when the receiving antenna is also a fraction of a wavelength long. Any source capable of producing electrical oscillations could become the basis of the transmitter; therefore, early designs used sparks, creating mass mixing of wavelengths. Later designs used mechanical generators to generate low-frequency waves, which required huge antennas. Radio carrier modulation always leads to sidebands [61—63]. For amplitude modulation, the difference between the sideband frequency and the carrier frequency is equal to the modulation frequency. Early amplitude modulation signal radio receivers consisted solely of an antenna, a crystal, and headphones. This arrangement can be used near the transmitter, and multiple transmitter signals can be tuned when coils and capacitors are added. The solution to the problem with medium wave radio is in the use of a supersonic heterodyne (superheterodyne) receiver. The principle is to eliminate as much carrier gain as possible, thus using variable tuning only at the beginning of the receiver block [64, 65].

The complexity of the antenna system design depends on the requirements for the radio receiver and the propagation characteristics of the environment. An antenna array system consisting of multiple antenna units can improve the performance and functionality of the antenna system significantly and have better anti-interference capabilities.

1.2. Overview of the development of antenna theory

The initial experiments illustrating the interaction of electric and magnetic fields and demonstrating their deterministic relationship were conducted by Faraday in the 1830s [58]. Faraday's innovative approach involved sliding a magnet around a coil connected to a galvanometer. During this motion, the magnet created a time-varying magnetic field, which produced a corresponding time-varying electric field, as predicted by Maxwell's equations. Essentially, the coil worked as a loop antenna, picking up electromagnetic radiation that was subsequently recorded by a galvanometer, essentially mirroring the fundamental principle of how antennas work. Significantly, these experiments preceded the formal proposal of electromagnetic waves as a concept.

In 1886, the German physicist Hertz (1857—1894) built the first antenna, an assembly that today can be described as a complete radio system, operating at meter wavelengths using terminal-loaded dipoles. The antenna is used as a transmitting antenna, and a resonant square ring is used as a receiving system [55].

In December 1901, Marconi, a researcher in Bologna, Italy, added a tuning circuit to the Hertzian system, equipped a large antenna and grounding system

for longer waves, and received a signal from Bordeaux, England, to St. John's, Newfoundland — 1.5 miles (2.5 km) of wireless telegraphy. The transmitting antenna in use at the time was a fan-shaped structure formed by stretching 50 copper wires diagonally from a horizontal wire 48 meters high. It can be considered the first practical monopole antenna. The source of oscillations was a 70 Hz spark generator. Later, four wooden towers were used to install a wire network to form a square single-cone antenna (radiation wavelength 1,000 m). With the invention and development of electron tubes in the early 20th century, long-wave communication was first used during this period, and then communication was developed. Thanks to the discovery of the formation, which was called the "ionosphere" around 1924, short-wave communication and long-distance broadcasting began. The basic theory of wire antennas was also created during this period [56].

On the eve of the Second World War, the invention of the microwave klystron and magnetron led to the introduction of microwave radar, the popularization of centimeter waves, and the radio spectrum was used more fully [62]. During this period, parabolic antennas or other forms of antennas with a reflecting surface were widely used. These antennas are zonal or aperture antennas. In addition, waveguide slot antennas, dielectric rod antennas, spiral antennas, etc., also appeared. Postwar programs such as microwave relay communications, radio broadcasting, and radio astronomy further developed and improved field and line antenna technology.

The launch of an artificial Earth satellite in 1957 was a pivotal moment in human history, ushering in a new era of space exploration. This development has created increased demands on antennas, requiring attributes such as high gain, accurate tracking, fast scanning, wide bandwidths, and low sidelobes [41]. At the same time, advances in electronic computers, microelectronics technology, and modern materials laid the foundation for the evolution of antenna theory and technology. Practical microstrip antennas [66], representing an important milestone, were first manufactured in 1972. In recent years, we have witnessed the introduction of miniature forms of antennas, such as fractal antennas [67—74], which were accompanied by the development of appropriate antenna signal processing technologies.

1.3. Review of studies of homogeneous and rarefied antenna arrays

Antenna arrays (AAs) provide higher gain and better radiation pattern (RP) than a single antenna. High directivity allows the array to limit its radiation or reception to certain directions of the directional pattern. As the size of the array increases (that is, as the number of array elements increases), its aperture also increases. Gratings with wider apertures provide a smaller beam

width and better angular resolution compared to matrices with smaller apertures [2, 20, 55, 58—60]. The spatial pattern or radiation pattern of an array represents the direction in which the array emits or receives energy. Due to the directional properties, arrays are often considered as spatial filters [75, 76]. AAs play a crucial role in improving wireless communication systems by offering improved directional patterns and extended coverage [75—83]. The development of arrays with low side lobe levels (SLL) is important for minimizing the interference level and saving energy [71—74, 84, 85, 167—169]. While aperiodic arrays can achieve this, their implementation presents challenges due to the complexity of physical rearrangement and increasing size. Thinning arrays by selectively deactivating elements is an alternative, offering advantages such as reduced weight and simplified beamforming networks [74, 86]. Traditional thinning methods face limitations, which prompts the study of global optimization methods, albeit with computational problems [87, 88]. Recent studies have focused on iterative Fourier transform and analytical methods [89] based on differential sets [90, 91], which provide computational efficiency but often compromises performance. Hybrid approaches aim to find a balance between SLL reduction and computational efficiency [92—95]. More new mathematical methods need to be introduced into this field of research.

From the point of view of the mathematical ensemble, sparse AAs (SAAs) are a subset of inhomogeneous gratings and have the advantage of requiring fewer sensor elements for a given aperture compared to uniform AAs (UAAs). Conversely, a sparse matrix with the same number of sensors can provide a larger aperture and increase the degree of freedom in the estimation of the direction of arrival. These arrays have less impact on connections comparatively from UAAs. Although minimally AA redundant and AAs with holes of minimum size have been studied for more than 50 years [1—24, 32—50, 58—66, 70—74, 80—86, 96—105], in recent years new sparse arrays have appeared, such as nested arrays, single arrays and nested arrays. The last decade has been marked by various modifications and improvements of sensor arrays, highlighting the potential of SAAs in future communication systems due to their performance comparable to UAAs.

1.4. Review of possible applications of sparse antenna arrays

Sparse antenna arrays (SAAs), including two-dimensional non-equidistant AAs, offer a variety of applications in various fields [98—100, 106]. In radio astronomy, the use of SAA increases the accuracy and sensitivity of observations, reducing interference [17, 27, 28, 49, 107, 108]. In communication systems, wireless communication, in particular, SAAs support effective beamforming, improving signal quality in crowded environments [84]. Radar

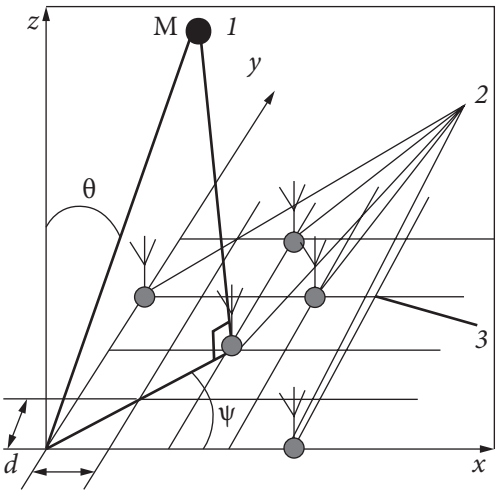

Fig. 1.1. Geometrical parameters of a planer sparse AA

systems benefit from sparse arrays with reduced side lobes and enhanced target detection capabilities [41, 48, 49, 78, 109—111, 162—164]. Medical imaging [116], remote sensing [117], and automotive radar systems [118, 160, 165—168] use SAAs to improve resolution and precision monitoring. In wireless sensor networks, these arrays contribute to energy-efficient monitoring of the environment. Security systems benefit from accurate tracking and monitoring capabilities. SAAs are used in satellite communication [41, 42], increasing communication efficiency [45, 51, 52]. In the context of 5G networks, SAAs facilitate beamforming and massive MIMO, improving overall network performance and spectral efficiency [86]. In general, the unique characteristics of SAAs make them valuable for many technological applications.

In particular, this work considers possible applications of SAAs in radio astronomy systems (Fig. 1.1). High-gain antennas, low-noise systems, and cooling (with low thermal noise) are critical for radio astronomy systems [17, 18, 27, 28, 311, 49, 107, 108, 119—121]. Because radio astronomy observations from the Earth's surface are inherently very sensitive to intentional or unintentional human interference. In nature, the main source of electromagnetic fields above about 30 megahertz (MHz) is blackbody radiation, while at lower frequencies the main source is lightning (ICNIRP, 2009) [122]. Anthropogenic sources of electromagnetic radiation include radio and television broadcast signals [123—127, 165—167], which have existed for decades, as well as new sources such as mobile phones, satellite communication, Wi-Fi, etc., which are ubiquitous in today's world society [38, 76]. A complex interaction between different sources can lead to the fact that one source will interfere with the operation of another source [128, 129]. A number of different procedures may be adopted, which may apply to specific frequency bands, specific time periods, and/or different levels of interference sources, and technical, geographical, and/or regulatory measures may be applied. In the United States, the Federal Communications Commission (Chapter 47, Part 15) regulates intentional and unintentional emissions of radio frequency electromagnetic fields [130, 156—158]. Engineers and designers of almost all electrical and electronic equipment work to make their designs resistant to external sources of interference (called electromag-

netic susceptibility) and to reduce the potential interference that their equipment can create (called electromagnetic interference) [131—144, 156—161, 165—168]. These terms are often combined into the single category of electromagnetic compatibility (EMC), which is defined as "the ability of systems, equipment, and devices to use the electromagnetic spectrum to operate in their intended operating environment without unacceptable performance degradation or damage, unintended deterioration due to electromagnetic radiation or reaction…" (ANSI, 2009) [133].

In the emerging field of radio astronomy, the focus is on increasing sensitivity at all frequencies. The parameters of existing receivers are approaching the quantum limits. The prevailing trend is a constant increase in antenna reception areas and an expansion of the surveillance band [145—147, 159, 163, 165—169]. Current international efforts, such as the Square Kilometer Array (SKA) project, aim to create a large radio jamming network with an antenna reception area of one square kilometer, covering a baseline of 3,000 km and operating from 100 MHz to 25 GHz. Initiatives such as the LOw Frequency ARray (LOFAR) in the Netherlands, with an antenna coverage area of 100,000 m^2 and a baseline of 1,000 km in the frequency range from 30 to 250 MHz, are examples of the desire for larger coverage areas. Similarly, the Atacama Large Millimeter/submillimeter Array (ALMA) operates in the frequency range from 30 to 850 GHz with 64 antenna arrays located 5 kilometers above sea level in the Andes Mountains. The development of SAAs is consistent with these changing requirements, advancing the capabilities of radio astronomy.

1.5. Antenna array model and parameters

The performance of these antenna systems strongly depends on the design of the antenna array (AA). Criteria important to AA design include beamwidth, sidelobe levels, directivity, noise sensitivity, reliability, and dynamic range of element excitation. In this book, two design criteria for evaluating the efficiency of antenna arrays are considered: criteria for the minimum main beam width (MBW) and the minimum side lobe level (SLL). There are compromises between these parameters [104].

This subsection presents the basic design methods and parameters used. As indicated in the literature review, assuming that the antenna elements work independently, that is, there is no obvious effect of electromagnetic interaction, the total electromagnetic radiation E emitted by point M can be considered as a superposition of the main fields:

$$E(M) = \sum_{i=1}^{N} \omega_i \cdot E_{A_i}(M), \tag{1.1}$$

where N is the number of antenna elements, ω_i is the complex weight or

relative power coefficients of the antenna element A_i, and the electromagnetic field E_{A_i} emitted at point M from the antenna A_i.

AA requirements (directivity, MBW, SLL, etc.) can be expressed by the radiation pattern (RP) of the E field in the domain of space Ω. The RP Γ corresponding to the required levels of lateral radiation, maximum permissible deviations, etc., can be used as a criterion for evaluating the acceptability of an AA.

For simplicity and practicality, the elementary elements of the antenna array are assumed to be omnidirectional (isotropic emitters) with uniform responses, with uniform transmission coefficients $\omega_i = \omega_0 = 1$, and have the same physical orientation (all points are oriented in the same direction). The radiating (or receiving) RP of AAs is simply the array factor (AF) multiplied by the directional pattern. This concept is known as AR multiplication.

In this case, the corresponding AF for planar AAs on a uniform grating x, y with a wavelength step d_x, d_y:

$$F(\theta,\psi)=\sum_{m=x_1}^{x_n}\sum_{p=y_1}^{y_n}\exp\left(j\frac{2\pi}{\lambda}\sin\theta(md_x\cos\psi+pd_y\sin\psi)\right), \tag{1.2}$$

where θ is the angle measured from the normal to the lattice/AA plane; ψ is the angle measured from the X-axis on the lattice or AA plane.

In this book, we use identical isotropic emitters $a_{m,p} = a_0 = 1$, and place the X and Y axes in the same wavelength intervals. If $d_x = d_y = d$, then the phase shift between two arbitrary emitters is equal to:

$$t=\frac{2\pi d}{\lambda}\sin\theta. \tag{1.3}$$

Further, formula (1.2) can be written in the following form for simulation calculation:

$$F(t,\psi)=\sum_{i=1}^{N}\exp(jt\sin\theta(x(i)\cos\psi+y(i)\sin\psi). \tag{1.4}$$

Based on the expression for RP of AA, the calculations of its parameters, MBW and SLL, are determined as follows:

MBW — the effective width of the main beam/lobe of AA RP ($\Delta\omega_{0.707}$) at the level of half the power;

SLL — average level of side beams/lobes of AA RP:

$$SLL=\sqrt{\sum_{\Delta\psi=-\pi}^{\pi}\left(\sum_{\Delta t=-\pi}^{-\Delta\omega/2}\sum_{n=1}^{N}\left|F(\Delta t,\Delta\psi)\right|+\sum_{\Delta t=\Delta\omega/2}^{\pi}\sum_{n=1}^{N}\left|F(\Delta t,\Delta\psi)\right|\right)^2}\Bigg/N_{\max}, \tag{1.5}$$

where the summation is performed outside the main petal along $N_{\max}$ pixels.

The main advantage of non-equidistant (sparse) AAs over equidistant ones is the simplification of the design due to the reduction of the number of

elements (emitters/receivers, phase shifters, etc.) while preserving the main properties. Therefore, for such gratings, the filling coefficient is an important parameter:

$$\alpha = \frac{N_0}{\nu}, \tag{1.6}$$

where N_0 is the number of lattice/AA elements; ν is the number of nodes of an equidistant lattice in which they can be located/placed.

Or the redundancy coefficient:

$$\beta = \frac{N_0}{\sqrt{S}} = \frac{N_0}{\sqrt{M_1 \times M_2}}, \tag{1.7}$$

where S, M_1, and M_2 are the effective area, length, and width of the corresponding equidistant lattice/AA. For rectangular lattices $M_1 = M_2 = M$, where M is the width (length) of the corresponding equidistant lattice (the AA coordinate plane) and $\beta = \sqrt{N_0 \times \alpha}$.

Referring to these parameters, the research problem can be transformed to obtain antenna arrays with a given number of elements that have the smallest MBW, the smallest SLL, and the smallest fill/redundancy coefficient. Of course, this is an ideal situation. In fact, we can only look at it holistically and make trade-offs depending on our situation and sacrifice some performance if necessary.

1.6. The traditional basic method of designing a two-dimensional non-equidistant antenna array using a matrix

The elements S_{lj} of the Latin/magic square can be considered as distances between adjacent elements of AAs. Then the coordinates of the elements that make up the AA can be written in terms of the S_{lj} values in row l and column j (as shown in Fig. 1.2):

$$x_{lj} = \sum_{j=1}^{j} S_{lj} = x_{lj-1} + S_{lj} \text{ and } y_{lj} = \sum_{l=1}^{l} S_{lj} = y_{lj-1} + S_{lj}, \tag{1.8}$$

where x_{lj} is the abscissa and y_{lj} is the ordinate.

The obtained complex integers $Z_{lj} = x_{lj} + iy_{lj}$ are Gaussian numbers that determine the coordinates of the AA elements. The coordinates of the element Z_{lj} are shifted from the previous elements along the abscissa and ordinate axes by the value S_{lj}. At the same time, the matrix $||Z||$, obtained on the basis of the matrix $||S||$, whose elements are the elements of a special square matrix (for example, a magic/Latin square), determines the coordinates of the elements of a two-dimensional sparse AA.

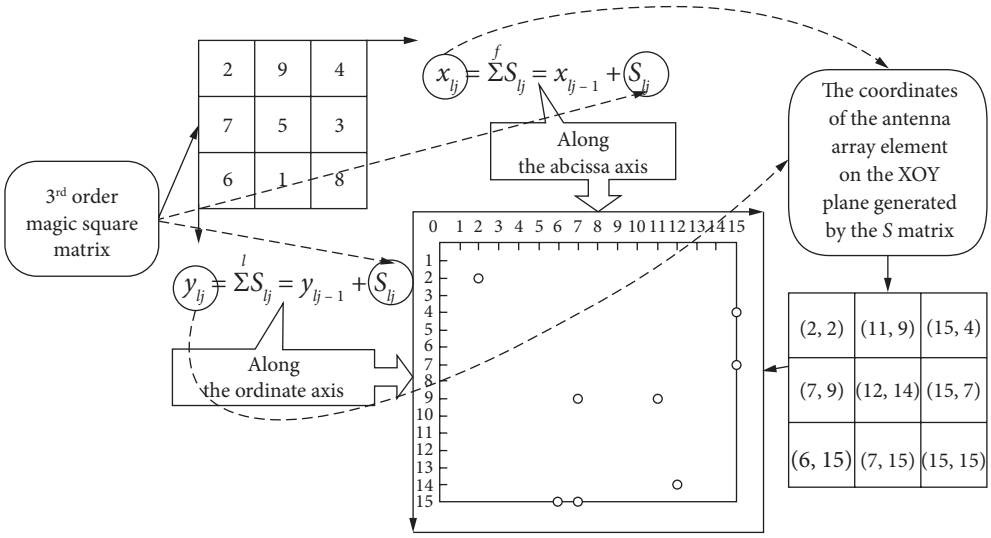

Fig. 1.2. Schematic diagram of the coordinates of the antenna array elements formed by the S matrix in the XOY plane

The corresponding spatial frequencies D_x and D_y, which are covered along the X and Y axes, are determined by the difference in the coordinates of the AA elements:

$$D_x = x_{ij} - x_{lk} \text{ and } D_y = y_{ij} - y_{lk}. \quad (1.9)$$

When the spatial frequencies are completely covered, the average level of the side lobes of the AAs' RP will be lower, because the spatial frequency represents the spatial phase difference between independent array elements. These phase differences lead to the fact that the AA will compensate for the additional side lobes of the RP.

It is worth mentioning that the AA obtained by the above-mentioned formula (1.8) using the Latin matrix has a very high redundancy compared to the magic square [22—24], although it is completely covered. The thesis presents improved methods of AA design using Latin squares to overcome this drawback.

1.7. Conclusion

The history of research on antennas, linear antenna arrays (AAs), and planar AAs has been reviewed. The application of sparse AAs is presented with a special emphasis on possible applications and urgent needs in the field of radio astronomy. Some of the parameters used in the thesis are explained (including pattern, main beam width, average side lobe level, fill

factor, redundancy, spatial frequency, etc.). The traditional matrix method of AA construction is explained.

The analysis conducted made it possible to formulate a list of problems to be solved in the monograph:

1. To analyze the current state of the problem of modeling two-dimensional non-equidistant antenna arrays for low-frequency radio telescopes and radars.

2. To create methods that allow transforming the values of matrices of a special form into the coordinates of the elements of the AA and a computer program for calculating the characteristics of the obtained AA, such as:

a) Radiation Pattern (RP), its width, and the average level of the side petals;

b) covering spatial frequencies and the method of their addition to full coverage;

c) filling and redundancy factors.

3. AA Model based on matrices of a special form (Latin squares, magic squares, triangular matrices) and compare the characteristics of the obtained AAs with those obtained earlier using cyclic difference sets.

4. Compare the characteristics of AAs obtained using the proposed approach based on special matrices with the attributes of previously known non-equidistant AAs.

5. Consider the possibility of using sparse planar AAs based on special matrices.

CHAPTER 2

DESIGN AND OPTIMIZATION OF SPARSE PLANAR ANTENNA ARRAY BASED ON LATIN SQUARES

In works [22, 23] and subsection 1.6, an attempt was made to use existing mathematical constructions, such as, for example, magic squares, to construct two-dimensional non-equidistant antenna arrays (AAs) and lattices. This made it possible to expand the possibilities of constructing two-dimensional lattices, for which previously two-dimensional sets [17—21] constructed artificially by L.E. Kopilovich and L.G. Sodin, taking into account the one-dimensional cyclic difference sets proposed by Liper [15, 16], were used. This section outlines the further development of these ideas. The possibility of using Latin squares for the construction of two-dimensional non-equidistant AAs/lattices was considered, and their characteristics were investigated.

2.1. Latin squares and their properties

The historical origins of the Latin square can be traced back to ancient China and India. The earliest record of the Latin square appeared in the book "Detailed Explanation of the Nine Chapters of Algorithm" by Yang Hui, a mathematician in the Southern Song Dynasty of China, which was completed around 1275. In the book, Yang Hui described a "vertical and horizontal diagram," which can be regarded as an early form of the Latin square. The modern definition of the Latin square was proposed by the Swiss mathematician Euler in the 18th century. He studied the properties of such squares and attempted to solve a famous mathematical problem, the "36 officer problem," which involves constructing a 6×6 Latin square that contains six different elements in each row and column, and each element appears exactly once. Although Euler failed to solve this problem, his work inspired in-depth research on the Latin square.

The Latin square is also widely used outside the field of mathematics. For example, in experimental design, the Latin square can be used to arrange experiments to reduce interference between variables, so as to more accurately evaluate the experimental results. In statistics, the properties of the Latin square are used to design more effective sampling methods to improve the quality and efficiency of data collection. With the development of mathematical theory, the study of Latin squares has gradually deepened. The generalized forms of Latin square, such as generalized Latin square and incomplete Latin square, have also become a hot topic of research. These studies have not only enriched the content of combinatorial mathematics but also provided new tools and perspectives for solving practical problems.

A Latin square of the n^{th} order is a matrix $L = (l_{ij})$ of size $n \times n$, filled with n elements of the set Q in such a way that in each row i, each column j, each element of Q occurs exactly once [30, 31]. An example of a Latin square of the 3rd order:

$$\begin{bmatrix} A & B & C \\ C & A & B \\ B & C & A \end{bmatrix}. \tag{2.1}$$

Let us consider the main stages of modeling the scattering of electromagnetic waves by objects of complex shape, the main components of the scattered field, and compare the obtained asymptotic models for objects that have analytical or known asymptotic solutions of the problem of diffraction of electromagnetic waves on them.

It can be represented in the form {(1, 1, A), (1, 2, B), (1, 3, C), (2, 1, C), (2, 2, A), (2, 3, B), (3, 1, B), (3, 2, C), (3, 3, A)}, where the first and second elements are the position of the element in the matrix, and the third is the value.

If the set Q is the set of natural numbers $\{1, 2, \ldots, n\}$ or the set $\{0, 1, \ldots, n-1\}$, then we will have for the 3rd order a Latin square according to the following formula ($A = 1$, $B = 2$, $C = 3$):

$$L_3 = \begin{bmatrix} 1 & 2 & 3 \\ 3 & 1 & 2 \\ 2 & 3 & 1 \end{bmatrix}. \tag{2.2}$$

If the set Q is a set based on the unit diagonal square matrix of natural numbers, namely:

$$A = U_{\text{D}} = \begin{bmatrix} 1 & 0 & 0 \\ 0 & 1 & 0 \\ 0 & 0 & 1 \end{bmatrix}, \tag{2.3}$$

$$A = U_{\text{D}} = \begin{bmatrix} 1 & 0 & 0 \\ 0 & 1 & 0 \\ 0 & 0 & 1 \end{bmatrix}, \tag{2.4}$$

$$B = 2 \cdot U_{\mathrm{D}} = \begin{bmatrix} 2 & 0 & 0 \\ 0 & 2 & 0 \\ 0 & 0 & 2 \end{bmatrix}, \tag{2.5}$$

$$C = 3 \cdot U_{\mathrm{D}} = \begin{bmatrix} 3 & 0 & 0 \\ 0 & 3 & 0 \\ 0 & 0 & 3 \end{bmatrix}, \tag{2.6}$$

then we will get a square of the 9th order of the following form:

$$L_{3\mathrm{UD}} = \begin{bmatrix} 1 & 0 & 0 & 2 & 0 & 0 & 3 & 0 & 0 \\ 0 & 1 & 0 & 0 & 2 & 0 & 0 & 3 & 0 \\ 0 & 0 & 1 & 0 & 0 & 2 & 0 & 0 & 3 \\ 3 & 0 & 0 & 1 & 0 & 0 & 2 & 0 & 0 \\ 0 & 3 & 0 & 0 & 1 & 0 & 0 & 2 & 0 \\ 0 & 0 & 3 & 0 & 0 & 1 & 0 & 0 & 2 \\ 2 & 0 & 0 & 3 & 0 & 0 & 1 & 0 & 0 \\ 0 & 2 & 0 & 0 & 3 & 0 & 0 & 1 & 0 \\ 0 & 0 & 2 & 0 & 0 & 3 & 0 & 0 & 1 \end{bmatrix}. \tag{2.7}$$

If we take the unit square matrix as the set *Q*, then we have:

$$U_{\mathrm{I}} = \begin{bmatrix} 1 & 1 & 1 \\ 1 & 1 & 1 \\ 1 & 1 & 1 \end{bmatrix}, \tag{2.8}$$

$$A = U_{\mathrm{I}} = \begin{bmatrix} 1 & 1 & 1 \\ 1 & 1 & 1 \\ 1 & 1 & 1 \end{bmatrix}, \tag{2.9}$$

$$B = 2 \cdot U_{\mathrm{I}} = \begin{bmatrix} 2 & 2 & 2 \\ 2 & 2 & 2 \\ 2 & 2 & 2 \end{bmatrix}, \tag{2.10}$$

$$C = 3 \cdot U_{\mathrm{I}} = \begin{bmatrix} 3 & 3 & 3 \\ 3 & 3 & 3 \\ 3 & 3 & 3 \end{bmatrix}, \tag{2.11}$$

$$L_{3\mathrm{UI}} = \begin{bmatrix} 1 & 1 & 1 & 2 & 2 & 2 & 3 & 3 & 3 \\ 1 & 1 & 1 & 2 & 2 & 2 & 3 & 3 & 3 \\ 1 & 1 & 1 & 2 & 2 & 2 & 3 & 3 & 3 \\ 3 & 3 & 3 & 1 & 1 & 1 & 2 & 2 & 2 \\ 3 & 3 & 3 & 1 & 1 & 1 & 2 & 2 & 2 \\ 3 & 3 & 3 & 1 & 1 & 1 & 2 & 2 & 2 \\ 2 & 2 & 2 & 3 & 3 & 3 & 1 & 1 & 1 \\ 2 & 2 & 2 & 3 & 3 & 3 & 1 & 1 & 1 \\ 2 & 2 & 2 & 3 & 3 & 3 & 1 & 1 & 1 \end{bmatrix}. \tag{2.12}$$

If Q is the set of the magic squares of natural numbers of the 3rd order M_3, then we have:

$$M_3 = \begin{bmatrix} 8 & 1 & 6 \\ 3 & 5 & 7 \\ 4 & 9 & 2 \end{bmatrix}, \tag{2.13}$$

$$A = M_3 = \begin{bmatrix} 8 & 1 & 6 \\ 3 & 5 & 7 \\ 4 & 9 & 2 \end{bmatrix}, \tag{2.14}$$

$$B = 2 \cdot M_3 = \begin{bmatrix} 16 & 2 & 12 \\ 6 & 10 & 14 \\ 8 & 18 & 4 \end{bmatrix}, \tag{2.15}$$

$$C = 3 \cdot M_3 = \begin{bmatrix} 24 & 3 & 18 \\ 9 & 15 & 21 \\ 12 & 27 & 6 \end{bmatrix}, \tag{2.16}$$

$$L_{3M3} = \begin{bmatrix} 8 & 1 & 6 & 16 & 2 & 12 & 24 & 3 & 18 \\ 3 & 5 & 7 & 6 & 10 & 14 & 9 & 15 & 21 \\ 4 & 9 & 2 & 8 & 18 & 4 & 12 & 27 & 6 \\ 24 & 3 & 18 & 8 & 1 & 6 & 16 & 2 & 12 \\ 9 & 15 & 21 & 3 & 5 & 7 & 6 & 10 & 14 \\ 12 & 27 & 6 & 4 & 9 & 2 & 8 & 18 & 4 \\ 16 & 2 & 12 & 24 & 3 & 18 & 8 & 1 & 6 \\ 6 & 10 & 14 & 9 & 15 & 21 & 3 & 5 & 7 \\ 8 & 18 & 4 & 12 & 27 & 6 & 4 & 9 & 2 \end{bmatrix}. \tag{2.17}$$

If Q is the set of the magic squares of natural numbers M_3, M_3' (with a rotation of 90 degrees), and M_3'' (with a rotation of 180 degrees), then we have:

$$B = M_3' = \begin{bmatrix} 6 & 7 & 2 \\ 1 & 5 & 9 \\ 8 & 3 & 4 \end{bmatrix}, \tag{2.18}$$

$$C = M_3'' = \begin{bmatrix} 2 & 9 & 4 \\ 7 & 5 & 3 \\ 6 & 1 & 8 \end{bmatrix}, \tag{2.19}$$

$$L_{3M3R} = \begin{bmatrix} 8 & 1 & 6 & 6 & 7 & 2 & 2 & 9 & 4 \\ 3 & 5 & 7 & 1 & 5 & 9 & 7 & 5 & 3 \\ 4 & 9 & 2 & 8 & 3 & 4 & 6 & 1 & 8 \\ 2 & 9 & 4 & 8 & 1 & 6 & 6 & 7 & 2 \\ 7 & 5 & 3 & 3 & 5 & 7 & 1 & 5 & 9 \\ 6 & 1 & 8 & 4 & 9 & 2 & 8 & 3 & 4 \\ 6 & 7 & 2 & 2 & 9 & 4 & 8 & 1 & 6 \\ 1 & 5 & 9 & 7 & 5 & 3 & 3 & 5 & 7 \\ 8 & 3 & 4 & 6 & 1 & 8 & 4 & 9 & 2 \end{bmatrix}. \tag{2.20}$$

The approaches discussed above give an idea of the broad possibilities for constructing Latin squares of various types and, based on them, non-equidistant AAs.

As you can see, some of the considered constructions of Latin squares are a more general case compared to magic squares. At the same time, if in the magic square of the n^{th} order, each of the n^2 numbers occurs only once, then in the Latin squares of the n^{th} order, each of the n numbers occurs only once in a row or column, and occurs n times in total. This means that in the Latin square, the numbers of which they are composed will occur n times. Since each element of the Latin square will be considered in the future as the distance between the elements of the interferometer, then in the AA built based on the Latin square, the redundancy factor n is first introduced for all frequencies covered from 1 to n.

It is worth mentioning that in the field of combinatorial design in mathematics, the Latin square, as a matrix with rich symmetric properties, has always been the focus of researchers. Using permutation groups to construct Latin squares is one of the most effective methods. A permutation group is a group composed of permutations, which refers to the operation of rearranging a set of elements. When constructing Latin squares, permutation groups provide a systematic method to generate square matrices with specific arrangement characteristics. For example, consider a 3rd order Latin square, which we can construct using permutations in S_3 (symmetry group). S_3 contains six permutations of elements, and through these permutations, we can obtain six different 3rd order Latin squares.

This construction method not only has great theoretical significance but also shows its strong application potential in practical applications such as experimental design, coding theory, and statistics.

2.2. Modeling, evaluation and optimization of the characteristics of sparse planar antenna arrays based on the traditional Latin square

The coordinates of the elements of the antenna array (AA), calculated according to formula (1.8), and their location are shown in Fig. 2.1 and the view of the directional diagrams in the Cartesian and polar coordinate systems are shown in Fig. 2.2. In Fig. 2.1, points show the location of the initial elements of the lattice obtained based on the Latin square (hereinafter they will be denoted as AA $(X, Y)_{L3}$), the "star" shows the elements additionally introduced into the AR that provide full coverage of spatial frequencies — they will be denoted as $(X, Y)_{L3+}$, and "excessive" elements of the antenna array are marked with "non-filled dots (hollow)," after removing which the full coverage of spatial

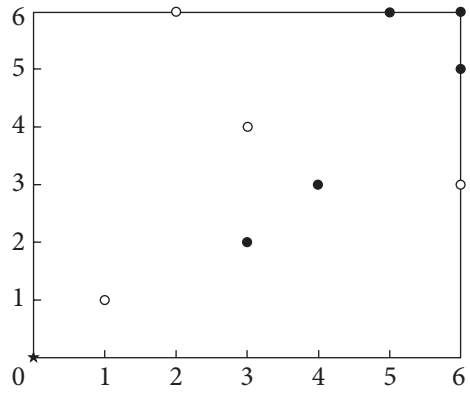

Fig. 2.1. Coordinates of AA elements and their location on the XOY coordinate plane

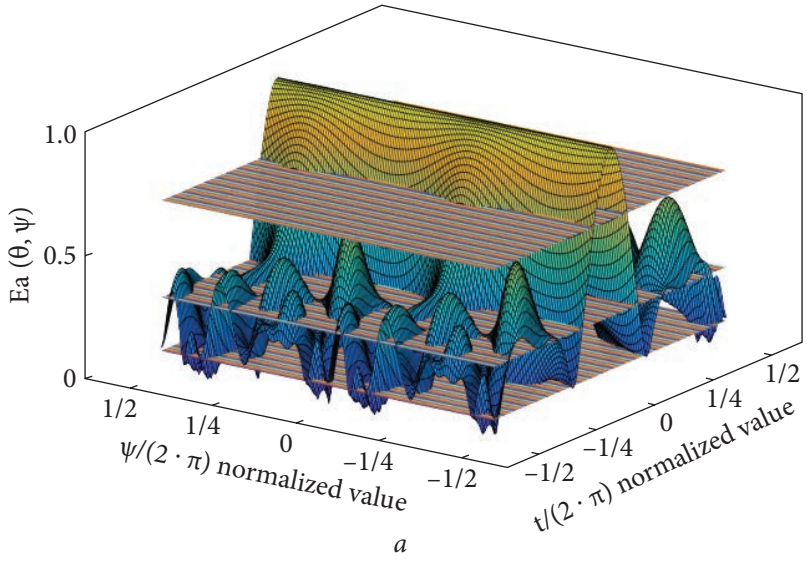

a

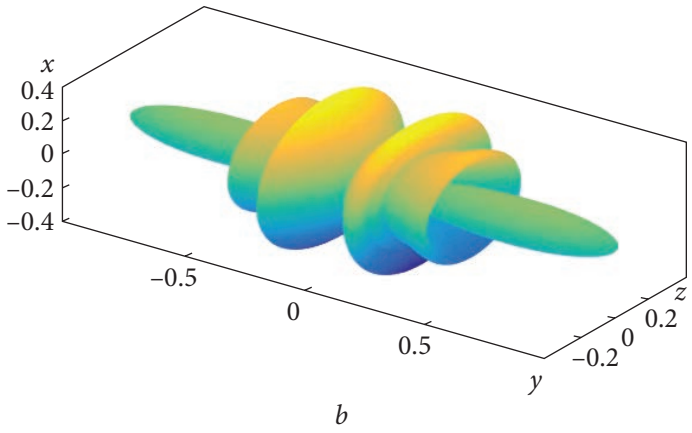

b

Fig. 2.2. Radiation pattern of the AA based on the Latin square of the 3rd order in the Cartesian (*a*) and polar (*b*) coordinate systems

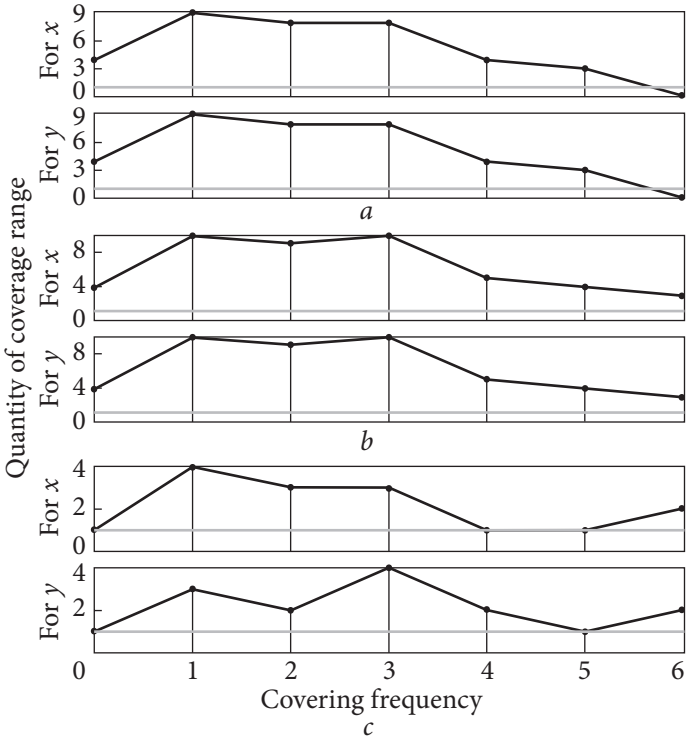

Fig. 2.3. Distribution of covered spatial frequencies along the *x*-axis and *y*-ordinate for the original AA ($(X, Y)_{L3}$) (*a*), with added points ($(X, Y)_{L3+}$) (*b*), and after removing redundant points ($(X, Y)_{L3-}$) (*c*)

frequencies is preserved. They will be denoted as $(X, Y)_{L3-}$.

$$(X,Y)_{L3} = \begin{bmatrix} (1,1) & (3,2) & (6,3) \\ (3,4) & (4,3) & (6,5) \\ (2,6) & (5,6) & (6,6) \end{bmatrix}. \tag{2.21}$$

Using the Latin square matrix of the third order, the radiation pattern (RP) of the AA, which is built on the basis of formula (1.8), is displayed in the Cartesian coordinate system and the polar coordinate system, as shown in Fig. 2.2.

The spatial frequency ranges covered by each of these structures: $(X, Y)_{L3}$, $(X, Y)_{L3+}$, and $(X, Y)_{L3-}$ are shown in Fig. 2.3, and RP of the new AA after removing redundant elements — in Fig. 2.4. RP of the AA, based on a truncated (with excess points removed) AA $(X, Y)_{L3-}$, is displayed in the Cartesian and polar coordinate systems, as shown in Fig. 2.4.

Comparing the distribution of frequency areas covering Fig. 2.3, it can be seen that the elimination of excess points leads to a more even distribution of the covered frequencies, but at the same time, the level of side lobes increases.

It should be noted that the analysis of the covered frequencies is carried out in the selected XOY coordinate system. Obviously, it should be required that a sufficiently dense (preferably complete) coverage of the area of spatial frequen-

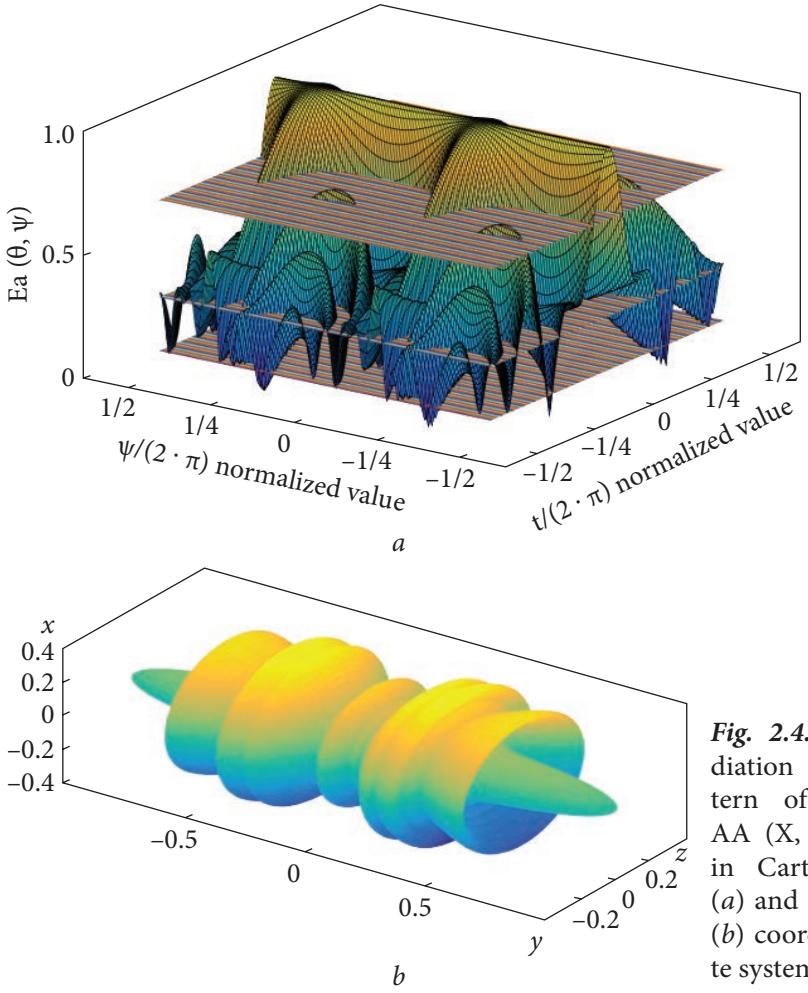

Fig. 2.4. Radiation pattern of the AA $(X, Y)_{L3-}$ in Cartesian (*a*) and polar (*b*) coordinate systems

cies is carried out when the selected coordinate system is rotated arbitrarily. Only in this case, it is expected that the level of side lobes will remain acceptable in the entire range of working angles. If the number of frequencies covered by one of the axes sharply decreases, while rotating the coordinate system, which will happen when most of the elements lie on another axis, then such an AA is unlikely to have an acceptable level of petals in the entire range of angles.

Numerical values of the parameters obtained by AAs ($(X, Y)_{L3}$, $(X, Y)_{L3+}$, $(X, Y)_{L3-}$) are given in the Table 2.1. The last column of the table shows the relative change in the AA characteristics after the elimination of redundant elements compared to the original lattices (columns are filled with green and yellow). Those characteristics that improve are filled in green, and those that worsen are in red. From the analysis of the relative change in characteristics from $(X, Y)_{L3}$

Table 2.1. **Comparison of AA parameters ($(X, Y)_{L3}$, $(X, Y)_{L3+}$, $(X, Y)_{L3-}$)**

Array parameters	Initial AA $(X, Y)_{L3}$	AA with added elements $(X, Y)_{L3+}$	AA with removed elements $(X, Y)_{L3-}$	Relative change (%) $(X, Y)_{L3-}$ *Vs.* $(X, Y)_{L3}$
$\Delta\omega_{0.707}$ (radian)	0.9704	0.8763	1.1688	–20.4436
$\Delta\omega_0$ (radian)	2.9847	2.7541	2.5109	15.8729
m	0.3067	0.2803	0.3944	–28.5971
N_0	9	10	6	33.3333
$X_{max} \times Y_{max}$	6×6	6×6	6×6	0
S	36	36	36	0
α	0.2500	0.2778	0.1667	33.3333
β	1.5000	1.6667	1	33.3333

Table 2.2. **Comparison of AA parameters ($(X, Y)_{L3}$, $(X, Y)_{L3UD}$, $(X, Y)_{L3UD-}$)**

Array parameters	Initial AA $(X, Y)_{L3}$	Initial AA $(X, Y)_{L3UD}$	AA with remote elements $(X, Y)_{L3UD-}$	Relative change (%) $(X, Y)_{L3UD-}$ *Vs.* $(X, Y)_{L3UD}$
$\Delta\omega_{0.707}$ (radian)	0.9704	0.8213	0.9632	–17.2845
$\Delta\omega_0$ (radian)	2.9847	2.7826	2.0064	27.8974
m	0.3067	0.1900	0.3899	–105.1551
N_0	9	81	6	92.5926
$X_{max} \times Y_{max}$	6×6	6×6	6×6	0
S	36	36	36	0
α	0.2500	2.2500	0.1667	92.5926
β	1.5000	13.5000	1	92.5926

to $(X, Y)_{L3-}$ it can be concluded that the removal of redundant points leads to a deterioration of the RP characteristics (an increase in the width and level of the side lobes), however, other lattice parameters are significantly improved (filling and redundancy factors are reduced). Moreover, the magnitude of improvement in characteristics is somewhat greater than the observed deterioration.

2.3. Modeling, evaluation, and optimization of characteristics of sparse planar antenna arrays based on nested Latin squares

In [22, 23], we showed the possibility of creating large-sized antenna arrays (AAs) using nested magic squares. A similar approach can be used when using nested Latin squares. Using several simple squares and nesting one inside the other, the size of the synthesized AA can be increased significantly.

Different combinations of squares can be used, which means various generating matrices for AA formation.

2.3.1. Unit diagonal matrices as nested submatrices

As mentioned in CHAPTER 1 of this book, a nested Latin square of the 3rd order has a nesting of a set of unit diagonal matrices in the form (U_D), while we obtain the matrix (L_{3UD}) and further calculate the coordinates according to the formula (1.8). We have:

$$(X,Y)_{L3UD} = \begin{bmatrix} (1,1) & (1,0) & (1,0) & (3,2) & (3,0) & (3,0) & (6,3) & (6,0) & (6,0) \\ (0,1) & (1,1) & (1,0) & (1,2) & (3,2) & (3,0) & (3,3) & (6,3) & (6,0) \\ (0,1) & (0,1) & (1,1) & (1,2) & (1,2) & (3,2) & (3,3) & (3,3) & (6,3) \\ (3,4) & (3,1) & (3,1) & (4,3) & (4,2) & (4,2) & (6,5) & (6,3) & (6,3) \\ (0,4) & (3,4) & (3,1) & (3,3) & (4,3) & (4,2) & (4,5) & (6,5) & (6,3) \\ (0,4) & (0,4) & (3,4) & (3,3) & (3,3) & (4,3) & (4,5) & (4,5) & (6,5) \\ (2,6) & (2,4) & (2,4) & (5,6) & (5,3) & (5,3) & (6,6) & (6,5) & (6,5) \\ (0,6) & (2,6) & (2,4) & (2,6) & (5,6) & (5,3) & (5,6) & (6,6) & (6,5) \\ (0,6) & (0,6) & (2,6) & (2,6) & (2,6) & (5,6) & (5,6) & (5,6) & (6,6) \end{bmatrix}. \quad (2.22)$$

The coordinates of the elements of the AA and its distribution are shown in Fig. 2.5 and Fig. 2.6.

AA is built based on third-order nested Latin squares (L_{3UD}) using a set of unit diagonal (U_D) matrices as submatrices. The radiation pattern (RP) of this developed AA is shown in Fig. 2.6.

It can be seen that this square and the produced AA are characterized by a large number of overlapping frequencies (great redundancy). In Fig. 2.5, the elements of the AA are shown with colored round dots — the AA $(X, Y)_{L3UD}$; open circles show points that can be removed while providing full coverage of the spatial frequency — the AA $(X, Y)_{L3UD-}$. Those points that had multiple coverage and part of which was removed are shown as filled and empty at the same time. After deleting redundant points, you can compare the spatial frequencies covered using AA $(X, Y)_{L3UD}$ and AA $(X, Y)_{L3UD-}$. The obtained results are presented in Fig. 2.7. It can be seen that the original grid was characterized by a very large redundancy of elements and a very high multiplicity of covering frequencies, as shown in Fig. 2.7, *a*.

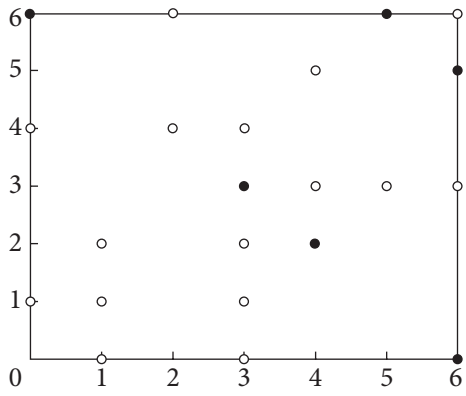

Fig. 2.5. Coordinates of AA elements $(X, Y)_{L3UD}$ based on a Latin square of 3rd order with a nested set of single diagonal matrices of 3rd order and their location

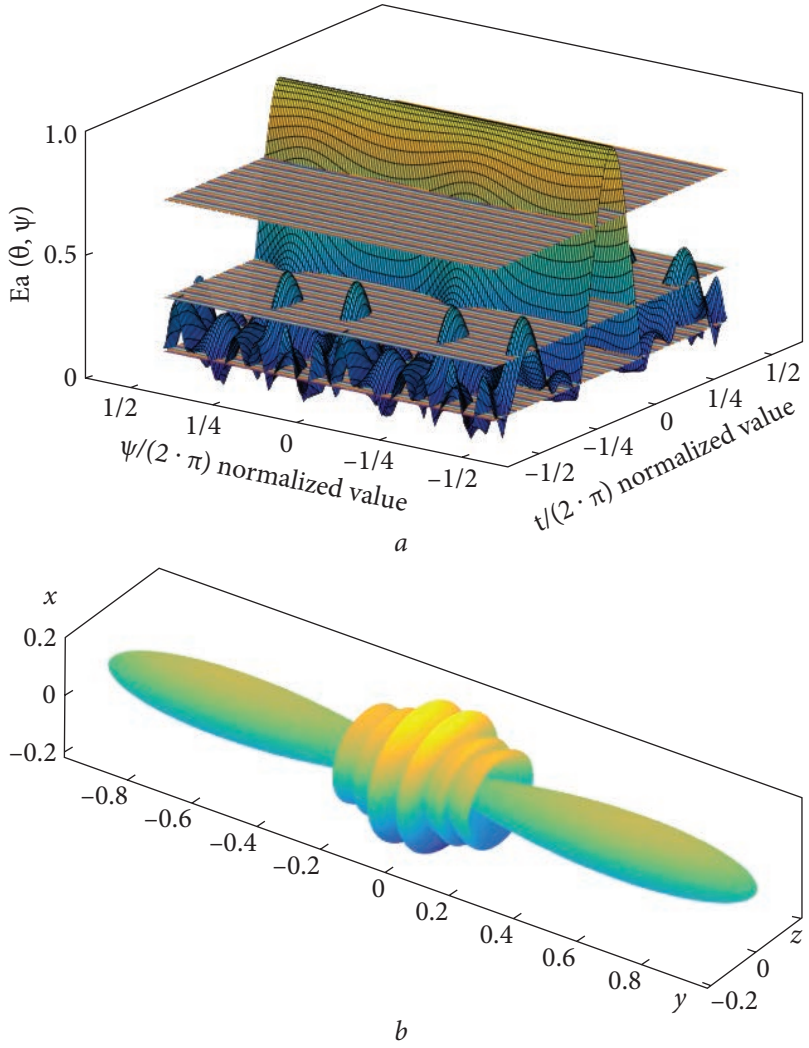

Fig. 2.6. The radiation pattern of the AA $(X, Y)_{L3UD}$ in Cartesian (*a*) and polar (*b*) coordinate systems

After the removal of redundant points, the multiplicity of frequency coverage decreased significantly — Fig. 2.7, *b*. At the same time, it should be noted that after removing the excess points, the remaining points are placed unevenly in space, most of them are grouped at angles of –45° and 135°. This means that in the coordinate system rotated by this angle, frequency coverage may be incomplete, which is manifested in large values of the side lobes at certain angles — Fig. 2.7.

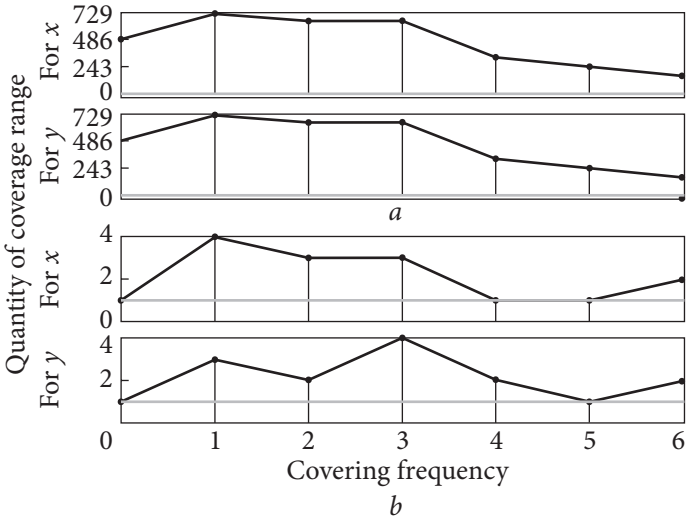

Fig. 2.7. Distribution of covered spatial frequencies along the *x*-axis and *y*-ordinate for the original AA ($(X, Y)_{L3UD}$) (*a*), and after removing redundant points ($(X, Y)_{L3UD-}$) (*b*)

Table 2.2 shows a comparison of the characteristics of the simple $(X, Y)_{L3}$ and the nested AA of the original $(X, Y)_{L3UD}$ and after removing the redundant elements $(X, Y)_{L3UD-}$, respectively.

RP of the AA $(X, Y)_{L3UD-}$, based on the truncated (with distant excess points) AA $(X, Y)_{L3UD}$, is displayed in the Cartesian and polar coordinate systems, as shown in Fig. 2.8.

Analyzing the relative change in the characteristics of AA $(X, Y)_{L3UD}$ and $(X, Y)_{L3UD-}$, it can be concluded that the removal of points leads to the deterioration of the characteristics of the RP — the expansion of the main beam and the increase in the level of the side lobe levels, but it significantly reduces the coefficients of filling and redundancy of the AA.

From the comparison of AA $(X, Y)_{L3}$ and $(X, Y)_{L3UD}$, it follows that the creation of the generating matrix based on Latin squares and the matrix of units does not lead to an increase in the size of AA, but improves its quality. This does not lead to a narrowing of the width of the main petal, but allows to for a reduction in the average level of the side lobes.

2.3.2. Unit square matrices as nested submatrices

As was mentioned in the first section of this chapter, the embedded Latin square of the 3rd order has an embedding of a set of unit square matrices in the form (U_I), we get the matrix (L_{3UI}), and further, after calculating the

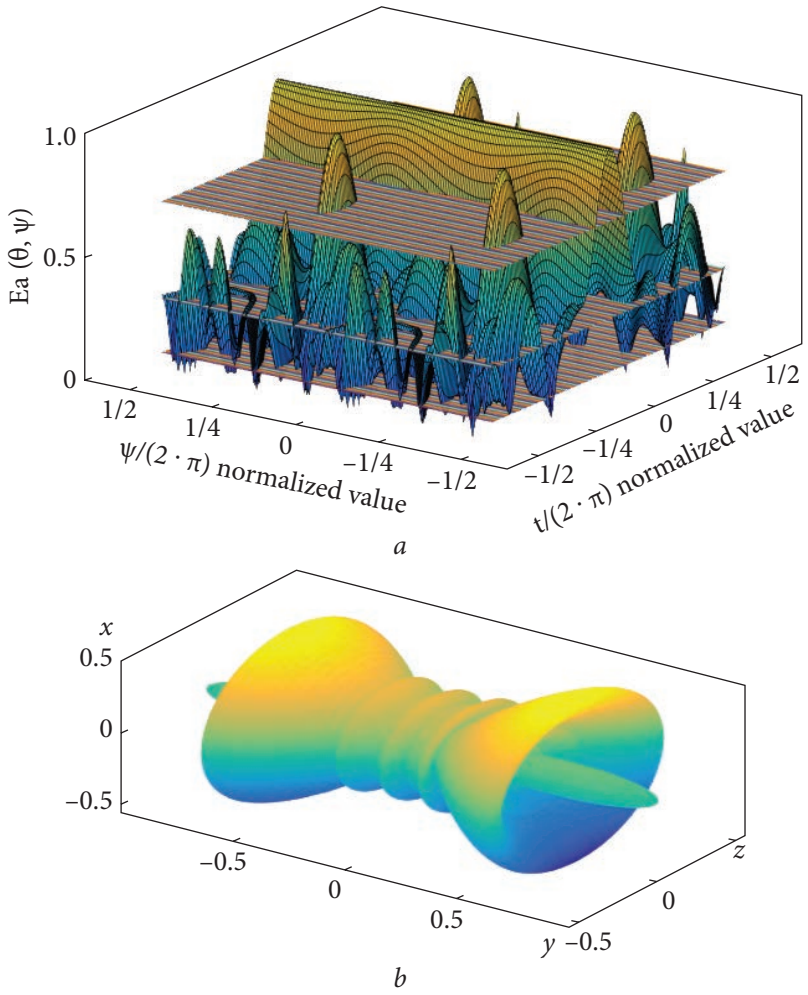

Fig. 2.8. Radiation pattern of the AA $(X, Y)_{L3UD-}$ in the Cartesian (*a*) and polar (*b*) coordinate systems

coordinates according to the formula (1.6), we get:

$$(X,Y)_{L3UI}=\begin{bmatrix} (1,1) & (2,1) & (3,1) & (5,2) & (7,2) & (9,2) & (12,3) & (15,3) & (18,3) \\ (1,2) & (2,2) & (3,2) & (5,4) & (7,4) & (9,4) & (12,6) & (15,6) & (18,6) \\ (1,3) & (2,3) & (3,3) & (5,6) & (7,6) & (9,6) & (12,9) & (15,9) & (18,9) \\ (3,6) & (6,6) & (9,6) & (10,7) & (11,7) & (12,7) & (14,11) & (16,11) & (18,11) \\ (3,9) & (6,9) & (9,9) & (10,8) & (11,8) & (12,8) & (14,13) & (16,13) & (18,13) \\ (3,12) & (6,12) & (9,12) & (10,9) & (11,9) & (12,9) & (14,15) & (16,15) & (18,15) \\ (2,14) & (4,14) & (6,14) & (9,12) & (12,12) & (15,12) & (16,16) & (17,16) & (18,16) \\ (2,16) & (4,16) & (6,16) & (9,15) & (12,15) & (15,15) & (16,17) & (17,17) & (18,17) \\ (2,18) & (4,18) & (6,18) & (9,18) & (12,18) & (15,18) & (16,18) & (17,18) & (18,18) \end{bmatrix}. \quad (2.23)$$

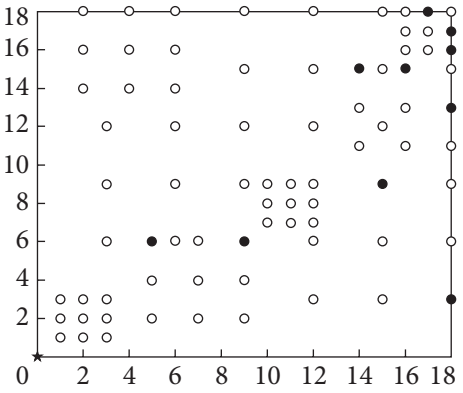

Fig. 2.9. Coordinates of AA elements $(X, Y)_{L3UI}$, $(X, Y)_{L3UI+}$, and $(X, Y)_{L3UI-}$ based on the Latin square of the 3rd order with a nested unit square matrix of the third order as submatrices, and their location on the coordinate plane

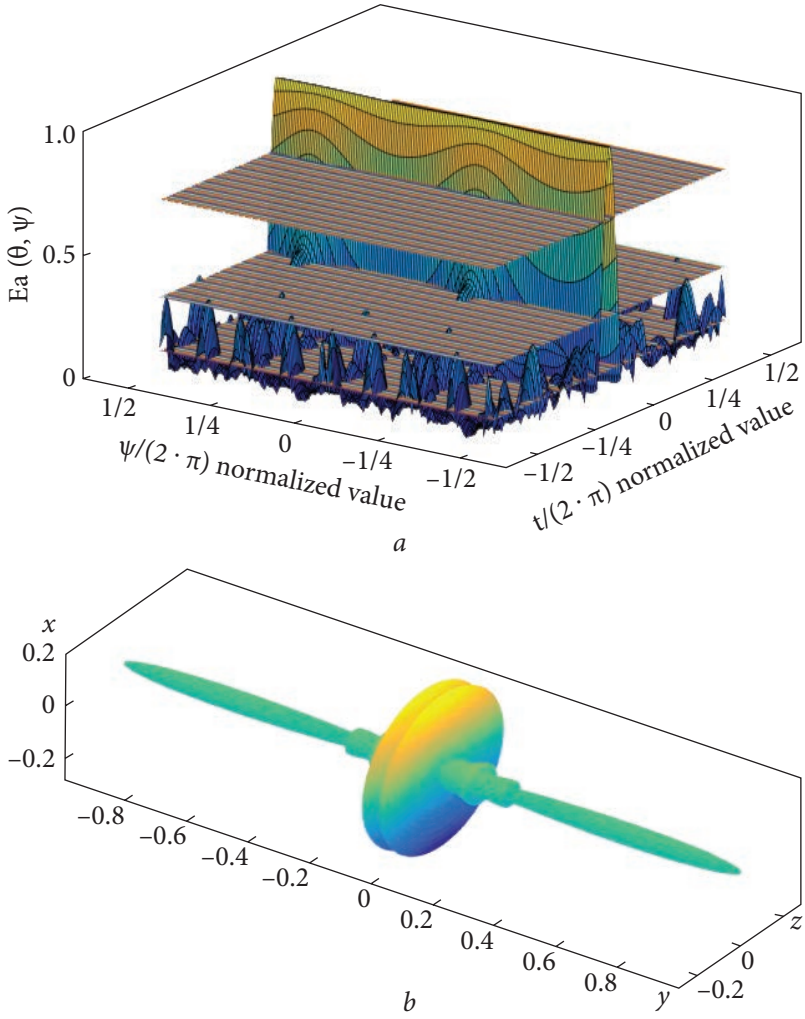

Fig. 2.10. Radiation pattern of the AA $(X, Y)_{L3UI}$ in Cartesian (*a*) and polar (*b*) coordinate systems

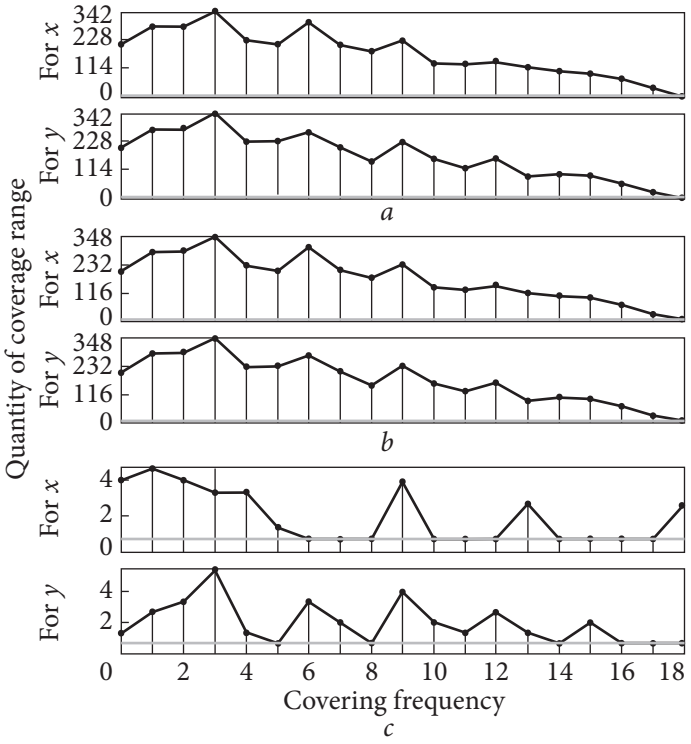

Fig. 2.11. Distribution of covered spatial frequencies along the *x*-axis and *y*-ordinate for AAs: *a* — $(X, Y)_{L3UI}$, *b* — $(X, Y)_{L3UI+}$, and *c* — $(X, Y)_{L3UI-}$

Table 2.3. **Comparison of AA parameters ($(X, Y)_{L3}$, $(X, Y)_{L3UD}$, $(X, Y)_{L3UI}$, and $(X, Y)_{L3UI-}$)**

Antenna array parameters	Initial AA $(X, Y)_{L3}$	Initial AA $(X, Y)_{L3UD}$	Initial AA $(X, Y)_{L3UI}$	AA with removed elements $(X, Y)_{L3UI-}$	Relative change (%) $(X, Y)_{L3UI-}$ *Vs.* $(X, Y)_{L3UI}$
$\Delta\omega_{0.707}$ (radian)	0.9704	0.8213	0.3099	0.3339	–7.7597
$\Delta\omega_0$ (radian)	2.9847	2.7826	1.6582	1.7321	–4.4617
m	0.3067	0.1900	0.1070	0.2983	–178.9076
N_0	9	81	81	11	86.4198
$X_{max} \times Y_{max}$	6×6	6×6	18×18	18×18	0
S	36	36	324	324	0
α	0.2500	2.2500	0.2500	0.0340	86.4198
β	1.5000	13.5000	4.500	0.6111	86.4198

Built on this type of square, AA will consist of 3 types of equidistant fully filled lattices with distances between elements {1, 2, 3}. It is obvious that it will have a large redundancy factor. The coordinates of the location of AR elements are shown in Fig. 2.9. In this case, the "points" are the original points of AA $(X, Y)_{L3UI}$; An additional point is marked with an "asterisk", providing full

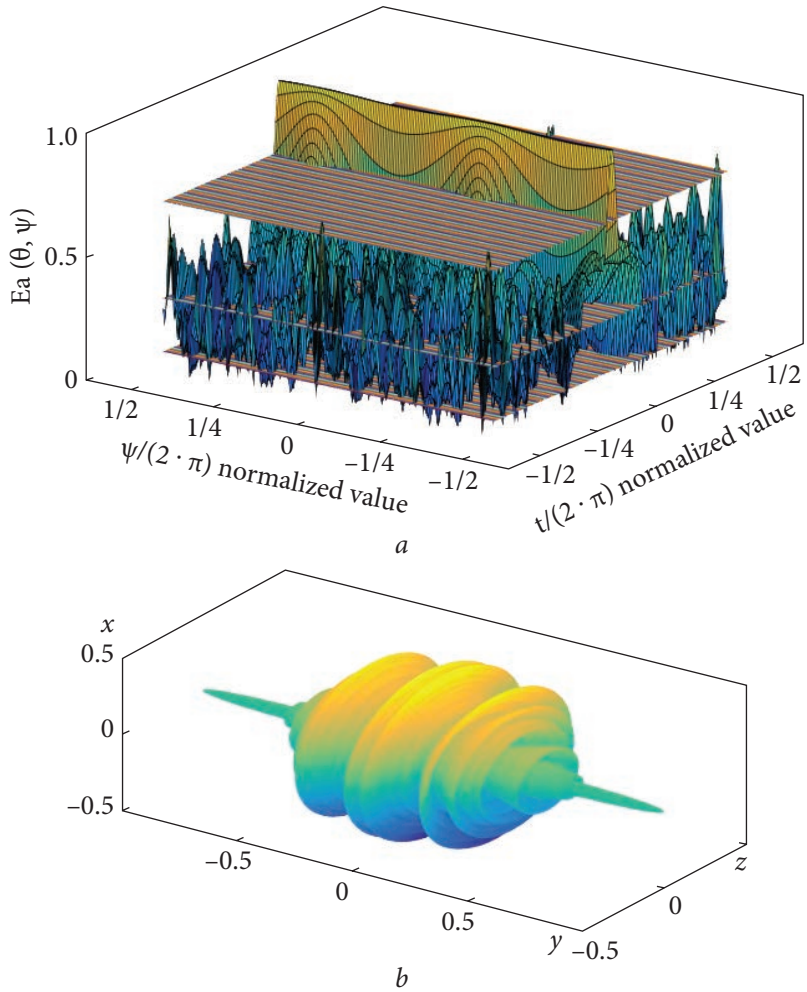

Fig. 2.12. Radiation pattern of the AA $(X, Y)_{L3UI-}$ in Cartesian (*a*) and polar (*b*) coordinate systems

frequency coverage ($(X, Y)_{L3UI+}$); "Empty dots" show remote points with full coverage of ($(X, Y)_{L3UI-}$) frequencies, filled points show the ones remaining after removal.

Consider the areas of spatial frequencies covered by each of these structures: $(X, Y)_{L3UI}$, $(X, Y)_{L3UI+}$, and $(X, Y)_{L3UI-}$. The results are shown in Fig. 2.12. From the comparison of Fig. 2.12, *a*, Fig. 2.12, *b*, and Fig. 2.12, *c*, it can be seen that a significant reduction in the redundancy in the covered frequencies, as well as a more even distribution of the frequencies covering the grids with the redundant points removed.

AA is built based on third-order nested Latin squares (L_{3UI}) using a set of unit matrices (U_1) as submatrices. The RP of this developed AA is shown in Fig. 2.10.

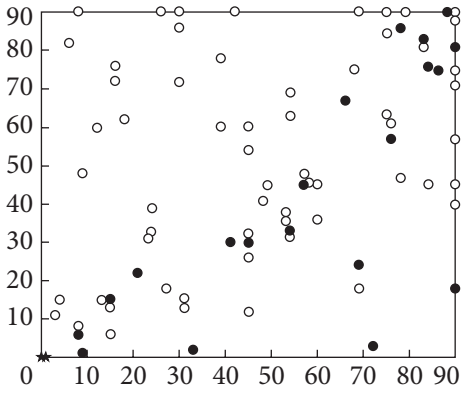

Fig. 2.13. Coordinates of AA elements $(X, Y)_{L3M3}$, $(X, Y)_{L3M3+}$, and $(X, Y)_{L3M3-}$ based on the Latin square of the 3rd order with a nested identity square of the third order and their location on the coordinate plane

Distribution of covered spatial frequencies along the *x*-axis and *y*-ordinate for the original AA ($(X, Y)_{L3UI}$), AA with added point ($(X, Y)_{L3UI+}$), and AA after removing extra points ($(X, Y)_{L3UI-}$) are shown in Fig. 2.11.

RP of the AA $(X, Y)_{L3UI-}$, based on the truncated (with redundant points removed) AA $(X, Y)_{L3UI}$, is displayed in the Cartesian coordinate system and the polar coordinate system, as shown in Fig. 2.12.

The results of comparing the characteristics of AAs ($(X, Y)_{L3UI}$, $(X, Y)_{L3UI+}$, $(X, Y)_{L3UI-}$) are shown in the Table 2.3. If we analyze the relative change in characteristics for AAs $(X, Y)_{L3UI}$ and $(X, Y)_{L3UI-}$, we can conclude that the removal of redundant points significantly reduces the coefficients of filling and redundancy of AAs, but leads to a significant increase in the average level of side petals. At the same time, the main petal expands a little, although the value changes slightly. From the analysis of the relative changes in the AA characteristics from $(X, Y)_{L3UI}$ to $(X, Y)_{L3UI+}$, it can be concluded that adding another point to the origin of the coordinates is useful for reducing the levels of the side lobes and narrowing the width of the main beam.

Comparing the RP parameters for AAs $(X, Y)_{L3UD}$ and $(X, Y)_{L3UI}$, it can be seen that the combination of the Latin square with the unit square allows to increase the size of the AA, narrow the width of the main petal, and reduce the level of the side petals, better than the previously synthesized square on based on the unit square.

Comparing the RP parameters for AAs $(X, Y)_{L3}$ and $(X, Y)_{L3UI}$, it can be seen that for a Latin square nested with the n^{th} order single square, the size of the AA will expand by $n \times n$ times, and the width of the main beam will decrease by n times Similarly, for the average level of the side lobes — they will decrease by n times. Therefore, using the nesting of the n^{th} order of the unit square, it is possible to increase the size of the AA by n times, reduce the effective width of the main petal by n times, and also reduce the average level of the side lobes by n times.

From the analysis of Fig. 2.9, *a* for the coordinates of the AA elements, it can be seen that for the matrix generating $(X, Y)_{L3UI}$, within each block, the abscissa coordinates on the column do not change in the same way as the ordinates on the row.

2.3.3. Magic squares as nested submatrices

As mentioned in the first section of this chapter, a nested Latin square of order 3 has a nesting of a set of nested magic square matrices of the form (M_3). At the same time, we obtain the matrix (L_{3M3}) and calculate the coordinates further according to the formula (1.6). We have:

$$(X,Y)_{L3M3} =$$

$$= \begin{bmatrix} (8,8) & (9,1) & (15,6) & (31,16) & (33,2) & (45,12) & (69,24) & (72,3) & (90,18) \\ (3,11) & (8,6) & (15,13) & (21,22) & (31,12) & (45,26) & (54,33) & (69,18) & (90,39) \\ (4,15) & (13,15) & (15,15) & (23,30) & (41,30) & (45,30) & (57,45) & (84,45) & (90,45) \\ (24,39) & (27,18) & (45,33) & (53,38) & (54,31) & (60,36) & (76,61) & (78,47) & (90,57) \\ (9,48) & (24,33) & (45,54) & (48,41) & (53,36) & (60,43) & (66,67) & (76,57) & (90,71) \\ (12,60) & (39,60) & (45,60) & (49,45) & (58,45) & (60,45) & (68,75) & (86,75) & (90,75) \\ (16,76) & (18,62) & (30,72) & (54,69) & (57,48) & (75,63) & (83,83) & (84,76) & (90,81) \\ (6,82) & (16,72) & (30,86) & (39,78) & (54,63) & (75,84) & (78,86) & (83,81) & (90,88) \\ (8,90) & (26,90) & (30,90) & (42,90) & (69,90) & (75,90) & (79,90) & (88,90) & (90,90) \end{bmatrix}. \quad (2.24)$$

Obtained based on the matrix that generates the coordinates and type of AA $(X, Y)_{L3M3}$ are shown in Fig. 2.13 and the RP of AA $(X, Y)_{L3M3}$ in the Cartesian and polar coordinate systems in Fig. 2.14. The notation used is the same as before: "filled dots" are the starting points ($(X, Y)_{L3M3}$), "asterisks" are additional points for full coverage ($(X, Y)_{L3M3+}$), "empty dots" are remote ones points with full frequency coverage ($(X, Y)_{L3M3-}$).

AA $(X, Y)_{L3M3}$ is built on third-order nested Latin squares (L_{3M3}) using a set of M_3 magic matrices as submatrices. The RP of this developed AA is shown in Fig. 2.14**.**

Distribution of covered spatial frequencies along the x-axis and y-axis for the original/initial AA ($(X, Y)_{L3M3}$), AA with an added point ($(X, Y)_{L3M3+}$), and AA after removing extra points ($(X, Y)_{L3M3-}$) are shown in Fig. 2.15.

Consider the areas of spatial frequencies covered by each of these structures: AA $(X, Y)_{L3M3}$, $(X, Y)_{L3M3+}$, and $(X, Y)_{L3M3-}$. The results are shown in Fig. 2.15. It can be seen that, in contrast to the previous cases ($(X, Y)_{L3}$, $(X, Y)_{L3UD}$, $(X, Y)_{L3UI}$, $(X, Y)_{L3M3}$), with this method of construction of the AAs, it is possible to obtain a more uniform coverage of the spatial frequency grid with a lower frequency of repetition of the same frequencies (Fig. 2.15 *a*, *b*). Removing redundant elements makes it more uniform (Fig. 2.15 *c*). The directional diagrams of this AA $(X, Y)_{L3M3-}$ are shown in Fig. 2.16.

Table 2.4 shows the characteristics of AA $(X, Y)_{L3}$ based on a simple Latin square and AA $(X, Y)_{L3M3}$ obtained by inserting a magic square of 3rd order into a Latin square.

RP of AA $(X, Y)_{L3M3-}$, based on the truncated (with excess points removed) AA $(X, Y)_{L3M3}$, is displayed in the Cartesian and polar coordinate systems, as shown in Fig. 2.16.

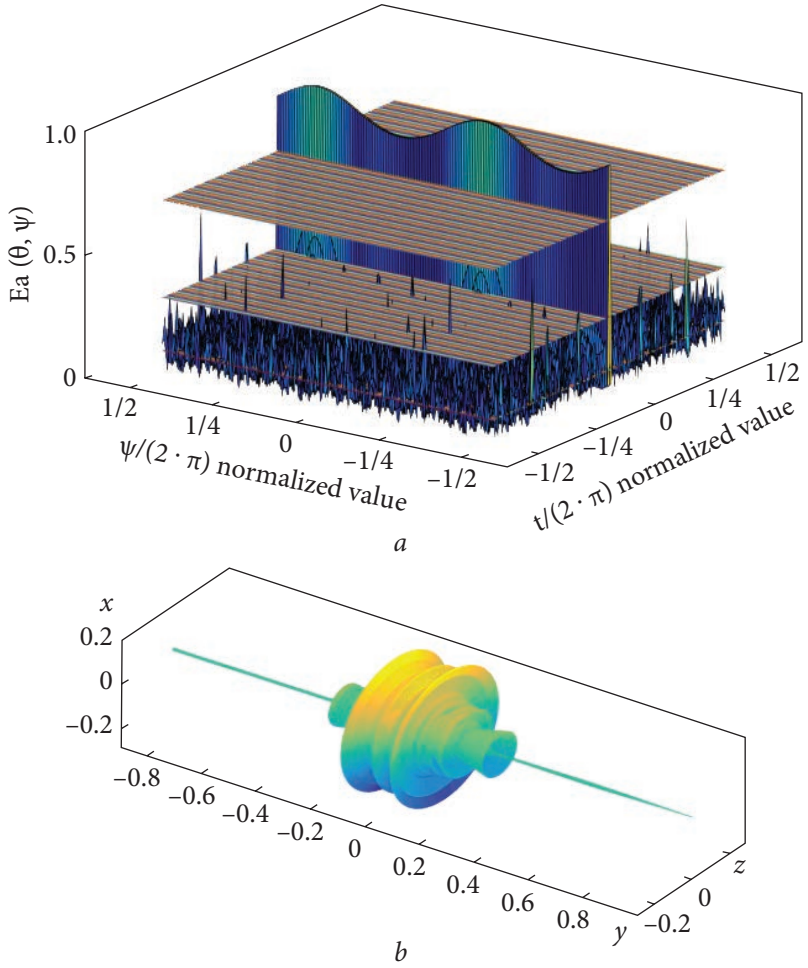

Fig. 2.14. Radiation pattern of the AA $(X, Y)_{L3M3}$ in Cartesian (*a*) and polar (*b*) coordinate systems

Observing the relative change in the characteristics of AAs from AA $(X, Y)_{L3M3}$ to AA $(X, Y)_{L3M3-}$, we can conclude that the removal of redundant points allows for a significant reduction in the coefficients of redundancy and filling of AA, but leads to a significant increase in the average level of side lobes. At the same time, the width of the main petal expands a little, although this change is small. From the changes in the AA's characteristics when going from AA $(X, Y)_{L3M3}$ to AA $(X, Y)_{L3M3+}$, it can be concluded that adding an AA element to the origin of the coordinates is useful for reducing the level of the side petals and narrowing the width of the main beam.

Comparing the RP parameters for AA $(X, Y)_{L3}$ and AA $(X, Y)_{L3M3}$, we can conclude that the use of the Latin square, with the addition of the n^{th} order of

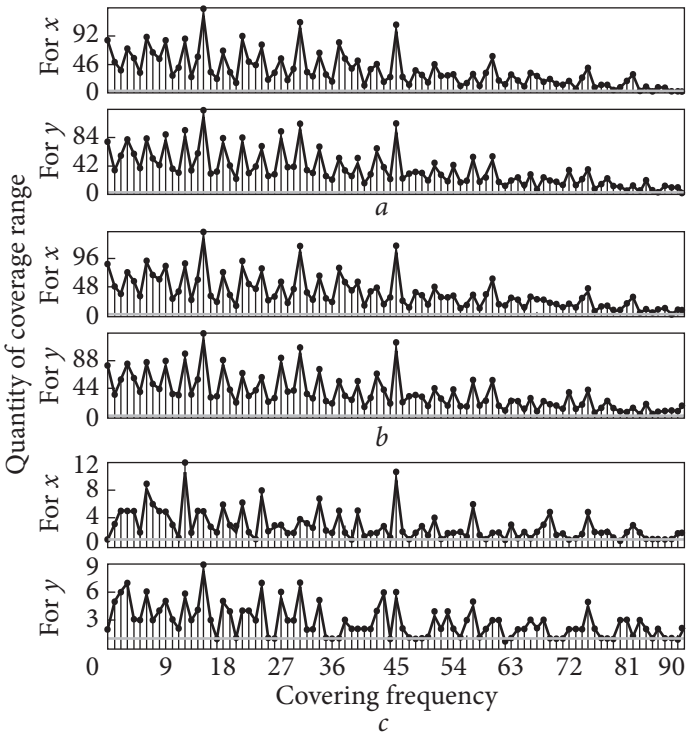

Fig. 2.15. Distribution of covered spatial frequencies along the *x*-axis and *y*-ordinate for AAs: *a* — $(X, Y)_{L3M3}$, *b* — $(X, Y)_{L3M3+}$, and *c* — $(X, Y)_{L3M3-}$

the magic square, allows you to expand the size of the AA aperture by $M \times M$ times, and reduce the width of the main petal by M times, while reducing the average level of the side petals by n times. Therefore, we can, when nesting the n^{th} order of the unit square, increase the size of the AA by M times, and reduce the width of the main petal by M times, as well as reduce the average level of the side petals by n times, where M is a magic constant equal to $(n^2 + 1) \cdot n/2$. This made it possible to reduce the fill factor by $(M/n)^2$ times, reducing the redundancy factor by n^2/M times.

2.3.4. A magic square and its rotation matrices as nested submatrices

As mentioned in the first section of this chapter, a third-order nested Latin square has a nest of magic square matrices and their rotation matrices of the form (M_3, M_3', M_3''). We obtain the matrix (L_{3M3R}), and the further

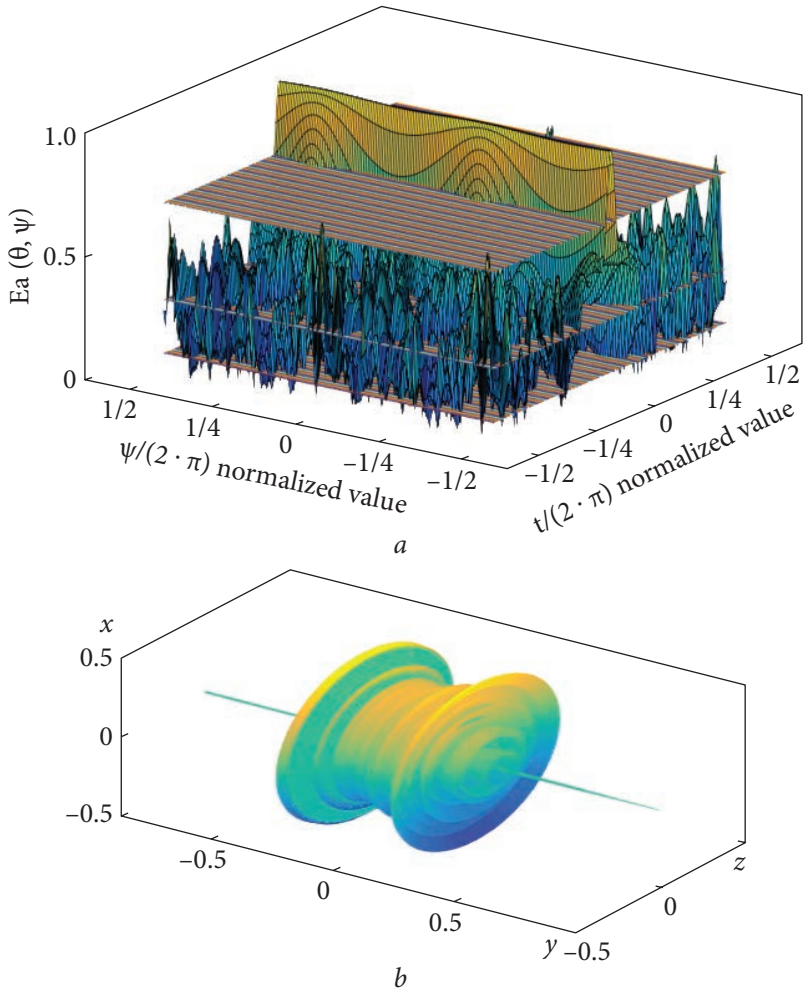

Fig. 2.16. Radiation pattern of the AA $(X, Y)_{L3M3-}$ in Cartesian (*a*) and polar (*b*) coordinate systems

calculation of coordinates can be obtained from formula (1.6):

$$(X,Y)_{L3M3R} =$$

$$= \begin{bmatrix} (8,8) & (9,1) & (15,6) & (21,6) & (28,7) & (30,2) & (32,2) & (41,9) & (45,4) \\ (3,11) & (8,6) & (15,13) & (16,7) & (21,12) & (30,11) & (37,9) & (42,14) & (45,7) \\ (4,15) & (13,15) & (15,15) & (23,15) & (26,15) & (30,15) & (36,15) & (37,15) & (45,15) \\ (2,17) & (11,24) & (15,19) & (23,23) & (24,16) & (30,21) & (36,21) & (43,22) & (45,17) \\ (7,24) & (12,29) & (15,22) & (18,26) & (23,21) & (30,28) & (31,27) & (36,27) & (45,26) \\ (6,30) & (7,30) & (15,30) & (19,30) & (28,30) & (30,30) & (38,30) & (41,30) & (45,30) \\ (6,36) & (13,37) & (15,32) & (17,32) & (26,39) & (30,34) & (38,38) & (39,31) & (45,36) \\ (1,37) & (6,42) & (15,41) & (22,39) & (27,44) & (30,37) & (33,41) & (38,36) & (45,43) \\ (8,45) & (11,45) & (15,45) & (21,45) & (22,45) & (30,45) & (34,45) & (43,45) & (45,45) \end{bmatrix}. \quad (2.25)$$

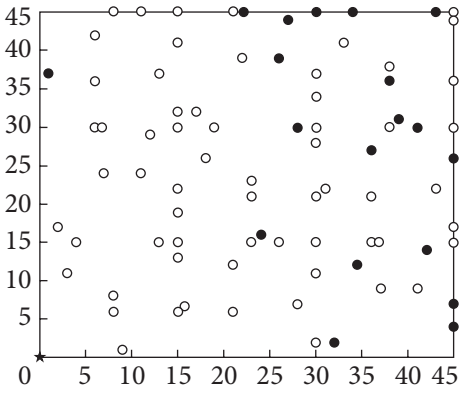

Fig. 2.17. Coordinates of AA elements $(X, Y)_{L3M3R}$, $(X, Y)_{L3M3R+}$, and $(X, Y)_{L3M3R-}$ based on the Latin square of the 3rd order with a nested identity square of the third order, their location on the coordinate plane

In this case, the element of the Latin square is the original magic square transformed with the help of a rotation (transpose) o+peration.

The coordinates of AA elements and their location on the plane are shown in Fig. 2.17. The type of RP of the original AA $(X, Y)_{L3M3R}$ is also given here.

An AA constructed from third-order nested Latin squares (L_{3M3R}) by taking the set of magic matrices and their rotation matrices of the form (M_3, M_3', M_3'') as a submatrix. The RP of the developed AA is shown in Fig. 2.18.

Spatial frequencies are shown in Fig. 2.19, which are covered along the *x*-axis (red curves), the *y*-ordinate (blue curves) for the original AA ($(X, Y)_{L3M3R}$) — *a*, with the added point ($(X, Y)_{L3M3R+}$) — *b*, and after removing redundant points ($(X, Y)_{L3M3R-}$) — *c*.

Marks in Fig. 2.17 are used the same as before: with a "dot" — the original AA elements are marked, with an "asterisk" there is an additional element that provides full coverage of the AA frequencies, with "empty dots" — deleted points are shown when full coverage is provided. Let's consider the areas of spatial frequencies covered by each of these structures: AA $(X, Y)_{L3M3R}$, AA $(X, Y)_{L3M3R+}$, and AA $(X, Y)_{L3M3R-}$. The results are shown in Fig. 2.19. It can be seen that the addition of a point at the origin of the coordinates does not lead to a significant

Table 2.4. **Comparison of AA parameters ($(X, Y)_{L3}$, $(X, Y)_{L3M3}$, $(X, Y)_{L3M3+}$, and $(X, Y)_{L3M3-}$)**

Array parameters	Initial AA $(X, Y)_{L3}$	Initial AP $(X, Y)_{L3M3}$	AA with added elements $(X, Y)_{L3M3+}$	AR with remote elements $(X, Y)_{L3M3-}$	Relative change (%) $(X, Y)_{L3M3-}$ *Vs.* $(X, Y)_{L3M3}$
$\Delta\omega_{0.707}$ (radian)	0.9704	0.0609	0.0607	0.0673	–10.5096
$\Delta\omega_0$ (radian)	2.9847	1.2878	1.3164	1.2910	–0.2485
m	0.3067	0.1093	0.1083	0.2100	–92.1482
N_0	9	81	83	23	71.6049
$X_{max} \times Y_{max}$	6×6	90×90	90×90	90×90	0
S	36	8100	8100	8100	0
α	0.2500	0.0100	0.0102	0.0028	71.6049
β	1.5000	0.900	0.9222	0.2556	71.6049

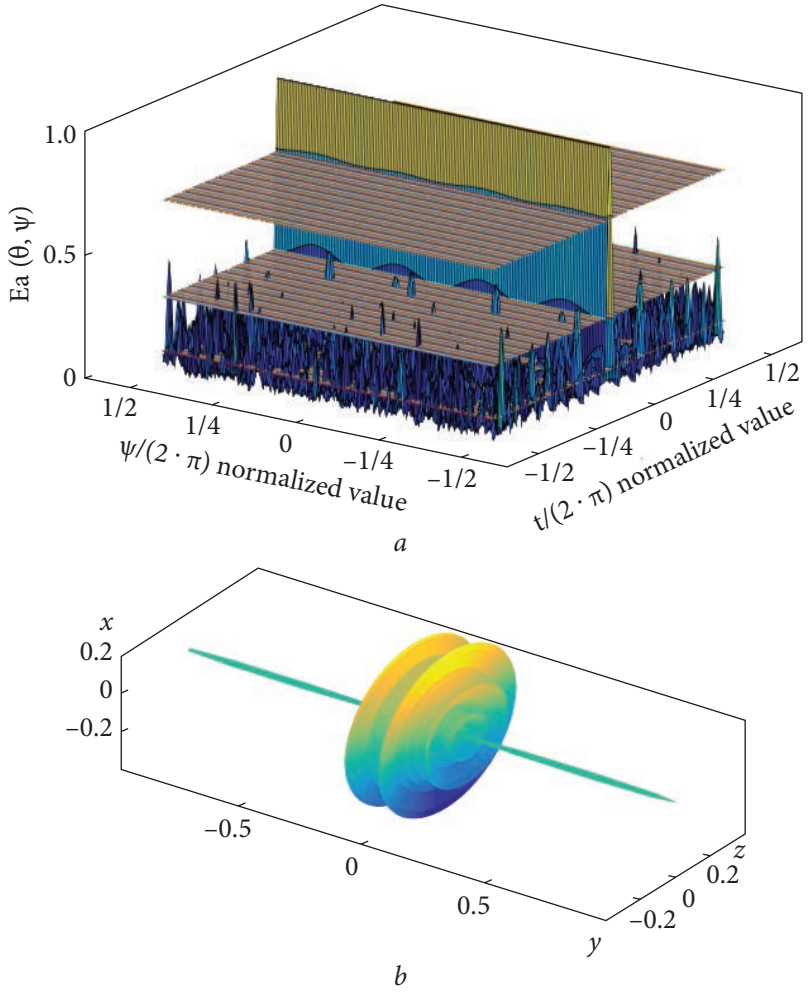

Fig. 2.18. Radiation pattern of the AA $(X, Y)_{L3M3R}$ in Cartesian (*a*) and polar (*b*) coordinate systems

change in the type of frequency distribution covered (Fig. 2.19, *b*), but only to a certain increase in the frequency of their coverage. After the removal of excess points (Fig. 2.19, *c*), the distribution of covered frequencies becomes more uniform with a significant reduction in multiplicity. The obtained RP of AA $(X, Y)_{L3M3R-}$ is shown in Fig. 2.20, and the results of comparison of AA parameters are shown in the Table 2.5. RP of AA $(X, Y)_{L3M3R-}$, based on the truncated (with redundant points removed) AA $(X, Y)_{L3M3}$, is displayed in the Cartesian coordinate system and the polar coordinate system, as shown in Fig. 2.20.

By comparing the change in the characteristic change from AA $(X, Y)_{L3M3R}$ to AA $(X, Y)_{L3M3R-}$, it can be concluded that the removal of points significantly reduces the value of the power coefficients and filling of the AA, but at the same

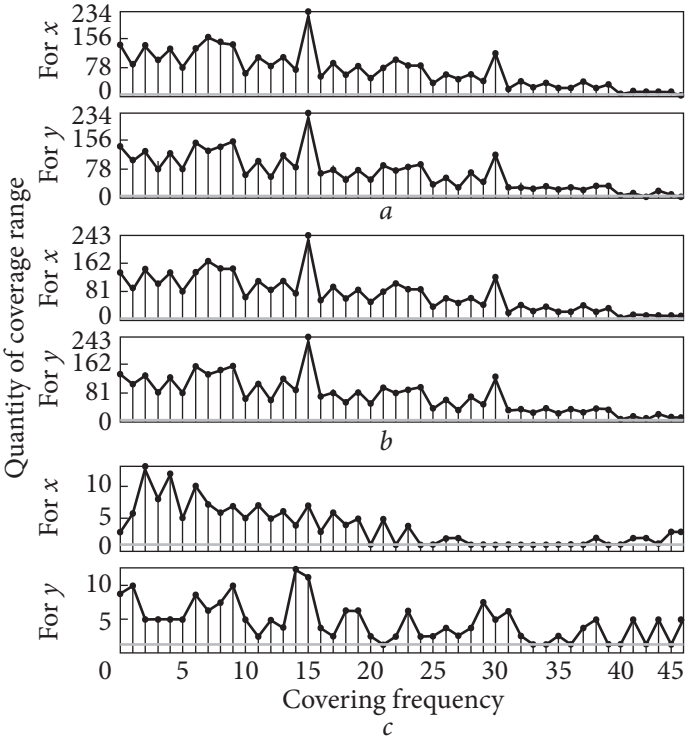

Fig. 2.19. Distribution of covered spatial frequencies along the *x*-axis and *y*-ordinate for AAs: *a* — $(X, Y)_{L3M3R}$, *b* — $(X, Y)_{L3M3R+}$, and *c* — $(X, Y)_{L3M3R-}$

Table 2.5. **Comparison of AA parameters ($(X, Y)_{L3}$, $(X, Y)_{L3M3R}$, $(X, Y)_{L3M3R+}$, $(X, Y)_{L3M3R-}$)**

Array parameters	Initial AA $(X, Y)_{L3}$	Initial AA $(X, Y)_{L3M3R}$	AA with added elements $(X, Y)_{L3M3R+}$	AA with remote elements $(X, Y)_{L3M3R-}$	Relative change (%) $(X, Y)_{L3M3R-}$ *Vs.* $(X, Y)_{L3M3R}$
$\Delta\omega_{0.707}$ (radian)	0.9704	0.1222	0.1222	0.1247	–2.0635
$\Delta\omega_0$ (radian)	2.9847	1.3335	1.3845	1.3947	–4.5881
m	0.3067	0.1077	0.1075	0.2274	–111.1939
N_0	9	81	82	19	76.5432
$X_{max} \times Y_{max}$	6×6	45×45	45×45	45×45	0
S	36	2025	2025	2025	0
α	0.2500	0.0400	0.0415	0.00 94	76.5432
β	1.5000	1.8000	1.8222	0.4222	76.5432

time, the average level of the side petals is significant. At the same time, the width of the main petal changes slightly (it expands a little). From the comparison of changes in the characteristic when going from AA $(X, Y)_{L3M3R}$ to $(X, Y)_{L3M3R+}$, it can be concluded that adding points to the origin of coordinates is useful for reducing the level of side petals, although it does not cause a practical width of the main beam.

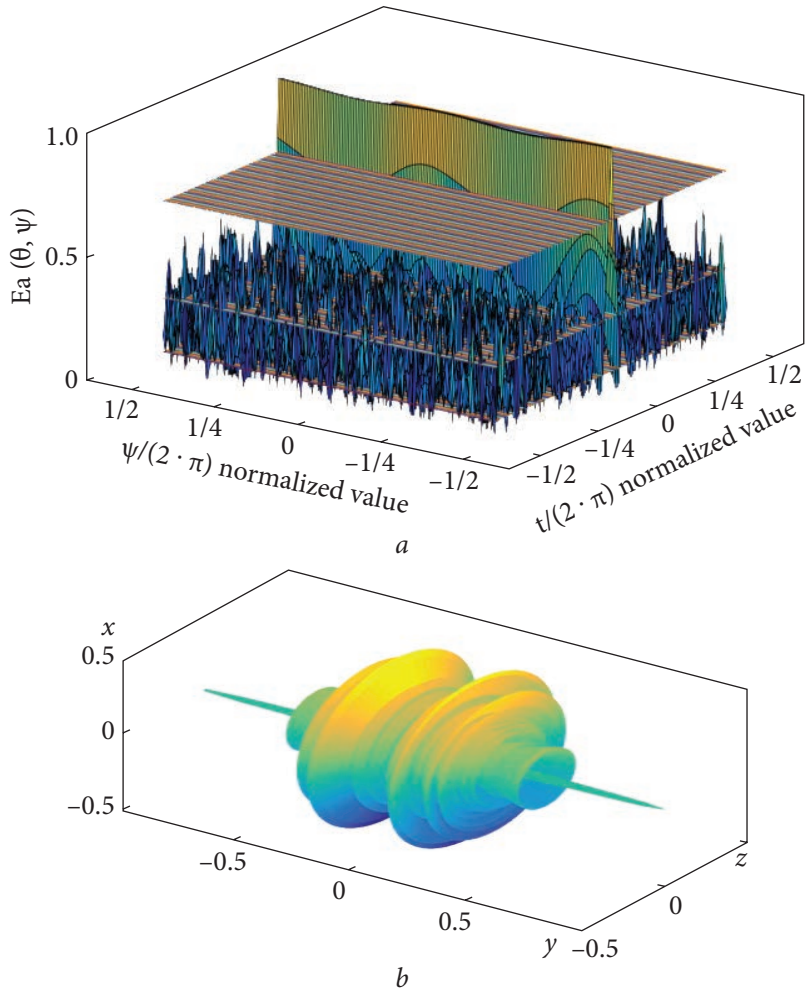

Fig. 2.20. Radiation pattern of the AA $(X, Y)_{L3M3\,R}$— in Cartesian (*a*) and polar (*b*) coordinate systems

A comparison of the RP parameters for AA $(X, Y)_{L3}$ and $(X, Y)_{L3M3R}$ shows (refer to Table 2.5) that for a Latin square, in which element there is no number, and the rotation operation nested in the n^{th} order of the magic square can be significantly increase the area of the AA by $(M/(2\times n)) \times (M/(2\times n))$ times, and reduce the width of the main petal by approximately $M/(2\times n)$ levels. At the same time, the average level of the side petals decreases by n times. Here, M is a magic constant equal to $(n^2 + 1)\cdot(n/2)$. In this case, the replenishment coefficients are reduced by $(M/(2\times n^2))^2$ times, and the efficiency factor is added by $2\times n\times n^2/M$ times.

2.4. Discussion

Comparing the antenna array considered in this chapter with a traditional non-equidistant AA using cyclic different sets (CDSs) with 16 elements of Z_{CDS16} [32—34] and an AA constructed using a third-order magic square matrix [22], we obtain a Table 2.6. It can be seen that the characteristics of the AR for the Latin square with a nested magic square of the n^{th} order are better than for other options. Although the use of magic squares nested in a Latin square for the synthesis of AA generally provides better characteristics

Table 2.6. **Comparison of AA characteristics for different configurations of constituent "Latin" squares and different types of nested other generating squares.**

Square type	Array parameters							
	$\Delta\omega_{0.707}$ (radian)	$\Delta\omega_0$ (radian)	m	N_0	$X_{max} \times Y_{max}$	S	α	β
Z_{CDS16}	0.3739	1.0389	0.2396	16	15×12	180	0.0889	1.1926
$(X, Y)_{L3}$	0.9704	2.9847	0.3067	9	6×6	36	0.2500	1.5000
$(X, Y)_{L3UD}$	0.8213	2.7826	0.1900	81	6×6	36	2.2500	13.5000
$(X, Y)_{L3UD-}$	0.9632	2.0064	0.3899	6	6×6	36	0.1667	1.0000
$(X, Y)_{L3UI}$	0.3099	1.658 2	0.1070	81	18×18	324	0.2500	4.5000
$(X, Y)_{L3UI-}$	0.3339	1.7321	0.2983	11	18×18	324	0.0340	0.6111
$(X, Y)_{L3M3}$	0.0609	1.2878	0.1093	81	90×90	8100	0.0100	0.9000
$(X, Y)_{L3M3+}$	0.0607	1.3164	0.1083	83	90×90	8100	0.0102	0.9222
$(X, Y)_{L3M3-}$	0.0673	1.2910	0.2100	23	90×90	8100	0.0028	0.2556
$(X, Y)_{L3M3R}$	0.1222	1.3335	0.1077	81	45×45	2025	0.0400	1.8000
$(X, Y)_{L3M3R+}$	0.1222	1.3845	0.1075	82	45×45	2025	0.0415	1.8222
$(X, Y)_{L3M3R-}$	0.1247	1.3947	0.2274	19	45×45	2025	0.0094	0.4222
$(X, Y)_{M3}$	0.3900	1.6443	0.3412	9	15×15	225	0.0400	0.6000

than the use of CDS, among this type of nested squares, the characteristics obtained by AA based on a Latin square, in which a magic square is nested, with a multiplicative shift of elements (such as AA $(X, Y)_{L3M3}$, AA $(X, Y)_{L3M3-}$).

In general, it can be concluded that the approach that uses a combination of nesting the magic square in the Latin one allows for implementing AA of significant sizes with small values of the filling factor and redundancy.

2.5. Conclusion

The possibility of constructing non-equidistant antenna arrays (AAs) based on Latin squares is considered. The algorithm for calculating the AA coordinates, which uses the values of the elements of "Latin" squares, is the same as when constructing the AAs based on magic squares. It is based on using the value of the element of the generating matrix (forming a square) as the basis of the interferometer formed by neighboring elements.

It is shown that the obtained AAs provide full coverage of the spatial frequency grid in the area of elements placement, but have a rather large redundancy factor. The radiation pattern (RP) was studied, and the levels of the side lobes of the obtained AAs were estimated. The elimination of redundancy in antenna arrays based on Latin squares does not practically affect the width of the main lobe but allows for a significant reduction in the coefficients of filling and redundancy. However, the average level of the side lobes increases significantly.

The possibility of synthesizing large AAs based on component squares using the nesting of Latin squares is shown. The characteristics of the lattices obtained using the parameters of additive and multiplicative shifts, as well as rotation, were studied. It is shown that by using mutual rotations of individual layers included in the synthesized lattice, it is possible to improve its characteristics.

It has been established that the best characteristics are obtained by nesting a magic square with an additive shift of elements in a Latin square, which leads to the formation of a new Latin square, including when using a rotation operation.

The obtained results open up new possibilities for creating non-equidistant antenna arrays with small filling/redundancy factors and acceptable values of side-beam radiation. According to their characteristics, they are superior to non-equidistant two-dimensional AAs built on the basis of cyclic difference sets (CDSs), which have been used until now. More derivative design solutions are proposed for AA design based on Latin square and nested matrices.

CHAPTER 3

DEVELOPMENT AND OPTIMIZATION OF SPARSE PLANAR ANTENNA ARRAY BASED ON LATIN SQUARE AND CYCLIC DIFFERENCE SET

Non-equidistant antenna arrays (AAs) reduce the number of antenna elements, maintaining high resolution and a sufficiently low level of side lobes [148—154]. Large antennas of radio telescopes and long-range radars almost always use irregularly spaced uniform aperture gratings. The method presented in this study is novel and unconventional, using sets of Latin squares and cyclic difference sets (CDS) to construct non-equidistant antenna arrays (AAs).

3.1. Introduction

Non-equidistant AAs allow for reducing the number of antenna elements while maintaining high resolution and low side lobes. Most large antennas of radio telescopes and long-range radars use a non-equidistant arrangement of elements and unfilled aperture arrays. Recently, when creating radars of the decameter range, there has been an interest in using non-equidistant AAs to improve their operational characteristics. There have already been attempts to use mathematical constructions such as magic squares [22] and the method of Latin squares [23] to construct two-dimensional non-equidistant AAs. Cyclic difference sets (CDSs) are widely used in various areas of research. This section of the work explores the possibilities of using the structure of Latin squares and CDSs for constructing two-dimensional non-equidistant AAs, and their characteristics, as a continuation of the idea of works [17—25, 32, 33].

3.2. CDS and the new Latin square matrix, taking it as element

Cyclic difference sets (CDSs) — $A_{CDS}(\nu, \kappa, \lambda)$ is a subset $\mathbf{D} = \{d_1, d_2, ..., d_k\}$ of integers modulo ν such that each $\{1,2, ..., \nu - 1\}$ can be represented in exactly λ various ways as a difference $(d_i - d_j)$ modulo ν [35].

In other words, $A_{CDS}(\nu, k, \lambda)$, a difference set **D,** is a subset of k deductions modulo ν such that for any remainder $\delta \neq 0 \pmod{\nu}$, the congruence

$$d_i - d_j \equiv \alpha \pmod{\nu} \tag{3.1}$$

has exactly λ pairs of solutions (d_i, d_j) d_i and d_j in the set **D**. It is worth noting that the terms: difference set, CDS and ν, k, λ — difference set are interchangeable below: "the last two are used when there is a reason emphasize either the contrast with general group difference sets, or the specific parameters ν, k, λ."

As a direct consequence of this definition, the parameters ν, k, λ should hold:

$$k(k-1) = \lambda(\nu - 1). \tag{3.2}$$

For any positive integer ν, there exist some obvious difference sets modulo ν, which are:

1) a zero set **D** = {};
2) a singleton **D** = {i}, $0 \leq i \leq \nu - 1$;
3) a singleton **D** = {0,1, …, ν – 1};
4) a singleton **D** = {0,1, …, i – 1, i + 1, …, ν – 1},$0 \leq i \leq \nu - 1$.

Difference sets are called trivial and are quite often either ignored or treated only as borderline cases. Note that the parameters for these difference sets are {ν, k, λ} = {ν, 0, 0}; {ν, 1, 0}; {ν, ν, ν} and {ν, ν – 1, ν – 2} respectively. If we introduce an additional parameter $n = k - \lambda$, then formula (3.2) above shows that these trivial difference sets arise if and only if n = 0 or 1. Therefore, the assumption $n \geq 2$, which is often made implicitly, allows us to eliminate all trivial difference sets. Some non-trivial difference sets (i.e., CDSs) will be used below as shown in the Table 3.1.

Latin squares and their properties were presented fully in Chapter 2. In combinatorics [36, 37] and in the experimental setting, a Latin square is a square of size $n \times n$ filled with n different symbols, each of which appears exactly once in each row and exactly once in each column. An example of a 3×3

Table 3.1. **Cyclic Difference Sets (CDSs)**

Name	ν	k	λ	n	**D** = {d_1, …, d_k}
CDS3	7	3	1	2	1, 2, 4
CDS4	13	4	1	3	0, 1, 3, 9
CDS5	21	5	1	4	3, 6, 7, 12, 14
CDS6	31	6	1	5	1, 5, 11, 24, 25, 27
CDS7	15	7	3	4	0, 1, 2, 4, 5, 8, 10
CDS8	57	8	1	7	0, 1, 6, 15, 22, 26, 45, 55
CDS9s	19	9	4	5	1, 4, 5, 6, 7, 9, 11, 16, 17
CDS9m	37	9	2	7	1, 7, 9, 10, 12, 16, 26, 33, 34
CDS9b	73	9	1	8	0, 1, 12, 20, 26, 30, 33, 35, 57

Latin square:

$$\begin{bmatrix} A & B & C \\ C & A & B \\ B & C & A \end{bmatrix}. \tag{3.3}$$

Table 3.2. **New Latin squares taking CDSs as elements**

Name	CDS	The new matrix of Latin squares
L_{cds4}	$A_{\mathrm{CDS}}(13, 4, 1) = \{0, 1, 3, 9\}$	$\begin{bmatrix} 0 & 1 & 3 & 9 \\ 9 & 0 & 1 & 3 \\ 3 & 9 & 0 & 1 \\ 1 & 3 & 9 & 0 \end{bmatrix}$
L_{cds5}	$A_{\mathrm{CDS}}(21, 5, 1) = \{3, 6, 7, 12, 14\}$	$\begin{bmatrix} 7 & 12 & 14 & 3 & 6 \\ 6 & 7 & 12 & 14 & 3 \\ 3 & 6 & 7 & 12 & 14 \\ 14 & 3 & 6 & 7 & 12 \\ 12 & 14 & 3 & 6 & 7 \end{bmatrix}$
L_{cds6}	$A_{\mathrm{CDS}}(31, 6, 11) = = \{1, 5, 11, 24, 25, 27\}$	$\begin{bmatrix} 27 & 1 & 5 & 11 & 24 & 25 \\ 25 & 27 & 1 & 5 & 11 & 24 \\ 24 & 25 & 27 & 1 & 5 & 11 \\ 11 & 24 & 25 & 27 & 1 & 5 \\ 5 & 11 & 24 & 25 & 27 & 1 \\ 1 & 5 & 11 & 24 & 25 & 27 \end{bmatrix}$
L_{cds9s}	$A_{\mathrm{CDS}}(19, 9, 4) = \{1, 4, 5, 6, 7, 9, 11, 16, 17\}$	$\begin{bmatrix} 7 & 9 & 11 & 16 & 17 & 1 & 4 & 5 & 6 \\ 6 & 7 & 9 & 11 & 16 & 17 & 1 & 4 & 5 \\ 5 & 6 & 7 & 9 & 11 & 16 & 17 & 1 & 4 \\ 4 & 5 & 6 & 7 & 9 & 11 & 16 & 17 & 1 \\ 1 & 4 & 5 & 6 & 7 & 9 & 11 & 16 & 17 \\ 17 & 1 & 4 & 5 & 6 & 7 & 9 & 11 & 16 \\ 16 & 17 & 1 & 4 & 5 & 6 & 7 & 9 & 11 \\ 11 & 16 & 17 & 1 & 4 & 5 & 6 & 7 & 9 \\ 9 & 11 & 16 & 17 & 1 & 4 & 5 & 6 & 7 \end{bmatrix}$
L_{cds9m}	$A_{\mathrm{CDS}}(37, 9, 2) = \{1, 7, 9, 10, 12, 16, 26, 33, 34\}$	$\begin{bmatrix} 12 & 16 & 26 & 33 & 34 & 1 & 7 & 9 & 10 \\ 10 & 12 & 16 & 26 & 33 & 34 & 1 & 7 & 9 \\ 9 & 10 & 12 & 16 & 26 & 33 & 34 & 1 & 7 \\ 7 & 9 & 10 & 12 & 16 & 26 & 33 & 34 & 1 \\ 1 & 7 & 9 & 10 & 12 & 16 & 26 & 33 & 34 \\ 34 & 1 & 7 & 9 & 10 & 12 & 16 & 26 & 33 \\ 33 & 34 & 1 & 7 & 9 & 10 & 12 & 16 & 26 \\ 26 & 33 & 34 & 1 & 7 & 9 & 10 & 12 & 16 \\ 16 & 26 & 33 & 34 & 1 & 7 & 9 & 10 & 12 \end{bmatrix}$

End of Table 3.2

Name	CDS	The new matrix of Latin squares
L_{cds9b}	$A_{CDS}(73, 9, 1) = \{0, 1, 12, 20, 26, 30, 33, 35, 57\}$	$\begin{bmatrix} 35 & 57 & 0 & 1 & 12 & 20 & 26 & 30 & 33 \\ 33 & 35 & 57 & 0 & 1 & 12 & 20 & 26 & 30 \\ 30 & 33 & 35 & 57 & 0 & 1 & 12 & 20 & 26 \\ 26 & 30 & 33 & 35 & 57 & 0 & 1 & 12 & 20 \\ 20 & 26 & 30 & 33 & 35 & 57 & 0 & 1 & 12 \\ 12 & 20 & 26 & 30 & 33 & 35 & 57 & 0 & 1 \\ 1 & 12 & 20 & 26 & 30 & 33 & 35 & 57 & 0 \\ 0 & 1 & 12 & 20 & 26 & 30 & 33 & 35 & 57 \\ 57 & 0 & 1 & 12 & 20 & 26 & 30 & 33 & 35 \end{bmatrix}$

Let us consider some methods of forming Latin squares. If the set of natural numbers {1, 2, ..., *n*} or the set {0, 1, ..., *n* – 1} is taken as the set *Q*, then for the 3rd order of the Latin square we get the following formula ($A = 1$, $B = 2$, $C = 3$):

$$L_3 = \begin{bmatrix} 1 & 2 & 3 \\ 3 & 1 & 2 \\ 2 & 3 & 1 \end{bmatrix}. \tag{3.4}$$

If the set *Q* is taken on the basis of the CDS, then we get a Latin square for the third order, the set $Q = A_{CDS}(v, k, \lambda) = CDS3 = A_{CDS}(7, 3, 1) = \{d_1, d_2, d_3\} = \{1, 2, 4\}$ according to the following formula ($A = d_1 = 1$, $B = d_2 = 2$, $C = d_3 = 4$):

$$L_{CDS3} = \begin{bmatrix} 1 & 2 & 4 \\ 4 & 1 & 2 \\ 2 & 4 & 1 \end{bmatrix}. \tag{3.5}$$

Similarly, we can take $CDS4 = A_{CDS}(13, 4, 1) = \{0, 1, 3, 9\}$ as elements of the Latin square of the 4th order, $CDS5 = A_{CDS}(21, 5, 1) = \{3, 6, 7, 12, 14\}$ as elements of the Latin square of the 5th order, and $CDS6 = A_{CDS}(31, 6, 11) = \{1, 5, 11, 24, 25, 27\}$ as elements of the Latin square of the 6th order, by the following formulas L_{CDS4}, L_{CDS5}, L_{CDS6} in the Table 3.2. And similarly, we take $CDS9s = A_{CDS}(19, 9, 4) = \{1, 4, 5, 6, 7, 9, 11, 16, 17\}$, $CDS9s = A_{CDS}(19, 9, 4) = \{1, 4, 5, 6, 7, 9, 11, 16, 17\}$, $CDS9m = A_{CDS}(37, 9, 2) = \{1, 7, 9, 10, 12, 16, 26, 33, 34\}$, $CDS9b = A_{CDS}(73, 9, 1) = \{0, 1, 12, 20, 26, 30, 33, 35, 57\}$ as elements of Latin square of the 9th order, according to the following formulas L_{CDS9s}, L_{CDS9m}, L_{CDS9b} in the Table 3.2.

The approaches discussed above provide ample opportunities for constructing Latin squares of various types and creating non-equidistant antenna arrays (AAs) based on them. As shown in the paper, some of the considered designs of Latin squares, taking CDSs as elements, have better characteristics compared to magic squares and the method of L.E. Kopilovich, which uses CDSs to create a 2-dimensional AA [32]. At the same time, if in the magic square of the n^{th} order each of the numbers n^2 is used only once, then in the Latin squares of the n^{th}

order each of the *n* numbers occurs only once in a row or column, and in general each of the n numbers is used n times. It means that in the Latin square, the numbers, including when they are added, are used *n* times. Since each element of the Latin square will further be considered as the distance between the interferometer elements, in the antenna array built on the basis of the Latin square, the redundancy factor was introduced first for all frequencies covered from 1 to *n*. However, if we take the CDS as the set *Q* for a Latin square and use this new square to construct an AA, we end up with an AA that guarantees almost full coverage and greatly reduces array redundancy.

3.3. Comparison of characteristics of AAs constructed based on new / traditional Latin squares and the Kopilovich method

The results are shown in the Table 3.3, Fig. 3.1, Fig. 3.2, and Fig. 3.3. L_{CDS4}, L_{CDS5}, L_{CDS6} denote different types of generating matrices and AAs mentioned above, and Z_{CDS20} = {(0, 0), (0, 3), (0, 4), (0, 7); (4, 0), (4, 3), (4, 4), (4, 9); (5, 0), (5, 3), (5, 4), (5, 9), (6, 0), (6, 3), (6, 4), (6, 9); (13, 0), (13, 3), (13, 4), (13, 9)} — a 2D AA containing 20 points/elements created by L.E. Kopilovich using CDSs [18—21].

Analysis of Table 3.3 reveals that AAs constructed from Latin squares taking CDSs as elements exhibit superior performance compared to AAs composed of 20 elements using CDSs by L.E. Kopilovich. Specifically, L_{CDS4} and L_{CDS5} demonstrate:

1) enhanced main lobe width in radiation patterns (RP) of AAs,
2) lower average side lobe levels in AA's RP,
3) improved filling and redundancy factors.

Comparison of L_{CDS4}, L_{CDS5}, and L_{CDS6} underscores the pivotal role of ν (size of the matrix) in determining RP's main beam width for AAs based on Latin

Table 3.3. **Characteristics of AAs constructed based on Latin squares taking CDSs as elements and the Kopilovich method**

Array parameters	L_{CDS4}	Z_{CDS20}	L_{CDS5}	L_{CDS6}
$\Delta\omega_{0.707}$(radian)	0.3425	0.4497	0.1222	0.0524
m	0.2940	0.2396	0.1982	0.1673
N_0	16	20	25	36
$X_{max} \times Y_{max}$	13 × 13	13 × 9	42 × 42	93 × 93
S	169	117	1.764	8.649
α	0.0947	0.1709	0.0142	0.0042
β	1.2308	1.8490	0.5952	0.3871

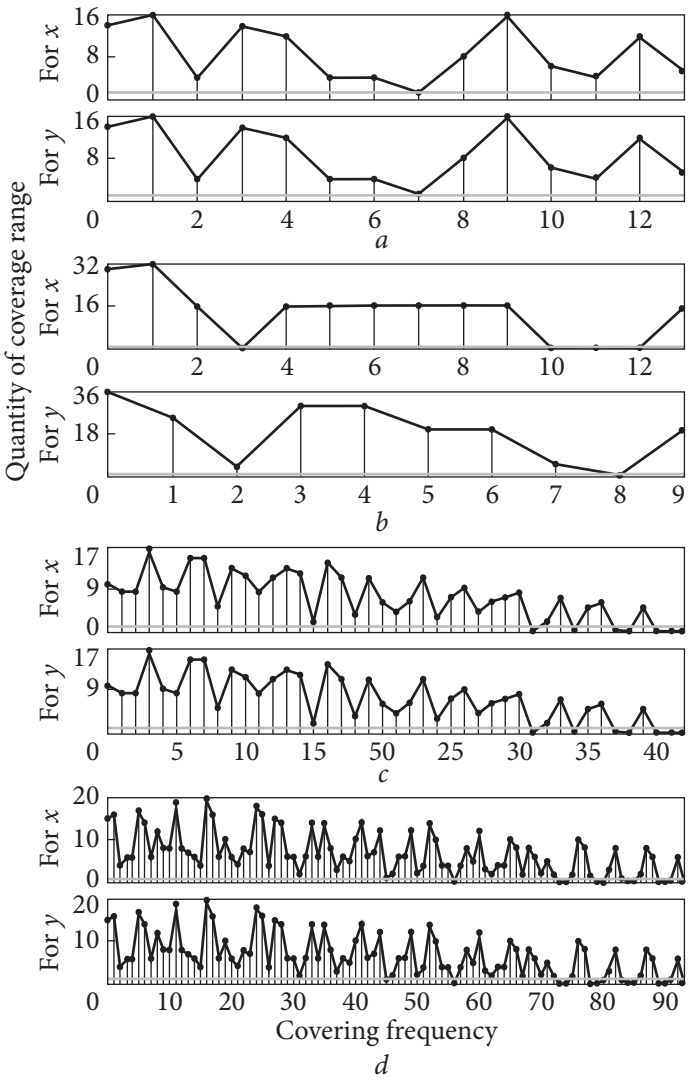

Fig. 3.1. Distribution of covered spatial frequencies along the *x*-axis and *y*-ordinate for AAs: *a* — L_{CDS4}, *b* — Z_{CDS20}, *c* — L_{CDS5}, and *d* — L_{CDS6}

squares taking CDSs as elements. The larger ν is, the narrower the width of the main beam will be. Given the definitions of *k* and λ in block design (combinatorial mathematics) [35—38], *k* means the number of points in a block (subset), and λ is the number of blocks (subsets) containing any two specific points (i.e., pairs). These two parameters will affect AA's redundancy. Having considered equation (3.2), it is possible to determine the ratio (ν, *k*, λ) for CDSs. These three parameters will affect the average level of the side lobes of the AA's RP. In addition, we can develop these design parameters according to the requirements of the task.

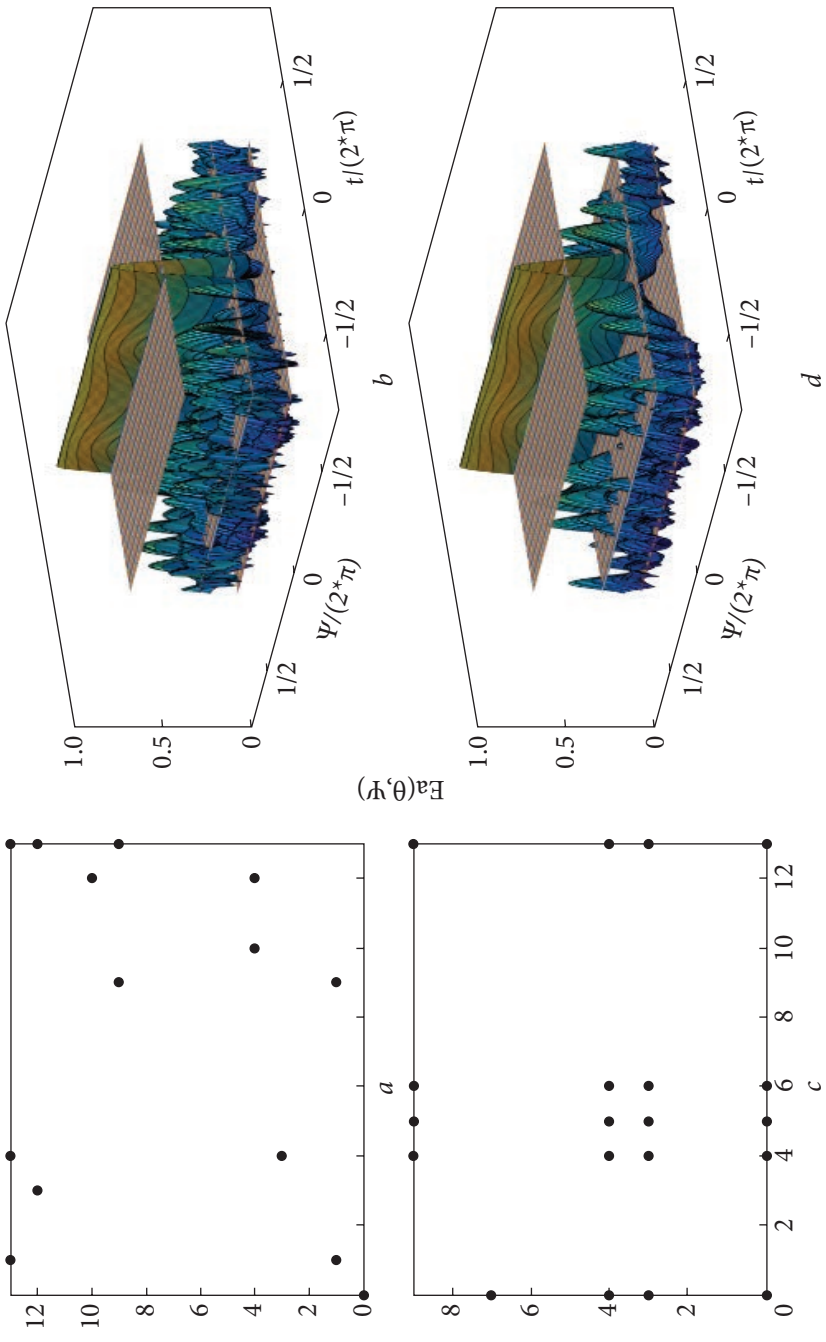

Fig. 3.2. The arrangement of AA's elements (*a*, *c*) and the corresponding RP in the Cartesian (*b*, *d*) coordinate system. AA based on L_{CDS4} (*a*, *b*), AA based on Z_{CDS20} (*c*, *d*)

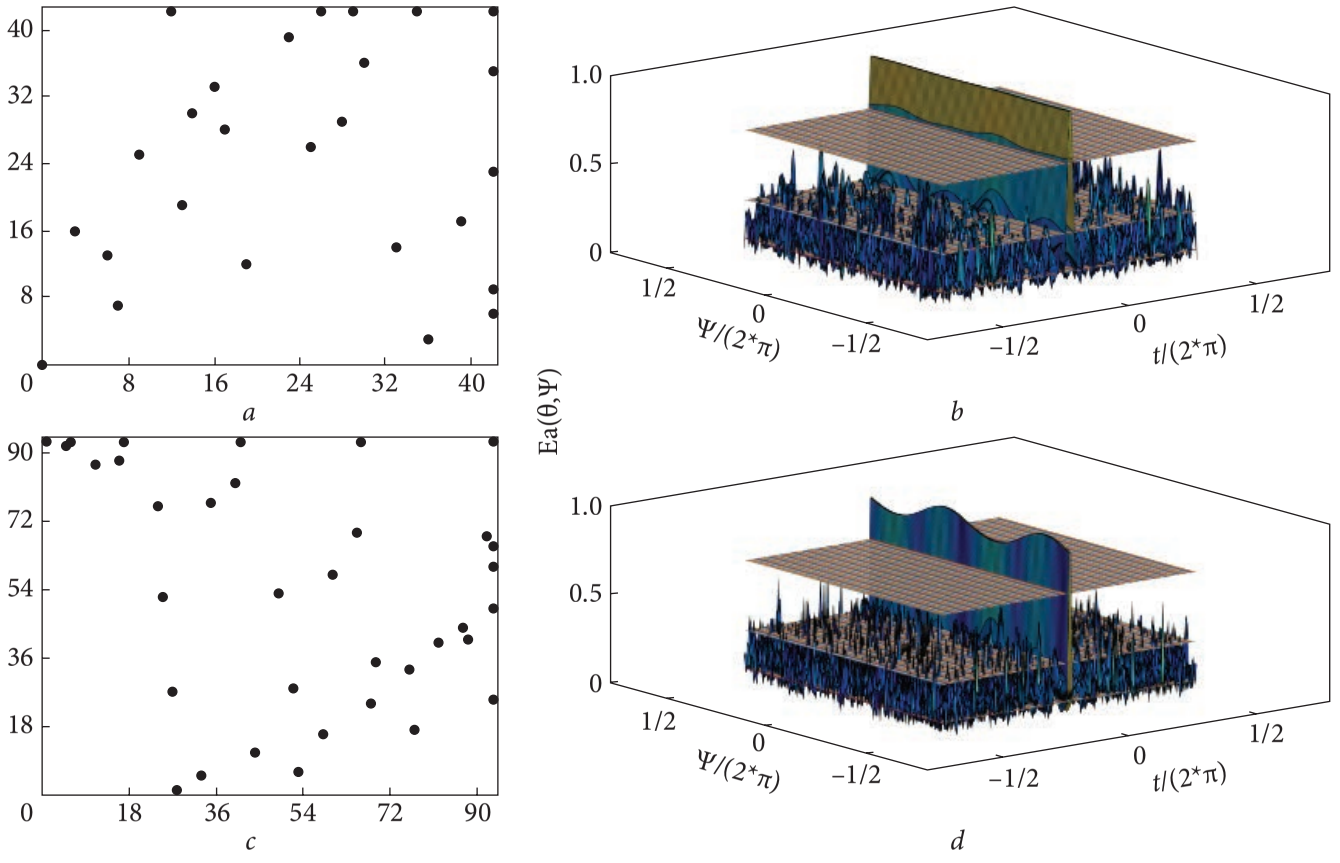

Fig. 3.3. The arrangement of AA's elements (*a*, *c*) and the corresponding RP in the Cartesian (*b*, *d*) coordinate system. AA based on L_{CDS5} (*a*, *b*) and AA based on L_{CDS6} (*c*, *d*)

3.4. Comparison of characteristics of large AAs constructed based on new / traditional Latin squares and magic squares

In this section, we compare the performance of a new Latin square using a CDS as an element and a magic square as a subarray with the performance of an AA constructed using a traditional magic square (Figs 3.4—3.6).

From Table 3.3, it follows that for the same number of points in the subset k, there are different design parameters v for CDS. When the number of lattice elements is constant, it is possible to construct a Latin square based on the generating matrix using the CDS of other ν and λ values to create lattices of various designs. Specifically, at $k = 9$, we have three different CDSs:

CDS9s = $A_{CDS}(19, 9, 4) = \{1, 4, 5, 6, 7, 9, 11, 16, 17\}$;

CDS9m = $A_{CDS}(37, 9, 2) = \{1, 7, 9, 10, 12, 16, 26, 33, 34\}$;

CDS9b = $A_{CDS}(73, 9, 1) = \{0, 1, 12, 20, 26, 30, 33, 35, 57\}$.

These CDSs can be used as elements of a 9th-order Latin square generating matrix to create various AA.

A third-order magic square can be nested as a submatrix in a third-order Latin square matrix. Refer to Chapter 2 for detailed information on coordinate distribution, spatial frequency distribution, and radiation pattern (RP).

$$L_{3M3} = \begin{bmatrix} 8 & 1 & 6 & 16 & 2 & 12 & 24 & 3 & 18 \\ 3 & 5 & 7 & 6 & 10 & 14 & 9 & 15 & 21 \\ 4 & 9 & 2 & 8 & 18 & 4 & 12 & 27 & 6 \\ 24 & 3 & 18 & 8 & 1 & 6 & 16 & 2 & 12 \\ 9 & 15 & 21 & 3 & 5 & 7 & 6 & 10 & 14 \\ 12 & 27 & 6 & 4 & 9 & 2 & 8 & 18 & 4 \\ 16 & 2 & 12 & 24 & 3 & 18 & 8 & 1 & 6 \\ 6 & 10 & 14 & 9 & 15 & 21 & 3 & 5 & 7 \\ 8 & 18 & 4 & 12 & 27 & 6 & 4 & 9 & 2 \end{bmatrix}. \quad (3.6)$$

M_9 means the generating matrix for the construction of AA based on the magic square of the 9th order [22], namely:

$$M_9 = \begin{bmatrix} 47 & 58 & 69 & 80 & 1 & 12 & 23 & 34 & 45 \\ 57 & 68 & 79 & 9 & 11 & 22 & 33 & 44 & 46 \\ 67 & 78 & 8 & 10 & 21 & 32 & 43 & 54 & 56 \\ 77 & 7 & 18 & 20 & 31 & 42 & 53 & 55 & 66 \\ 6 & 17 & 19 & 30 & 41 & 52 & 63 & 65 & 76 \\ 16 & 27 & 29 & 40 & 51 & 62 & 64 & 75 & 5 \\ 26 & 28 & 39 & 50 & 61 & 72 & 74 & 4 & 15 \\ 36 & 38 & 49 & 60 & 71 & 73 & 3 & 14 & 25 \\ 37 & 48 & 59 & 70 & 81 & 2 & 13 & 24 & 34 \end{bmatrix}. \quad (3.7)$$

The results obtained using the proposed approach are shown in Table 3.4. Meanwhile, L_{CDS9s}, L_{CDS9m}, L_{CDS9b}, L_{3M3}, and M_9 denote different types of genera-

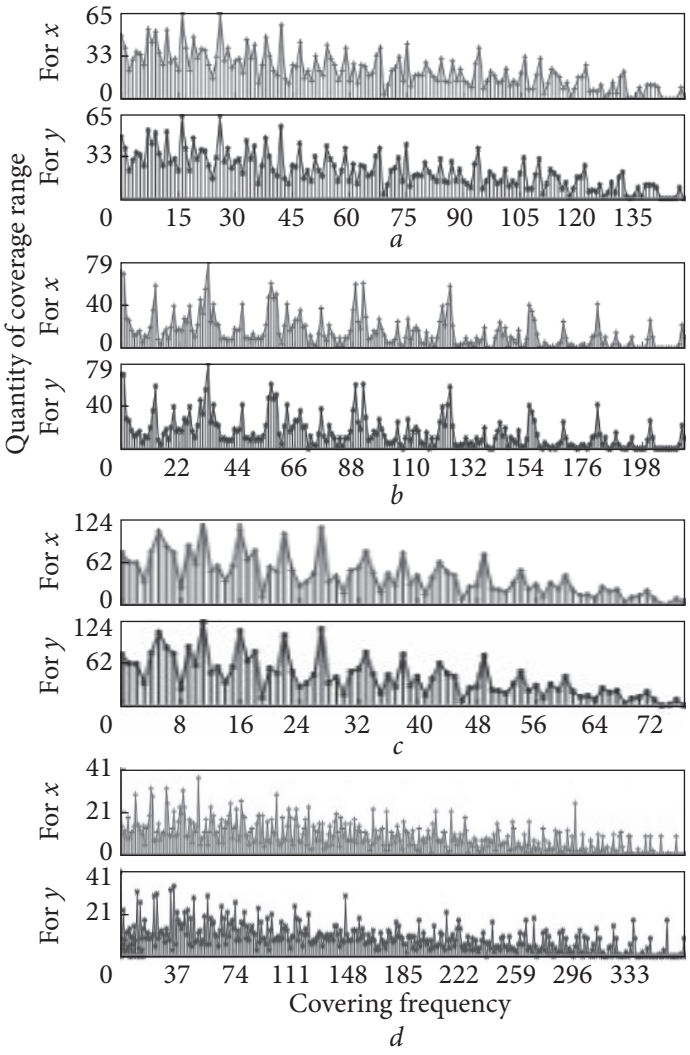

Fig. 3.4. Distribution of covered spatial frequencies along the *x*-axis and *y*-ordinate for different AAs: *a* — L_{CDS9m}, *b* — L_{CDS9b}, *c* — L_{CDS9S}, and *d* — M_9

ting matrices and AAs based on the Latin squares discussed above. Definition of parameters in the Table 3.4 is the same as in the Table 3.3.

From Table 3.4, the following conclusions can be drawn:

1) A comparison of the characteristics of L_{CDS9s}, L_{CDS9m} and L_{CDS9b} shows that in the antenna arrays based on the Latin square, taking CDS as elements, with the design parameters (ν, k, λ), the ν parameter will play a major role in the array size, that is, it will determine the width of the main beam of the AA's RP in the presence of a certain number of antenna elements k^2. The larger ν is, the narrower the width of the main lobe, and the smaller the redundancy and fill factors will be obtained. However, reducing the redundancy of the AA leads to an increase in the average level of the side lobes of the AA's RP and an increase

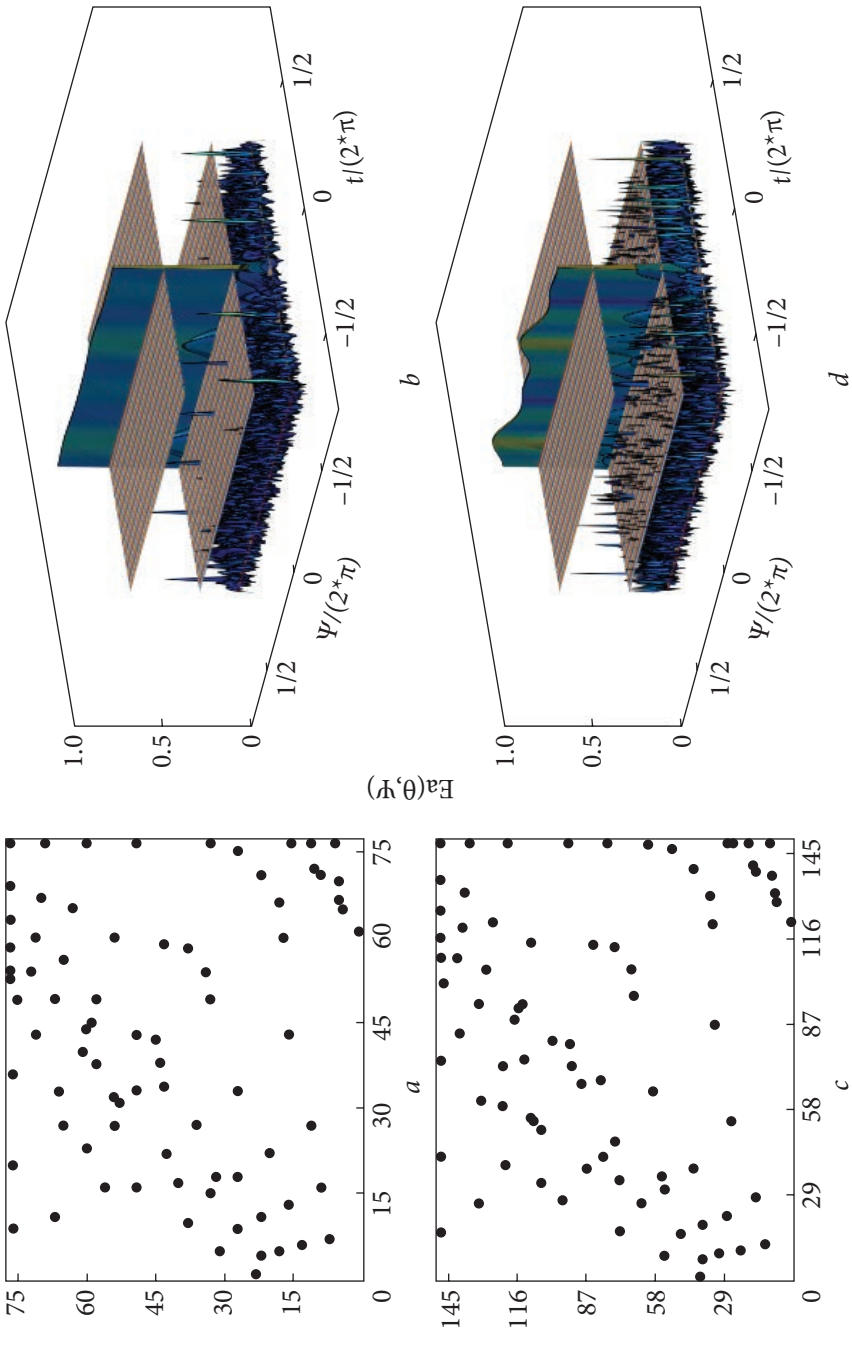

Fig. 3.5. The arrangement of AA's elements (*a*, *c*) and the corresponding RP in the Cartesian (*b*, *d*) coordinate system. AA based on L_{CDS9s} (*a*, *b*), AA based on L_{CDS9m} (*c*, *d*)

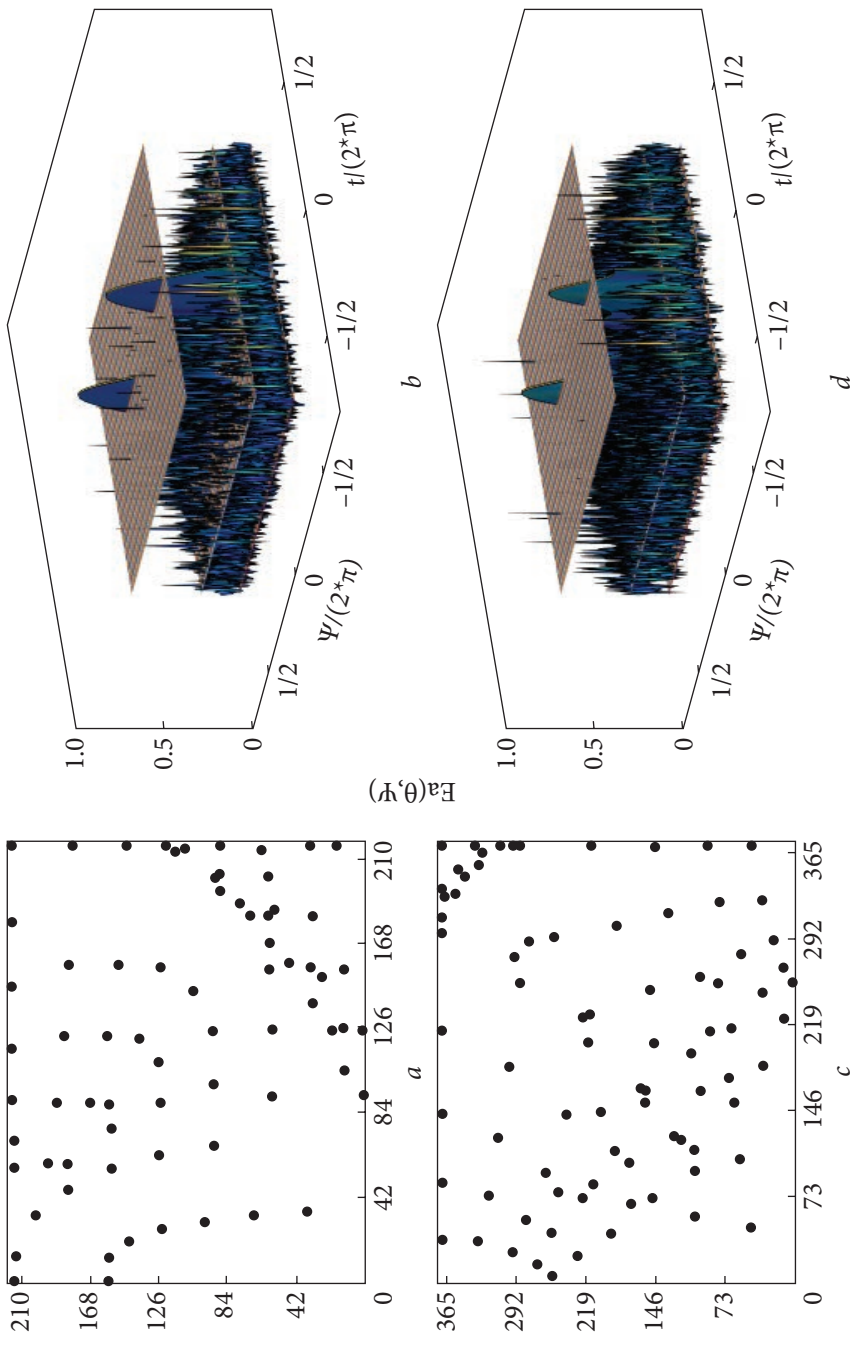

Fig. 3.6. The arrangement of AA's elements (*a*, *c*) and the corresponding RP in the Cartesian (*b*, *d*) coordinate system. AA based on L_{CDS9b} (a, *b*), AA based on M_9 (*c*, *d*)

Table 3.4. **Characteristics of AAs constructed based on Latin squares taking CDSs as elements and a magic square**

Array parameters	L_{CDS9s}	L_{CDS9m}	L_{CDS9b}	L_{3M3}	M_9
$\Delta\omega_{0.707}$(radian)	0.0636	0.0301	0.0175	0.0609	0.0175
m	0.1108	0.1118	0.1181	0.1093	0.1105
N_0	81	81	81	81	81
$X_{max} \times Y_{max}$	76×76	148×148	214×214	90×90	369×369
S	5,776	2,1904	4,5796	8,100	136,161
α	0.0140	0.0037	0.0018	0.0100	0.0059
β	1.0658	0.5473	0.3785	0.9000	0.2195

in the unevenness of the distribution of the spatial frequencies of the covered effective area, which may no longer satisfy the conditions of full coverage.

2) A comparison of the characteristics of L_{CDS9s}, L_{CDS9m}, L_{CDS9b}, and L_{3M3} shows that AAs based on the Latin square taking CDS as elements have better characteristics, are more diverse, and more flexible than the AAs constructed based on the Latin square nesting the magic square in the presence of a certain number of antenna elements k^2. Depending on the needs, it is possible to use AAs with narrower main lobes of the AA's RP, larger sizes, and with lower redundancy (filling) coefficients (such as, L_{CDS9b}), or AAs with a lower level of side lobes of the RP (such as, L_{CDS9s}), or AAs with intermediate characteristics (such as, L_{CDS9m}).

3) Comparing the characteristics of L_{CDS9s}, L_{3M3}, and M_9 shows that it is better to use a 9th order magic square antenna array as a generating square to obtain a larger AA with a certain number of antenna elements k^2. It should be noted that the obtained spatial frequency distributions are not the same for the abscissa and ordinate and do not provide complete coverage. A comparison of their RP shows that the RP of AAs is based on the magic square of the 9th order, as the generating square strongly depends on the azimuth Ψ. This angle is counted from the axis on the lattice plane, which does not contribute to its use in phased AA. In contrast, the RP of AAs, constructed based on the Latin square taking CDS as elements, is a good solution to this problem.

Moreover, having analyzed the Table 3.3 and Table 3.4, the following conclusions can be drawn:

From the comparison of L_{CDS5}, L_{CDS6}, and L_{3M3}, it can be concluded that the AAs based on the Latin square using CDS as elements have better characteristics than the Latin square nesting the magic square in RP's the main bean width, as well as in AA's filling and redundancy factors. It is worth noting that the average side lobes level of the RP of the AA, constructed based on Latin square nesting the magic square, is lower due to its fully covered spatial frequency, but has more redundancy.

3.5. Conclusion

1) The possibility of constructing non-equidistant antenna arrays (AA) based on Latin squares, which take cyclic difference sets (CDS) as elements, is considered. The algorithm for calculating the coordinates of antenna elements using the values of Latin square elements, in this case, is the same as when constructing AAs based on magic squares. It is based on using the value of the generating matrix element (formed square) as the basis of the interferometer formed by the neighboring elements. It is shown that the obtained AAs provide almost complete coverage of spatial frequencies in the area of the location of the elements and a rather small redundancy factor. AA's radiation pattern (RP) was studied, and the levels of the initial side lobes of non-equidistant AAs were estimated.

2) It was established that antenna arrays obtained on the basis of Latin squares, using CDS as elements, have better characteristics compared to AAs created by L.E. Kopilovich and the AAs, based on the Latin square, nesting magic squares. The obtained results open new possibilities for the creation of non-equidistant AAs with small filling/redundancy coefficients and permissible values of lateral radiation. According to their characteristics, they are better than the non-equidistant two-dimensional lattices that were used until now and were built only on the basis of CDSs.

3) It is shown that the possibility of synthesis of large AAs taking into account the composition of squares using CDS as elements of Latin squares. The characteristics of the obtained gratings were studied. It is shown that the use of the Latin square, which uses CDS as elements in the synthesized matrix, allows for a significant improvement in its characteristics. And also, it provides the possibility of more flexible change of design parameters (ν, k, λ) to better meet existing needs.

CHAPTER 4

A NEW METHOD OF CALCULATING COORDINATES FOR DIFFERENT SPARSE PLANAR ANTENNA ARRAYS

In this chapter, we propose a straightforward method for designing two-dimensional non-equidistant (sparse) antenna arrays (AAs). We focus on non-equidistant AAs structured using Latin squares and their triangular matrices. A novel construction method, distinct from existing approaches, is introduced. We investigate the properties of these AAs, which ensure full coverage of spatial frequencies with a high degree of sparsity and sufficiently low lateral/side-lobe radiation.

4.1. Introduction

First, we proposed a series of straightforward methods for the direct construction of two-dimensional non-equidistant antenna arrays (AAs) using fixed mathematical structures and their nested forms, such as magic squares [22] and Latin squares [23], which yielded promising results. Subsequently, we constructed a more complex two-dimensional non-equidistant AA by combining Latin squares with cyclic difference sets (CDS) [24]. However, this approach did not guarantee a non-redundant, fully covered AA without corrections (adding or removing elements).

Building on previous work, this chapter introduces a new construction method that employs a Latin square and a triangular matrix to generate the coordinate matrix of array elements. This method produces AAs that are nearly non-redundant and fully covered, satisfying the goal of minimizing the number of elements while maintaining the ability to obtain measurements at all distances up to the maximum, considering one defining angular resolution — the main beam width of the radiation pattern (RP).

4.2. Latin square and triangular matrix

In combinatorics [35] and experimental design, a Latin square is an $n \times n$ array filled with n different symbols, each occurring exactly once in each row and column. A key feature of the Latin square is that the same symbol appears only once per row and column. Both the transposed and rotated versions of a Latin square remain Latin squares. Typically, consecutive natural numbers are used as the elements of a Latin square.

It is worth mentioning that the well-known Sudoku puzzle, originally called Number Place [28], is a logical [29, 30] combinatorial [31] number arrangement puzzle based on a Latin square. Similar to Sudoku, where multiple solutions exist, there are numerous ways to arrange the symbols in a Latin square [32]. For simplicity, we will consider the most basic scenario: a Latin square filled with continuously increasing nonzero natural numbers, which behaves as follows:

$$L_n = Latin(n) = \begin{bmatrix} 1 & 2 & 3 & \cdots & n-1 & n \\ n & 1 & 2 & \cdots & n-2 & n-1 \\ n-1 & n & 1 & \cdots & n-3 & n-2 \\ \vdots & \vdots & \vdots & \ddots & \vdots & \vdots \\ 3 & 4 & 5 & \cdots & 1 & 2 \\ 2 & 3 & 4 & \cdots & n & 1 \end{bmatrix}. \tag{4.1}$$

In linear algebra, a triangular matrix is a square matrix in which all elements below (or above) the main diagonal are zero [33]. If all entries on the main diagonal are equal to 1, the matrix is called a one-triangular matrix, either upper or lower. These matrices are unipotent and are also known as unit triangular matrices, with "unit triangular" sometimes used as an abbreviation. Rarely, they are referred to as normalized triangular matrices [35, 36].

This chapter focuses on the synthesis of an AA using a lower one-triangular matrix, which behaves as follows:

$$UniTriL(n) = \begin{bmatrix} 1 & 0 & 0 & \cdots & 0 & 0 \\ n & 1 & 0 & \cdots & 0 & 0 \\ n-1 & n & 1 & \cdots & 0 & 0 \\ \vdots & \vdots & \vdots & \ddots & \vdots & \vdots \\ 3 & 4 & 5 & \cdots & 1 & 0 \\ 2 & 3 & 4 & \cdots & n & 1 \end{bmatrix} = \text{tril}[\text{Latin}(n)]. \tag{4.2}$$

This matrix *UniTriL* is obtained by zeroing the elements above the diagonal of the Latin square (4.1).

4.3. A new method of synthesis and estimation of antenna array parameters

In works [22, 23], attempts were made to use existing mathematical constructions, such as magic squares S_{lj}, to construct two-dimensional non-equidistant lattices. For the element (l, j) of the square, the S_{lj} value is set as the distance for the position of the element (l, j) along the abscissa and ordinate axes from the adjacent elements of the AA. Consequently, the coordinates of the elements that make up the antenna array can be expressed in terms of the values of the element S_{lj} of the square in row l and column j:

$$x_{lj} = \sum_{j=1}^{j} S_{lj} = x_{lj-1} + S_{lj}, \quad y_{lj} = \sum_{l=1}^{l} S_{lj} = y_{l-1\,j} + S_{lj}, \tag{4.3}$$

where x_{lj} is the abscissa and y_{lj} is the ordinate.

If the above relationship is expressed in matrix form, then:

$$X = S \cdot U = \begin{bmatrix} S_{1,1} & S_{1,2} & S_{1,3} & \dots & S_{1,n-1} & S_{1,n} \\ S_{2,1} & S_{2,2} & S_{2,3} & \dots & S_{2,n-1} & S_{2,n} \\ S_{3,1} & S_{3,2} & S_{3,3} & \dots & S_{3,n-1} & S_{3,n} \\ \vdots & \vdots & \vdots & \ddots & \vdots & \vdots \\ S_{n-1,1} & S_{n-1,2} & S_{n-1,3} & \dots & S_{n-1,n-1} & S_{n-1,n} \\ S_{n,1} & S_{n,2} & S_{n,3} & \dots & S_{n,n-1} & S_{n,n} \end{bmatrix}, \tag{4.4}$$

$$Y = L \cdot S = U^T \cdot S =$$

$$= \begin{bmatrix} 1 & 0 & 0 & \dots & 0 & 0 \\ 1 & 1 & 0 & \dots & 0 & 0 \\ 1 & 1 & 1 & \dots & 0 & 0 \\ \vdots & \vdots & \vdots & \ddots & \vdots & \vdots \\ 1 & 1 & 1 & \dots & 1 & 0 \\ 1 & 1 & 1 & \dots & 1 & 1 \end{bmatrix} \cdot \begin{bmatrix} S_{1,1} & S_{1,2} & S_{1,3} & \dots & S_{1,n-1} & S_{1,n} \\ S_{2,1} & S_{2,2} & S_{2,3} & \dots & S_{2,n-1} & S_{2,n} \\ S_{3,1} & S_{3,2} & S_{3,3} & \dots & S_{3,n-1} & S_{3,n} \\ \vdots & \vdots & \vdots & \ddots & \vdots & \vdots \\ S_{n-1,1} & S_{n-1,2} & S_{n-1,3} & \dots & S_{n-1,n-1} & S_{n-1,n} \\ S_{n,1} & S_{n,2} & S_{n,3} & \dots & S_{n,n-1} & S_{n,n} \end{bmatrix}, \tag{4.5}$$

where X, Y, and S are $n \times n$ square matrices; U/L is an upper/lower triangular matrix.

The matrix operation rules provide great opportunities for improvement. Because of this, we proposed to replace U/L with other matrices to synthesize the lattice. Considering the spatial frequency coverage, it was recommended to use other upper/lower unitriangular matrices without changing the main diagonal U/L. To make the resulting AA sufficiently sparse, without excessive redundancy, and fully covered, possible solutions were considered, and it was found that directly using the lower triangular Latin square matrix as L to synthesize the array, one can obtain the best coordinate matrix that has full coverage and is maximally sparse (without excess). The specific form of

calculations is as follows:

$$Y(n) = UniTriL(n) \cdot Latin(n) = \text{tril}[\text{Latin}(n)] \cdot Latin(n) = \\ = \begin{bmatrix} 1 & 0 & 0 & \dots & 0 & 0 \\ n & 1 & 0 & \dots & 0 & 0 \\ n-1 & n & 1 & \dots & 0 & 0 \\ \vdots & \vdots & \vdots & \ddots & \vdots & \vdots \\ 3 & 4 & 5 & \dots & 1 & 0 \\ 2 & 3 & 4 & \dots & n & 1 \end{bmatrix} \cdot \begin{bmatrix} 1 & 2 & 3 & \dots & n-1 & n \\ n & 1 & 2 & \dots & n-2 & n-1 \\ n-1 & n & 1 & \dots & n-3 & n-2 \\ \vdots & \vdots & \vdots & \ddots & \vdots & \vdots \\ 3 & 4 & 5 & \dots & 1 & 2 \\ 2 & 3 & 4 & \dots & n & 1 \end{bmatrix}, \tag{4.6}$$

$$X(n) = Y(n)^T \text{ or } Y(n)' \text{ or } Y(n)'' \text{ or } Y(n)''', \tag{4.7}$$

where n is the order of the Latin matrix, $Y(n)^T$ is a transposed matrix of $Y(n)$, $Y(n)'$, $Y(n)''$, and $Y(n)'''$ is a matrix obtained by rotating the matrix $Y(n)$ by 90, 180, and 270 degrees, respectively.

4.4. Modeling, calculation, and comparison of the AA design results

According to the method of calculation according to formulas (4.6) and (4.7), we actually received four types of arrays: $LTn^T = \{(x,y) \mid x \in Y(n)^T, y \in Y(n)\}$, $LTn' = \{(x,y) \mid x \in Y(n)', y \in Y(n)\}$, $LTn'' = \{(x,y) \mid x \in Y(n)'', y \in Y(n)\}$ and $LTn''' = \{(x,y) \mid x \in Y(n)''', y \in Y(n)\}$. And then we have:

$$Y(4) = UniTriL(4) \cdot Latin(4) = \text{tril}\left[\text{Latin}(4)\right] \cdot Latin(4) = \\ = \begin{bmatrix} 1 & 0 & 0 & 0 \\ 4 & 1 & 0 & 0 \\ 3 & 4 & 1 & 0 \\ 2 & 3 & 4 & 1 \end{bmatrix} \cdot \begin{bmatrix} 1 & 2 & 3 & 4 \\ 4 & 1 & 2 & 3 \\ 3 & 4 & 1 & 2 \\ 2 & 3 & 4 & 1 \end{bmatrix} = \begin{bmatrix} 1 & 2 & 3 & 4 \\ 8 & 9 & 14 & 19 \\ 22 & 14 & 18 & 26 \\ 28 & 26 & 20 & 26 \end{bmatrix}. \tag{4.9}$$

The locations of the antenna elements and the normalized RP of AAs ($LT4^T$, $LT4'$, $LT4''$, and $LT4'''$) are depicted in Fig. 4.1 and Fig. 4.2.

From Fig. 4.1 and Fig. 4.2, it is evident that the locations of the elements in the four types of AAs generated by formula (4.7) exhibit significant differences and distinct characteristics. Notably, the resulting AAs do not display prominent side lobes near the main lobe and show minimal variation with an angle, aligning well with theoretical expectations.

Referring to equations (4.4) and (4.5), the arrays generated by rotating/mirroring matrices demonstrate homogeneity. Subsequent analyses in this section will focus exclusively on such AAs.

A critical point is that since all coordinate matrices originate from geometric operations, the array geometric parameters for the four schemes mentioned above ($LT4^T$, $LT4'$, $LT4''$, and $LT4'''$) — spatial frequency, fill factor, and redundancy are identical. The spatial covering frequency distribution and coordinate layout are precisely mirrored along the X and Y axes, as depicted in Fig. 4.3.

Fig. 4.3 illustrates that the spatial covering frequencies are fully covered, with minimal redundancy in the coordinate distribution. All modulation results for the AAs ($LT4^{T}$, $LT4'$, $LT4''$, and $LT4'''$), including RP's parameters and geometric characteristics, are listed in Table 4.1.

Furthermore, according to formulas (4.6) and (4.7), a variety of two-dimensional non-equidistant AAs can be derived from Latin matrices of different orders: $LT2'$, $LT3'$, $LT5'$, $LT6'$, $LT7'$, $LT9'$, $LT10'$, $LT11'$, $LT12'$, $LT13'$, $LT14'$, $LT15'$, $LT16'$, $LT17'$, $LT18'$, $LT19'$, $LT20'$, $LT25'$ $LT30'$, $LT40'$, $LT50'$, $LT60'$, $LT70'$, $LT80'$, $LT90'$, $LT100'$. Their characteristic parameters are also detailed in Table 4.1.

Based on the methodology from [21], a series of antenna arrays by L.Ye. Kopilovich was derived using the cyclic difference sets (CDSs). Numerical calculations and modulation results for these arrays are provided in Table 4.1. Specifically, the arrays Z_{CDS13}, Z_{CDS16}, Z_{CDS20}, Z_{CDS25}, and Z_{CDS30} correspond to Kopilovich square matrices based on the CDSs with aperture lengths of 13, 16, 20, 25, and 30, respectively.

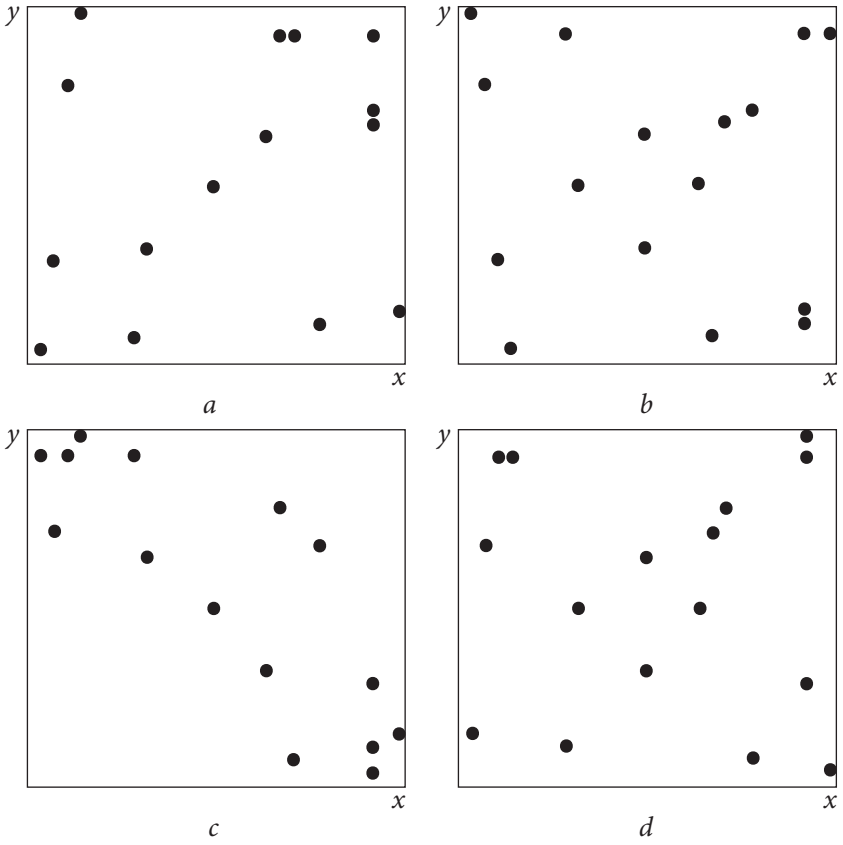

Fig. 4.1. Location of elements of AAs: ($LT4^{T}$(*a*), $LT4'$(*b*), $LT4''$(*c*) and $LT4'''$ (*d*)

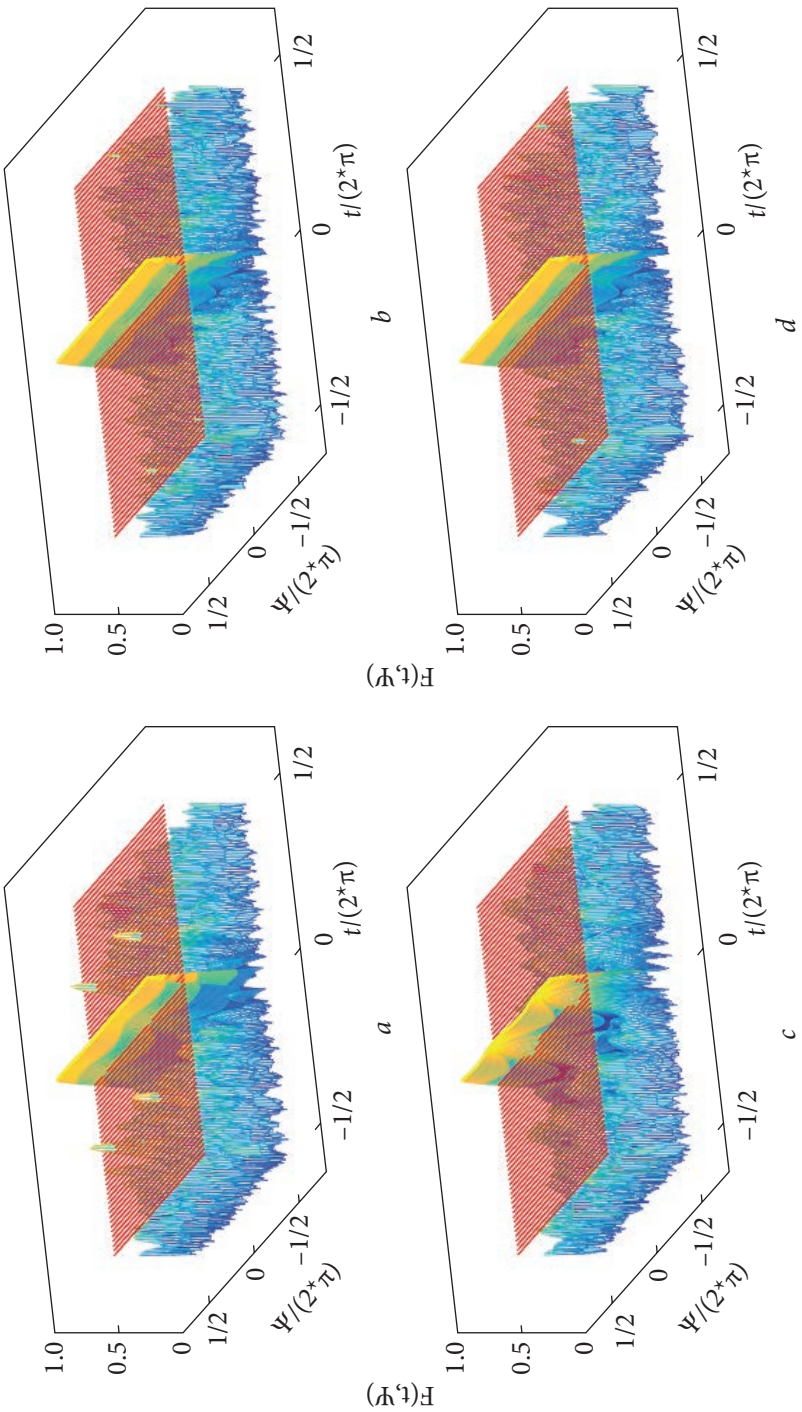

Fig. 4.2. Normalized RP of AAs: *LT4*‴(*a*), *LT4*′(*b*), *LT4*″(*c*) and *LT4*‴′(*d*)

Table 4.1. **Comprehensive comparison of AA characteristics**

Name of AAs or generative matrices	$\Delta\omega_{0.707}$ (radian)	m	N_0	S	β
$LT2'$	1.8504	0.5069	4	25	0.8000
$LT3'$	0.3758	0.3246	9	169	0.6923
Z_{CDS13}	0.4315	0.2343	17	169	1.3077
Z_{CDS16}	0.3244	0.2193	20	256	1.2500
Z_{CDS20}	0.2709	0.1919	26	400	1.3000
Z_{CDS25}	0.2259	0.1795	30	625	1.2000
Z_{CDS30}	0.1823	0.1670	35	900	1.1667
$LT4'$	0.1836	0.2728	16	784	0.5714
$LT4''$	0.1755	0.2519			
$LT4'''$	0.2147	0.2611			
$LT4''''$	0.1755	0.2519			
L_4	0.5597	0.2340	16	100	1.6000
M_4	0.1577	0.2573	16	1 156	0.4706
L_{CDS4}	0.3425	0.2940	16	169	1.2308
L_5	0.3681	0.1997	25	225	1.6667
M_5	0.0877	0.1986	25	4 225	0.3846
L_{CDS5}'	0.1222	0.1982	25	1 764	0.5952
$LT5'$	0.0894	0.1989	25	2 500	0.5000
$LT6'$	0.0524	0.1654	36	6 889	0.4337
$LT7'$	0.0524	0.1422	49	15 876	0.3889
$LT8'$	0.0175	0.1242	64	33 856	0.3478
$LT9'$	—	0.1128	81	65 025	0.3176
$LT10'$	—	0.1001	100	119 025	0.2899
$LT11'$	—	0.0909	121	203 401	0.2683
$LT12'$	—	0.0832	144	336 400	0.2483
$LT13'$	—	0.0768	169	529 984	0.2321
$LT14'$	—	0.0713	196	815 409	0.2171
$LT15'$	—	0.0665	225	1 210 000	0.2045
$LT16'$	—	0.0627	256	1 763 584	0.1928
$LT17'$	—	0.0586	289	2 499 561	0.1828
$LT18'$	—	0.0557	324	3 493 161	0.1734
$LT19'$	—	0.0526	361	4 774 225	0.1652
$LT20'$	—	0.0500	400	6 451 600	0.1575
$LT25'$	—	0.0402	625	23 765 625	0.1282
$LT30'$	—	0.0337	900	69 472 225	0.1080
$LT40'$	—	0.0256	1 600	379 470 400	0.0821
$LT50'$	—	0.0207	2 500	1.4232e + 09	0.0663
$LT60'$	—	0.0175	3 600	4.2016e + 09	0.0555
$LT70'$	—	0.0151	4 900	1.0509e + 10	0.0478
$LT80'$	—	0.0137	6 400	2.3275e + 10	0.0420
$LT90'$	—	0.0125	8 100	4.6961e + 10	0.0374
$LT100'$	—	0.0114	10 000	8.8031e + 10	0.0337

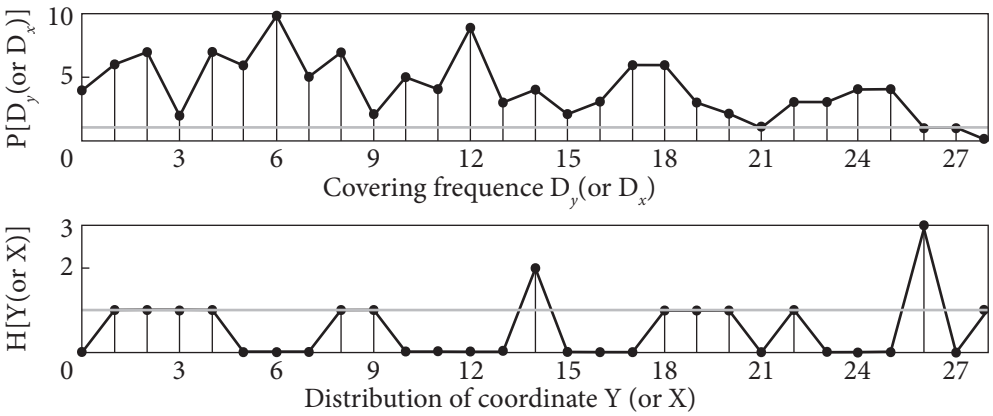

Fig. 4.3. Spatial covering frequency and coordinate distribution of AAs synthesized based on matrix $Y(4)$

Furthermore, Table 4.1 also presents the results of AAs' modeling synthesized using conventional methods proposed in the previous work. The AAs, corresponding to M_4 and M_5, are constructed using the magic square of the 4th and 5th order as generative matrices, respectively. The AAs, corresponding to L_4 and L_5, represent arrays constructed by using the Latin square of the 4th and 5th order as generative matrices. L_{CDS4} and L_{CDS5} represent AAs created using the CDS Latin square (taking CDS as elements) of the 4th and 5th order as generative matrices. It should be noted thats compared to the AAs constructed using magic squares, other AAs achieve full spatial frequency coverage.

4.5. Discussion

From the comparison and analysis of the parameters listed in the Table 4.1, it is obvious that:

1) The AA designed by L.E. Kopilovich based on CDS (abbreviated as Kopilovich-CDS AA), along with our AAs constructed based on the Latin square using both traditional and new methods, can achieve full spatial frequency coverage. The new synthesis method significantly enhances the effective coverage area of the grating without a notable degradation in sidelobe control. For the same effective coverage area, the number of elements required for a lattice based on the Latin square synthesized using the new method is less than half the number of elements in the Kopilovich-CDS AAs. This redundancy reduction allows for a narrower main lobe. The Kopilovich-CDS AAs, primarily intended for optical interferometric systems, are mainly used to solve imaging problems of space objects observed through a heterogeneous atmosphere. These optical systems with non-redundant apertures must be constructed in a mini-

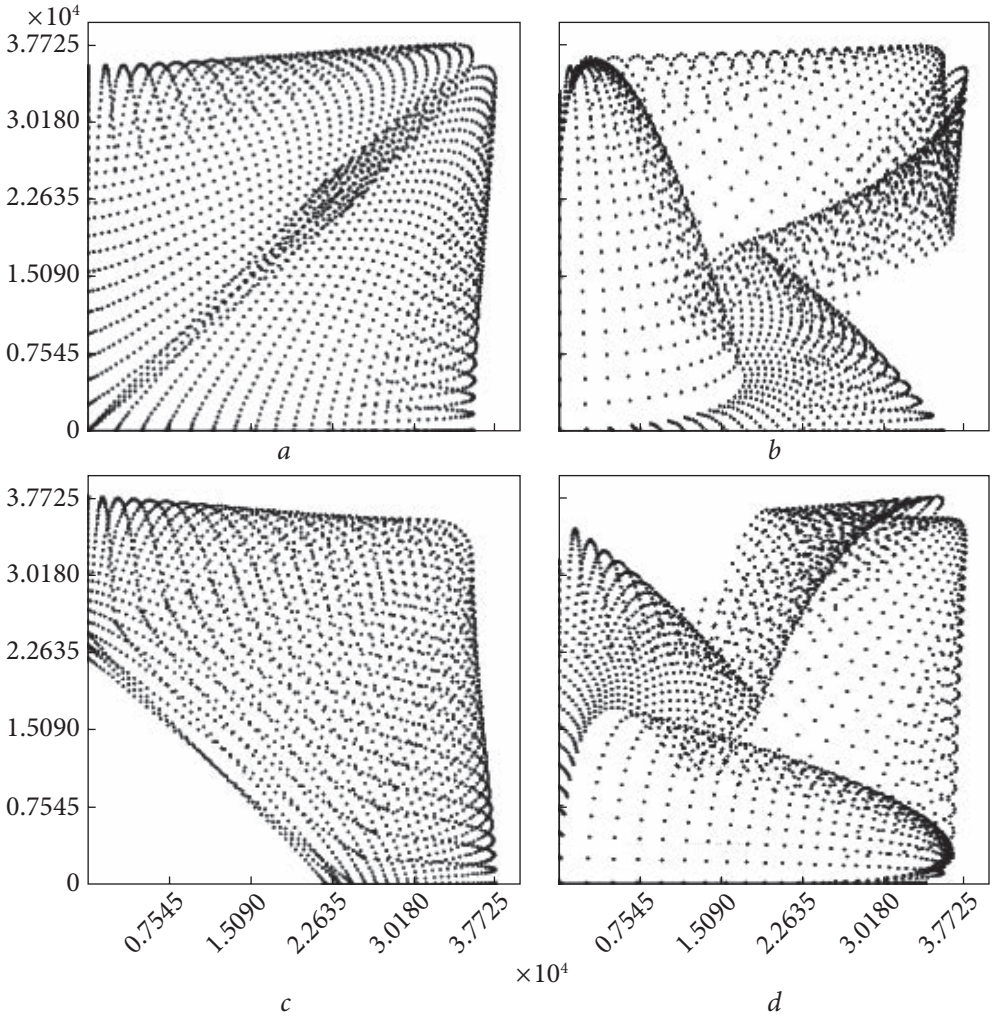

Fig. 4.4. The location of the AAs' elements created using the Latin square of the 50th order and its triangular matrix: *a* — $LT50^{T}$, *b* — $LT50'$, *c* — $LT50''$, *d* — $LT50'''$

mum size region to minimize influence of internal noise distribution. Consequently, array scanning accuracy is not their primary concern, but achieving the lowest possible sidelobe levels is [20, 21]. In many cases, the antenna array has greater requirements for the width of the main lobe (scanning accuracy), in which case it is more efficient to use the method proposed by us.

2) While magic squares can be used to construct an AA with a large coverage area and a very narrow main beam, the spatial frequency of the generated array cannot be fully covered, resulting in significant sidelobe levels. In comparison, AA synthesized using the new method based on the Latin square offers similar

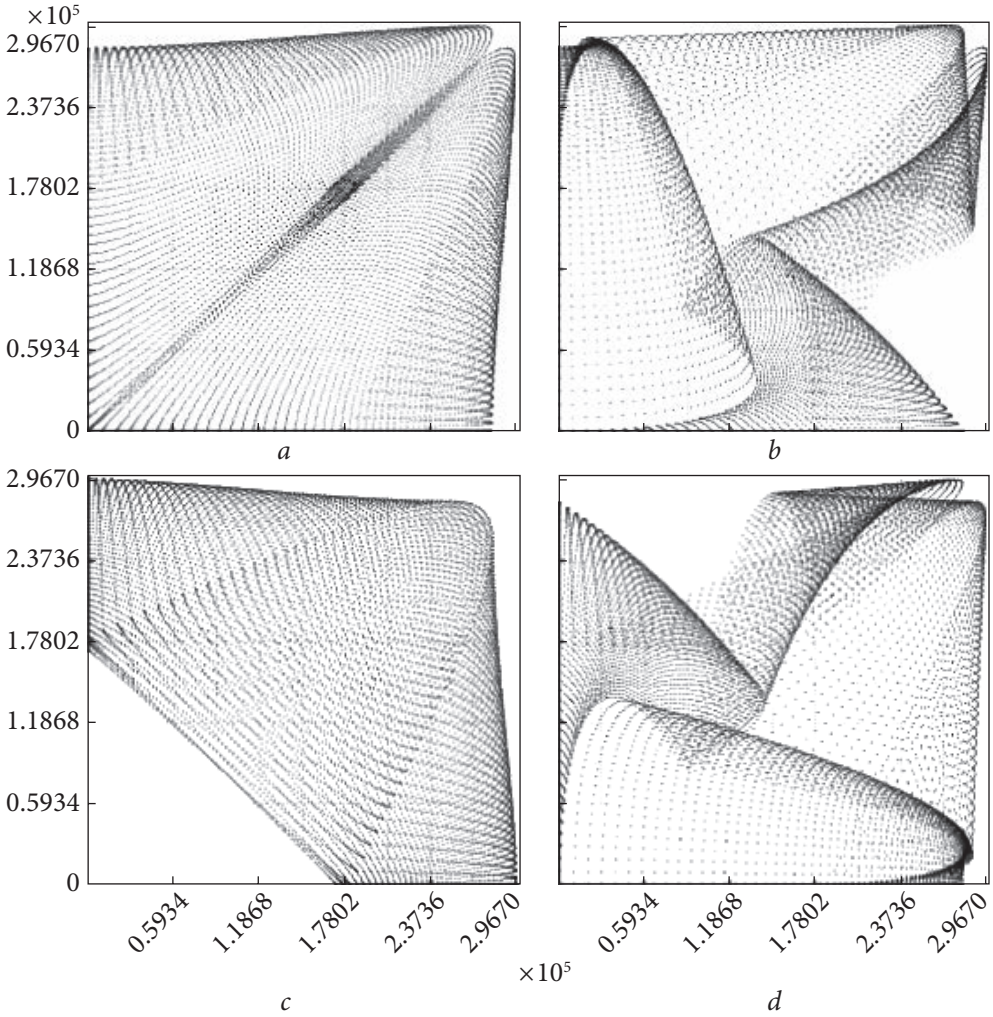

Fig. 4.5. The location of the AAs' elements created using the Latin square of the 100th order and its triangular matrix: *a* — $LT100^{T}$, *b* — $LT100'$, *c* — $LT100''$, *d* — $LT100'''$

coverage area, main beam width, and sidelobe levels but achieves full spatial frequency coverage. This ensures that the AA maintains some redundancy with more reliable performance, capable of extracting all information under extreme conditions.

3) AA synthesized using the new Latin squares (taking CDS as elements) does not achieve full spatial frequency coverage as the AA's geometric size increases. The previous research involved combining the Latin square with CDS, which expands the potential applications of the Latin square in AA design. Although the performance of the geometric size and main RP beam of the obtained AA's improves, the sidelobes worsen. The proposed new method effectively addresses this issue.

4) When using a new method of constructing AA, with an increase in the order n of the Latin square, the number of elements of the obtained AA (n^2) increases. In this case, the average level of the side lobes of the RP constantly decreases to a very small value, the space covered by the array expands, and the spatial frequency remains fully covered. Furthermore, observations of the array elements arrangement have shown that when the array elements are sufficiently large, the arrangement of the arrays exhibits a fixed geometry that does not change, as shown in Fig. 4.4 and Fig. 4.5.

4.6. Conclusion

The new method for synthesizing antenna arrays is a direct and efficient approach based on Latin squares and their triangular matrices. It ensures complete spatial covering frequency while minimizing array redundancy and the number of arrays required. This method also effectively controls side lobes, resulting in synthesized arrays with very narrow main lobes and low side lobe levels. These characteristics make the arrays multifunctional and suitable for various applications in radar, communications, radio astronomy, radiotherapy, remote sensing, automotive systems, biomedical imaging, navigation, and other fields.

When a large-number-elements AA is synthesized using this new method, the entire array maintains a consistent geometry. This means that when the number of elements is expanded or contracted in proportion, it exhibits consistently similar characteristics.

CHAPTER 5

APPLICATION OF DIFFERENT SPARSE PLANAR ANTENNA ARRAYS BASED ON SPECIAL MATRICES

The chapter is mainly devoted to describing of the design of the proposed antenna array (AA) and the application of the optimization method.

5.1. Introduction

This chapter presents individual definitions, examples, and simulation results of various mathematical concepts used in AA design. These concepts include:

1) Magic squares and their nested matrix;

2) Latin squares and their nested matrix;

3) cyclic difference sets (CDSs) and Latin squares using CDSs as elements;

4) triangular matrix and triangular matrix of Latin squares.

In particular, the designed AA will be analyzed and compared, taking into account aspects of the arrangement of grating elements, the characteristics of the radiation pattern (RP), and the spatial frequency of the AA. It should be taken into account that with the increase in the order of the used matrix, the number of AA elements also increases, which affects the overall performance of the designed AA.

Considering the practical application, the designed gratings are compared to the existing gratings in the Giant Ukrainian Radio Telescope (GURT), which is a low-frequency (8—80 MHz) radio telescope and consists of 25-element active gratings with analog time distribution of the phases of individual gratings between them [27, 28]. The work [27] shows the arrangement of antenna elements in GURT gratings; the distance between them along the X and Y axes is $dx = dy = 3.75$ m, which is $\lambda/2$ at a frequency of 40 MHz. Approximately the same parameters were used in the distributed AA that was developed.

In addition, the frequency ranges of the GURT subarray (5×5) are 8—32 MHz [28]. Let's assume that the AA works in the mode of receiving a plane electromagnetic wave of the same polarization coming from the zenith direction. RPs of AAs are calculated at a frequency of 25 MHz for four fixed planes Ψ. Two of which pass through the *X* (Ψ = 0°) and *Y* (Ψ = 90°) axes, and the two diagonal planes are E (Ψ = 45°) and H (Ψ = 135°).

5.2. AA design by using magic squares and their nested matrix

A magic square of the n^{th} order is a matrix filled with natural numbers from 1 to n^2. A magic square is called symmetric if the sum of any two numbers located symmetrically about the center of the square is $n^2 + 1$. Normal magic squares exist for all orders except $n = 2$. The case for $n = 1$ is trivial, as the square consists of only one number. The minimal nontrivial case has an order of 3

It is evident that the elements in the last column x_{lj}, i.e., at $j = n$, and in the last row y_{lj}, i.e., $i = n$, have values equal to the "magic" square constant, i.e., $x_{ln} = M, j \in (1, n)$ $x_{in} = M, j \in (1, n)$ and $y_{nj} = M, j \in (1, n)$.

Magic square matrices of the 3rd, 4th, and 9th orders are used as examples, and are denoted by M_3, M_4, and M_9 respectively [22]:

$$M_3 = \begin{bmatrix} 8 & 1 & 6 \\ 3 & 5 & 7 \\ 4 & 9 & 2 \end{bmatrix}, \tag{5.1}$$

$$M_4 = \begin{bmatrix} 16 & 2 & 3 & 13 \\ 5 & 11 & 10 & 8 \\ 9 & 7 & 6 & 22 \\ 4 & 14 & 15 & 1 \end{bmatrix}, \tag{5.2}$$

$$M_9 = \begin{bmatrix} 47 & 58 & 69 & 80 & 1 & 12 & 23 & 34 & 45 \\ 57 & 68 & 79 & 9 & 11 & 22 & 33 & 44 & 46 \\ 67 & 78 & 8 & 10 & 21 & 32 & 43 & 54 & 56 \\ 77 & 7 & 18 & 20 & 31 & 42 & 53 & 55 & 66 \\ 6 & 17 & 19 & 30 & 41 & 52 & 63 & 65 & 76 \\ 16 & 27 & 29 & 40 & 51 & 62 & 64 & 75 & 5 \\ 26 & 28 & 39 & 50 & 61 & 72 & 74 & 4 & 15 \\ 36 & 38 & 49 & 60 & 71 & 73 & 3 & 14 & 25 \\ 37 & 48 & 59 & 70 & 81 & 2 & 13 & 24 & 34 \end{bmatrix}. \tag{5.3}$$

A nested matrix essentially consists of two or more matrices nested layer by layer, similar to a component function. The structure of the nested magic square is shown in Fig. 5.1.

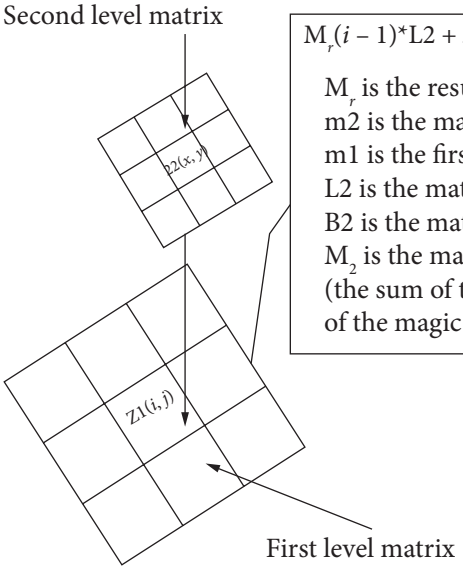

$M_r(i-1)*L2+x,\ (j-1)*B2+y) = m2(x, y) + (m1(i, j)-1)*M_2$

M_r is the resulting (nested) matrix.
m2 is the matrix of the second level ("magic" square).
m1 is the first level matrix.
L2 is the matrix length (m2) of the second level.
B2 is the matrix width (m2) of the second level.
M_2 is the matrix coefficient (m2) of the second level (the sum of the elements of the row/column/diagonal of the magic square).

Fig. 5.1. Schematic diagram of the structure of a nested magic square matrix

Actually, the nesting of the matrix is affected by the properties of the matrix itself, such that the nested magic square matrix remains a magic square. As an example, we use a nested matrix formed by combining two identical magic square matrices of the 3rd order, denoted as M_{r3*3}:

$$M_{r3*3} = M_3(M_3) = \begin{bmatrix} (8-1)*9+\begin{bmatrix}8&1&6\\3&5&7\\4&2&9\end{bmatrix} & (1-1)*9+\begin{bmatrix}8&1&6\\3&5&7\\4&2&9\end{bmatrix} & (6-1)*9+\begin{bmatrix}8&1&6\\3&5&7\\4&2&9\end{bmatrix} \\ (3-1)*9+\begin{bmatrix}8&1&6\\3&5&7\\4&2&9\end{bmatrix} & (5-1)*9+\begin{bmatrix}8&1&6\\3&5&7\\4&2&9\end{bmatrix} & (7-1)*9+\begin{bmatrix}8&1&6\\3&5&7\\4&2&9\end{bmatrix} \\ (4-1)*9+\begin{bmatrix}8&1&6\\3&5&7\\4&2&9\end{bmatrix} & (2-1)*9+\begin{bmatrix}8&1&6\\3&5&7\\4&2&9\end{bmatrix} & (9-1)*9+\begin{bmatrix}8&1&6\\3&5&7\\4&2&9\end{bmatrix} \end{bmatrix} =$$

$$= \begin{bmatrix} 71&64&69&8&1&6&53&46&51\\ 66&68&70&3&5&7&48&50&52\\ 67&72&65&4&9&2&49&54&47\\ 26&19&24&44&37&42&62&55&60\\ 21&23&25&39&41&43&57&59&61\\ 22&27&20&40&45&38&58&63&56\\ 35&28&33&80&73&78&17&10&15\\ 30&32&34&75&77&79&12&14&16\\ 31&36&29&76&81&74&13&18&11 \end{bmatrix}. \quad (5.4)$$

Obviously, M_{r3*3} is also a magic square of 9th order.

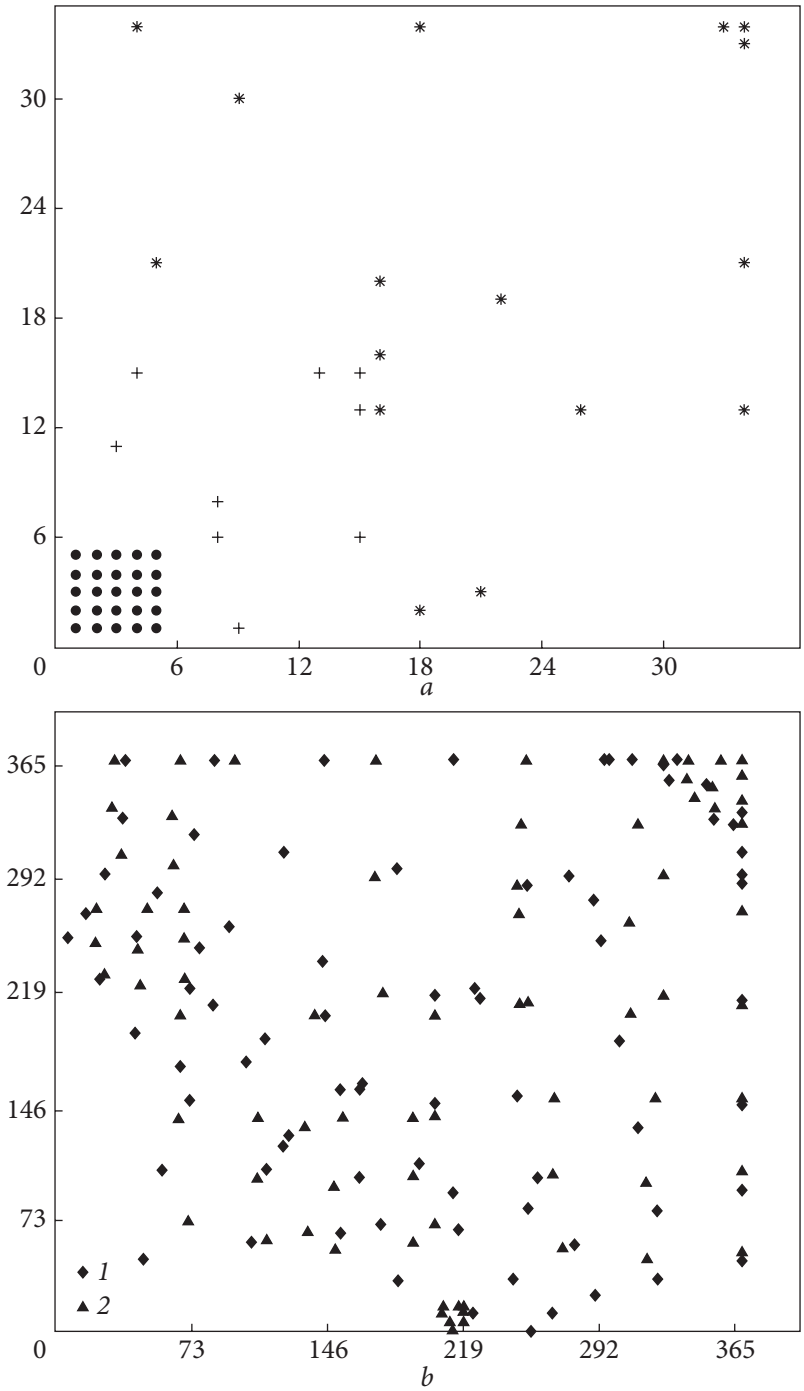

Fig. 5.2. Location of coordinates of AAs: • — GURT subarray (5×5), $(X, Y)_{M3}$, $(X, Y)_{M4}$; *b* — ◆ — $(X, Y)_{M9}$; ▲ — $(X, Y)_{Mr3*3}$

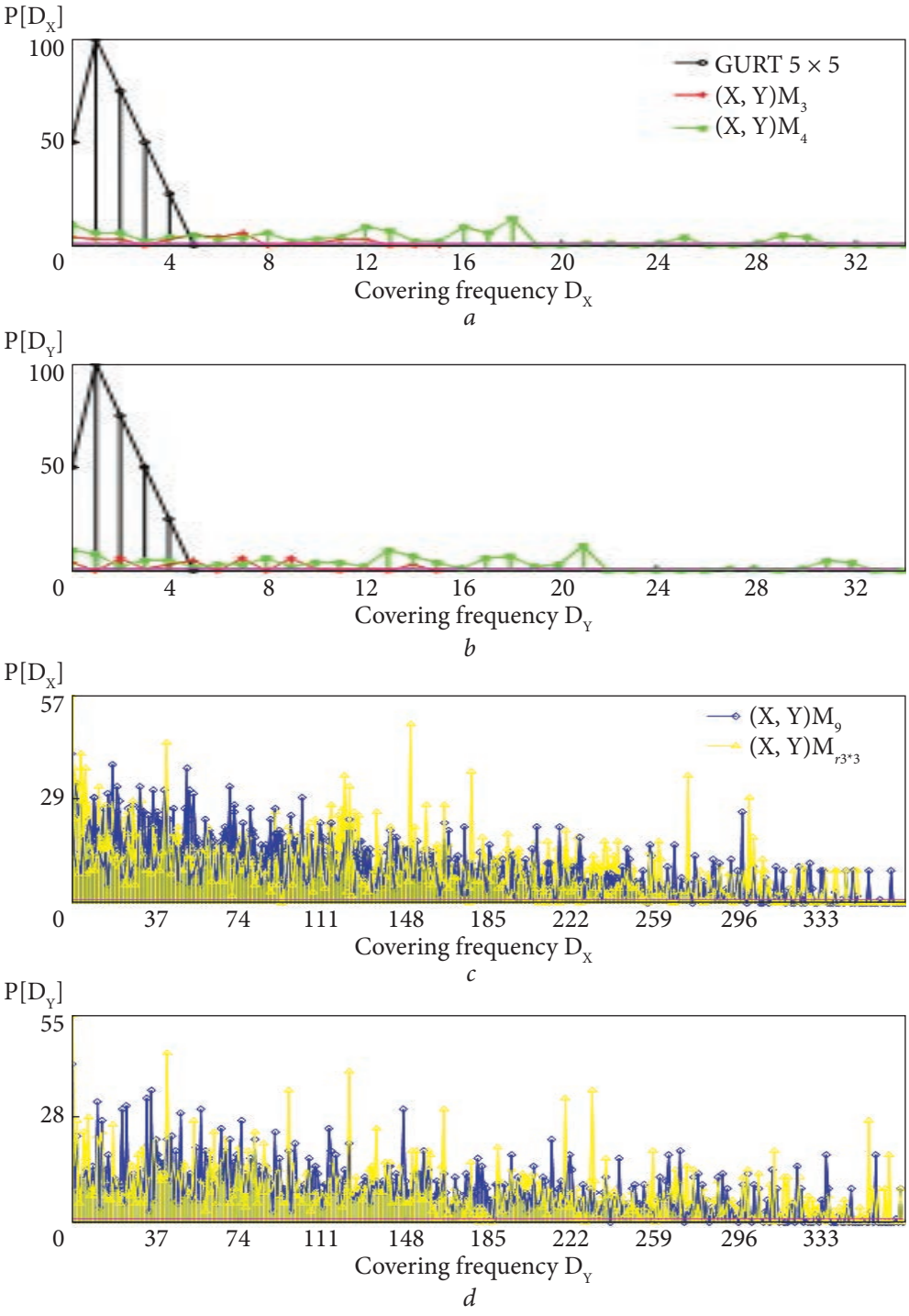

Fig. 5.3. Spatial frequencies covered by AAs: GURT subarray (5×5), $(X, Y)_{M3}$, $(X, Y)_{M4}$, $(X, Y)_{M9}$, and $(X, Y)_{Mr3*3}$, along the X (*a*, *c*) and Y (*b*, *d*) axes

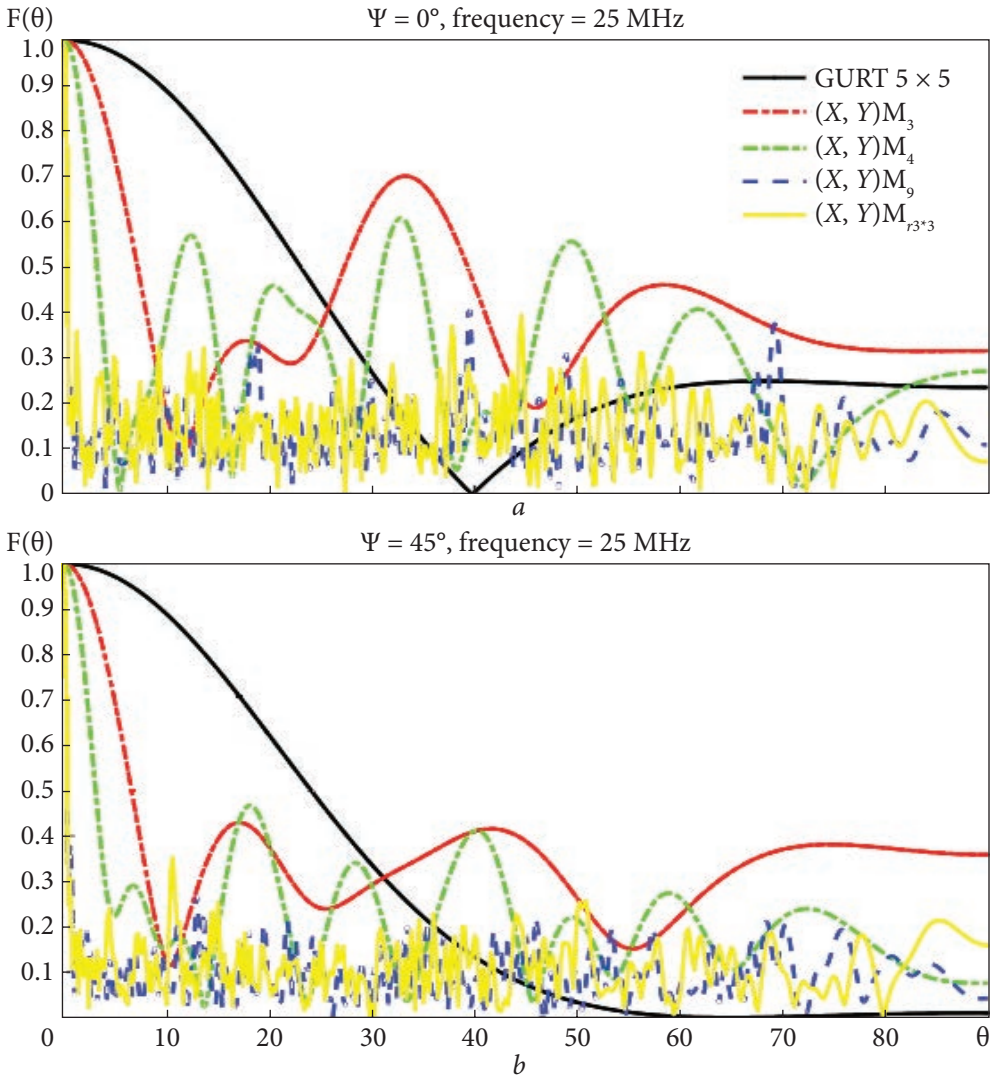

Fig. 5.4. Cross-section of the normalized RP in different planes Ψ (*a* — Ψ = 0°, *b* — Ψ = 45°, *c* — Ψ = 90°, *d* — Ψ = 135°) corresponding to the frequency of 25 MHz for the GURT subarray 5×5 sublattice and AAs developed based on the magic squares of the 3rd ($(X, Y)_{M3}$), 4th ($(X, Y)_{M4}$), of the 9th ($(X, Y)_{M9}$) orders and the nested magic square matrix of the 3rd order ($(X, Y)_{Mr3*3}$) (See also p. 84)

The synthesis method described in the previous chapter was used to construct the two-dimensional non-equidistant AA and calculate its RP. The location in the effective area of the designed antenna based on the matrices M_3, M_4, M_9, and the GURT subarray is shown in Fig. 5.2. And the corresponding covering spatial frequencies of the abscissa and ordinate are shown in Fig. 5.3. The

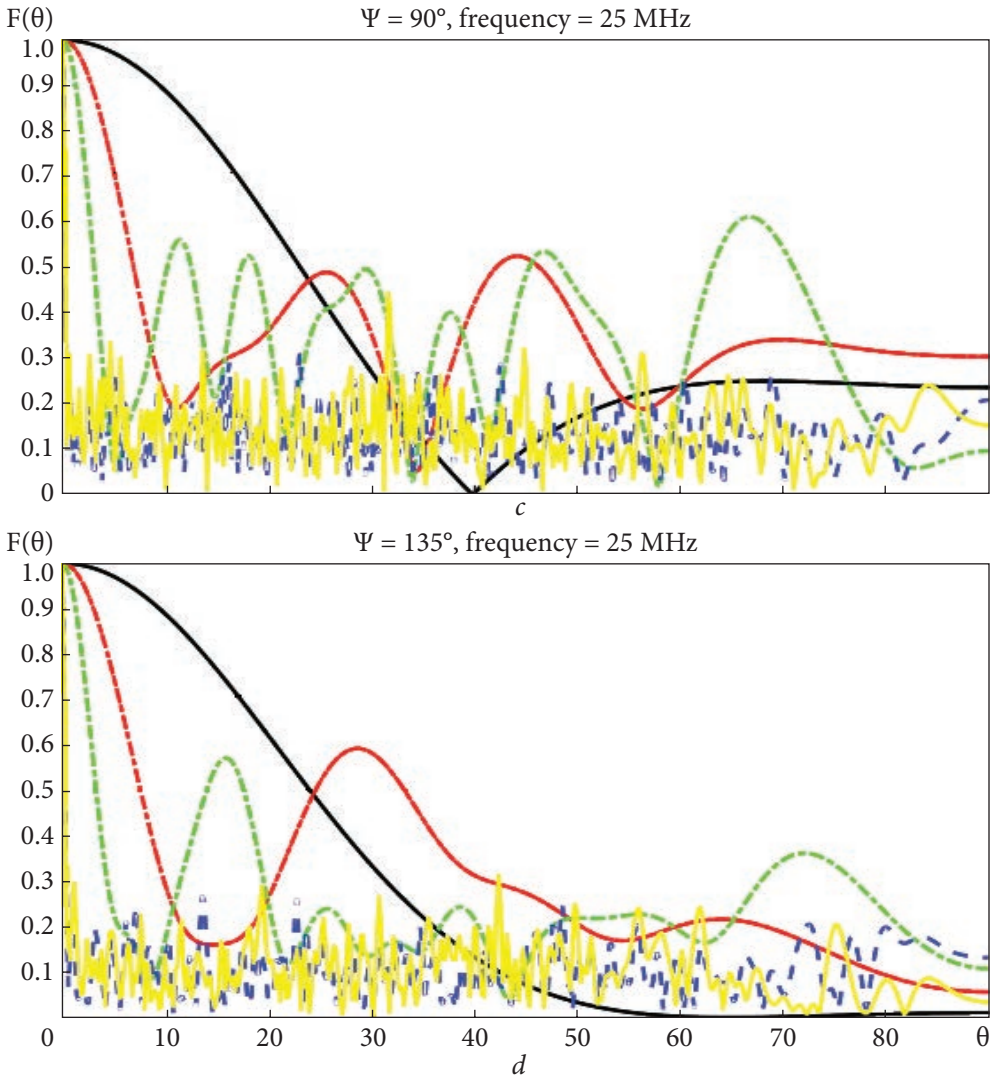

End of Fig. 5.4

simulation results of the AA's RP corresponding to the frequency 25 MHz are shown in Fig. 5.4. The corresponding AA parameter and the calculation time of these AAs are shown in the Table 5.1.

The location of GURT subarray (5 × 5) and the AAs developed on the basis of magic squares of the 3rd order ($(X, Y)_{M3}$), 4th order ($(X, Y)_{M4}$), 9th order ($(X, Y)_{M9}$) and the nested matrix of the magic square of the 3rd order ($(X, Y)_{Mr3*3}$) is shown in Fig. 5.2.

The spatial frequencies covered by GURT subarray (5 × 5) and the AAs developed based on magic squares of the 3rd order ($(X, Y)_{M3}$), 4th order ($(X, Y)_{M4}$),

Table 5.1. **A brief comparison of the characteristics of the GURT subarray and non-equidistant AAs developed based on magic squares and their nested matrix**

Comparison parameters	GURT (5×5)	$(X, Y)_{M3}$	$(X, Y)_{M4}$	$(X, Y)_{M9}$	$(X, Y)_{Mr3*3}$
MBW, °	67.8867	20.7751	9.4481	1.3992	1.0439
SLL, dB	–19.6258	–9.6896	–11.6884	–19.0479	–18.8707
The number of antenna elements	25	9	16	81	81
Effective covering area, d^2	25	225	1156	136161	136161
Calculation time, seconds	2.498235	1.987322	2.443966	7.093125	8.451823

9th order ($(X, Y)_{M9}$) and the nested matrix of the magic square of the 3rd order ($(X, Y)_{Mr3*3}$) are shown in Fig. 5.3.

The following points can be easily observed from the simulation results above:

1) The use of magic squares for the construction of AA can quickly and effectively expand the effective area and significantly reduce the width of the main lobe of the RP. As the order of magic squares increases, the width of the main lobe narrows, and the average level of the side lobes of the RP also decreases. AAs developed using this method have a nonlinear distribution, are flexible, and can be expanded with increasing matrix order.

2) The main RP beam of AAs, constructed based on a nested magic square matrix, is narrower than that of an AA constructed based on a magic square matrix of the same order. For a magic square of order n^2, synthesis is possible using two identical matrices of order n. For a magic square of order $m \times n$, synthesis is possible using a magic square of order m and order n (m and n being all natural numbers greater than or equal to three).

3) Unfortunately, AAs synthesized with the help of magic squares are unable to achieve full coverage of spatial frequencies, which is accompanied by the generation of side lobes with large amplitudes. To eliminate these side lobes, it is necessary to add additional antenna elements. In previous work, we used a greedy algorithm to achieve this goal [22].

5.3. AA design by using Latin squares and their nested matrix

This section focuses on the use of the general Latin square with natural numbers as elements for AA design. The Latin square of the n^{th} order has the following form [37]:

$$L_n = \begin{bmatrix} 1 & 2 & 3 & \cdots & n-1 & n \\ n & 1 & 2 & \cdots & n-2 & n-1 \\ n-1 & n & 1 & \cdots & n-3 & n-2 \\ \vdots & \vdots & \vdots & \ddots & \vdots & \vdots \\ 3 & 4 & 5 & \cdots & 1 & 2 \\ 2 & 3 & 4 & \cdots & n & 1 \end{bmatrix}. \tag{5.5}$$

Especially, as examples, the considered matrices of Latin squares of the 3rd, 4th, and 9th orders are marked as L_3, L_4, and L_9, respectively:

$$L_3 = \begin{bmatrix} 1 & 2 & 3 \\ 3 & 1 & 2 \\ 2 & 3 & 1 \end{bmatrix}, \tag{5.6}$$

$$L_4 = \begin{bmatrix} 1 & 2 & 3 & 4 \\ 4 & 1 & 2 & 3 \\ 3 & 4 & 1 & 2 \\ 2 & 3 & 4 & 1 \end{bmatrix}, \tag{5.7}$$

$$L_9 = \begin{bmatrix} 1 & 2 & 3 & 4 & 5 & 6 & 7 & 8 & 9 \\ 9 & 1 & 2 & 3 & 4 & 5 & 6 & 7 & 8 \\ 8 & 9 & 1 & 2 & 3 & 4 & 5 & 6 & 7 \\ 7 & 8 & 9 & 1 & 2 & 3 & 4 & 5 & 6 \\ 6 & 7 & 8 & 9 & 1 & 2 & 3 & 4 & 5 \\ 5 & 6 & 7 & 8 & 9 & 1 & 2 & 3 & 4 \\ 4 & 5 & 6 & 7 & 8 & 9 & 1 & 2 & 3 \\ 3 & 4 & 5 & 6 & 7 & 8 & 9 & 1 & 2 \\ 2 & 3 & 4 & 5 & 6 & 7 & 8 & 9 & 1 \end{bmatrix}. \tag{5.8}$$

The principle of nesting the Latin square matrix is essentially the same as in the case of the magic square, as shown in Fig. 5.1.

It is worth noting that a nested Latin square matrix remains a Latin square, meaning that nesting the matrix does not affect its properties. As an example, a nested matrix formed by combining two identical matrices of Latin squares of the 3rd order is used, denoted as:

$$L_{r3*3} = L_3(L_3) = \begin{bmatrix} (1-1)*3+\begin{bmatrix} 1 & 2 & 3 \\ 3 & 1 & 2 \\ 2 & 3 & 1 \end{bmatrix} & (2-1)*3+\begin{bmatrix} 1 & 2 & 3 \\ 3 & 1 & 2 \\ 2 & 3 & 1 \end{bmatrix} & (3-1)*3+\begin{bmatrix} 1 & 2 & 3 \\ 3 & 1 & 2 \\ 2 & 3 & 1 \end{bmatrix} \\ (3-1)*3+\begin{bmatrix} 1 & 2 & 3 \\ 3 & 1 & 2 \\ 2 & 3 & 1 \end{bmatrix} & (1-1)*3+\begin{bmatrix} 1 & 2 & 3 \\ 3 & 1 & 2 \\ 2 & 3 & 1 \end{bmatrix} & (2-1)*3+\begin{bmatrix} 1 & 2 & 3 \\ 3 & 1 & 2 \\ 2 & 3 & 1 \end{bmatrix} \\ (2-1)*3+\begin{bmatrix} 1 & 2 & 3 \\ 3 & 1 & 2 \\ 2 & 3 & 1 \end{bmatrix} & (3-1)*3+\begin{bmatrix} 1 & 2 & 3 \\ 3 & 1 & 2 \\ 2 & 3 & 1 \end{bmatrix} & (1-1)*3+\begin{bmatrix} 1 & 2 & 3 \\ 3 & 1 & 2 \\ 2 & 3 & 1 \end{bmatrix} \end{bmatrix} =$$

$$= \begin{bmatrix} 1 & 2 & 3 & 4 & 5 & 6 & 7 & 8 & 9 \\ 3 & 1 & 2 & 6 & 4 & 5 & 9 & 7 & 8 \\ 2 & 3 & 1 & 5 & 6 & 4 & 8 & 9 & 7 \\ 7 & 8 & 9 & 1 & 2 & 3 & 4 & 5 & 6 \\ 9 & 7 & 8 & 3 & 1 & 2 & 6 & 4 & 5 \\ 8 & 9 & 7 & 2 & 3 & 1 & 5 & 6 & 4 \\ 4 & 5 & 6 & 7 & 8 & 9 & 1 & 2 & 3 \\ 6 & 4 & 5 & 9 & 7 & 8 & 3 & 1 & 2 \\ 5 & 6 & 4 & 8 & 9 & 7 & 2 & 3 & 1 \end{bmatrix}. \quad (5.9)$$

Obviously, L_{r3*3} is also a Latin square of 9th order.

Use the synthesis method described in the previous section to generate the appropriate antenna array and calculate its RP. The spatial location of the designed AAs based on the matrices L_3, L_4, L_9, L_{r3*3}, and the GURT subarray (5 × 5) is shown in Fig. 5.5. The corresponding spatial covering frequencies of the ab-

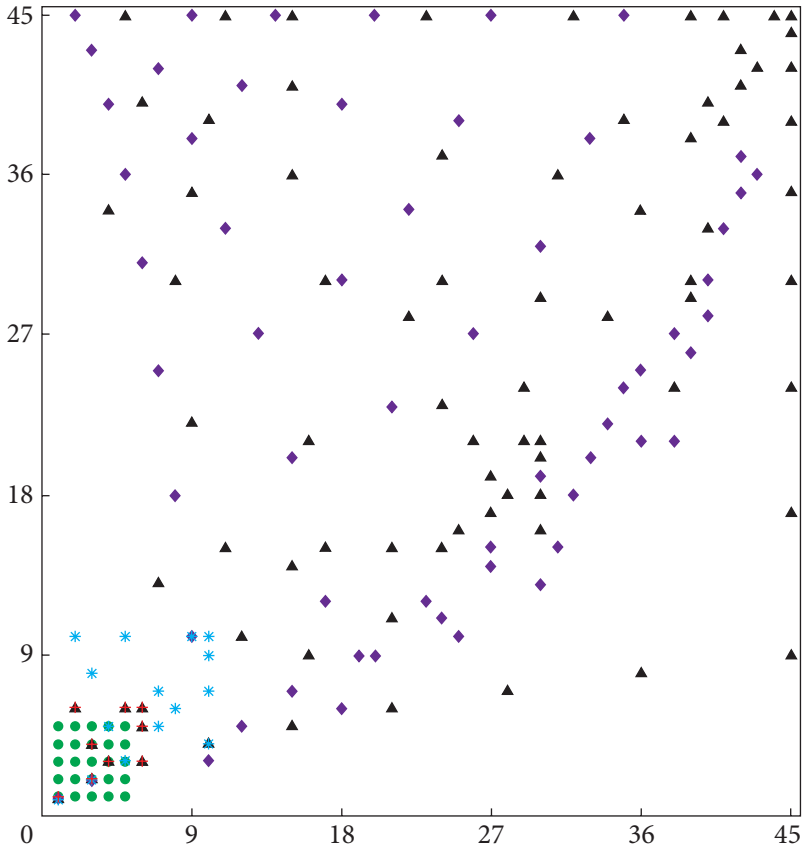

Fig. 5.5. Location of coordinates of AAs: • — GURT subarray (5 × 5), + — $(X, Y)_{L3}$, ✳ — $(X, Y)_{L4}$, ◆ — $(X, Y)_{L9}$, and ▲ — $(X, Y)_{Lr3*3}$

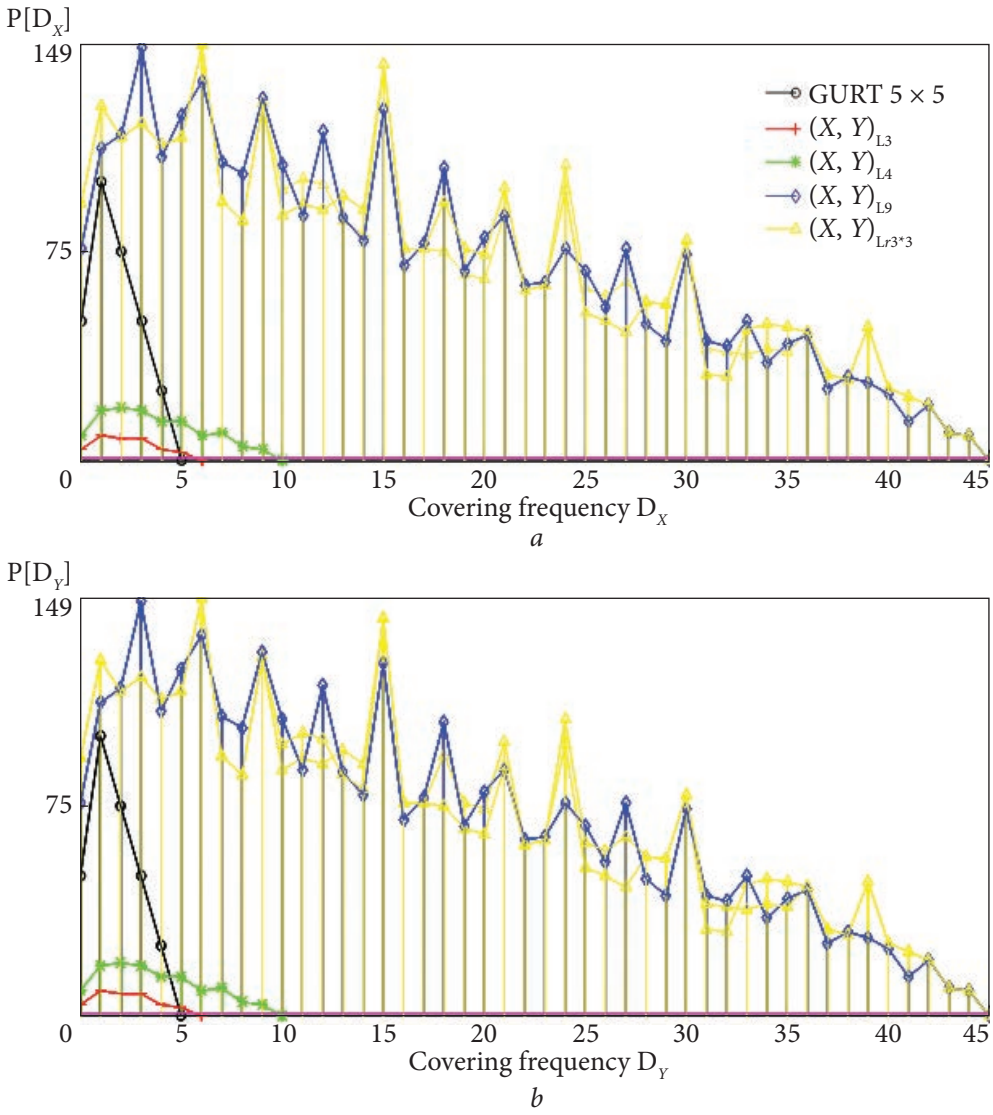

Fig. 5.6. Spatial frequencies covered by AAs: GURT subarray (5×5), $(X, Y)_{L3}$, $(X, Y)_{L4}$, $(X, Y)_{L9}$, and $(X, Y)_{Lr3*3}$, along the X (*a*) and Y (*b*) axes

scissa and ordinate are shown in Fig. 5.6. The comparison results of the simulation of the RP corresponding to the frequency of 25 MHz are shown in Fig. 5.7. The corresponding AA parameters and the calculation times for these AAs are demonstrated in Table 5.2.

The location of GURT subarray (5×5) and the AAs developed based on Latin squares of the 3rd order ($(X, Y)_{L3}$), 4th order ($(X, Y)_{L4}$), 9th order ($(X, Y)_{L9}$), and the nested matrix of the magic square of the 3rd order ($(X, Y)_{Lr3*3}$) is shown in Fig. 5.5.

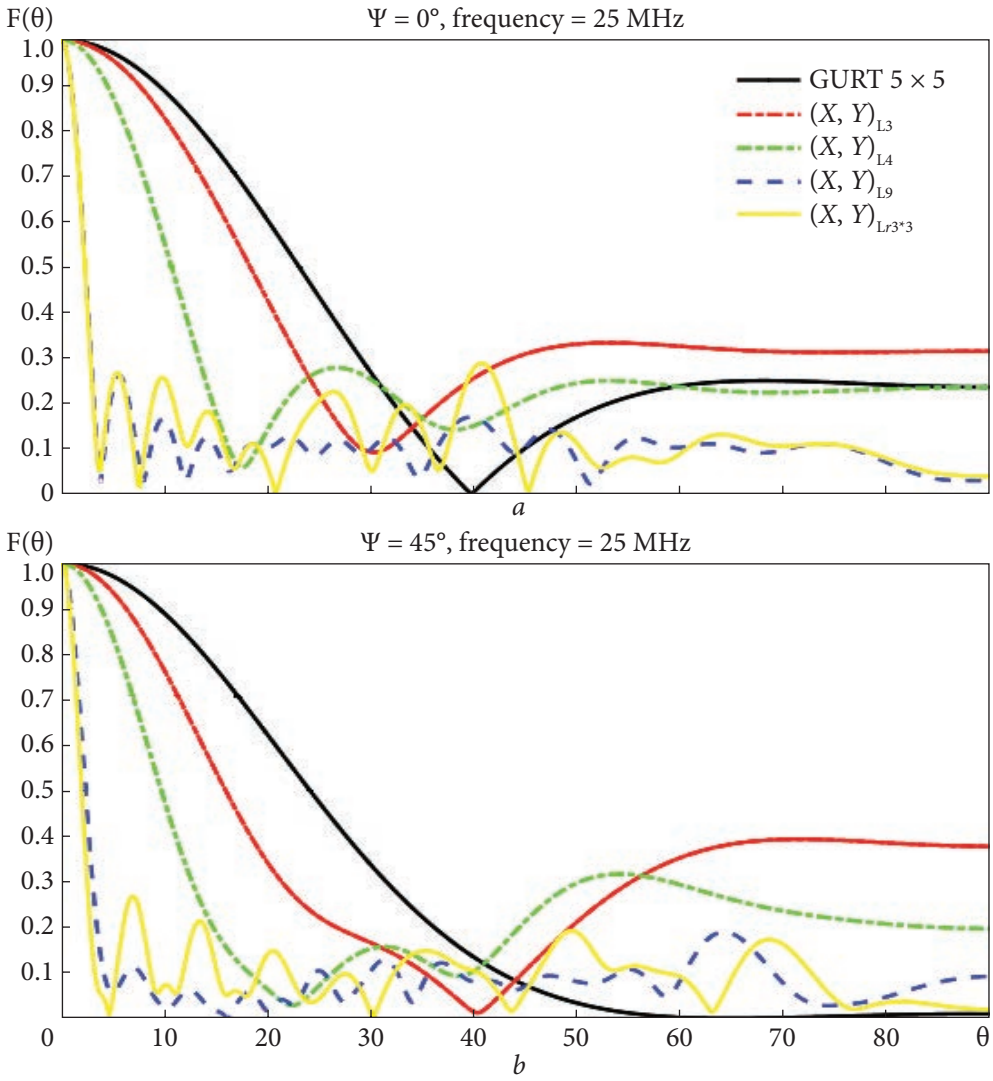

Fig. 5.7. Cross-section of the normalized RP in different planes Ψ (*a* — Ψ = 0°, *b* — Ψ = = 45°, *c* — Ψ = 90°, *d* — Ψ = 135°) corresponding to the frequency of 25 MHz for the GURT subarray 5×5 sublattice and AAs developed based on Latin squares of the 3rd ($(X, Y)_{L3}$), 4th ($(X, Y)_{L4}$), of the 9th ($(X, Y)_{L9}$) orders, and the nested Latin square matrix of the 3rd order ($(X, Y)_{Lr3*3}$) (See also p. 90)

The spatial frequencies covered by GURT subarray (5 × 5) and the AAs developed based on Latin squares of the 3rd order ($(X, Y)_{L3}$), 4th order ($(X, Y)_{L4}$), 9th order ($(X, Y)_{L9}$), and the nested matrix of the magic square of the 3rd order ($(X, Y)_{Lr3*3}$) are shown in Fig. 5.6.

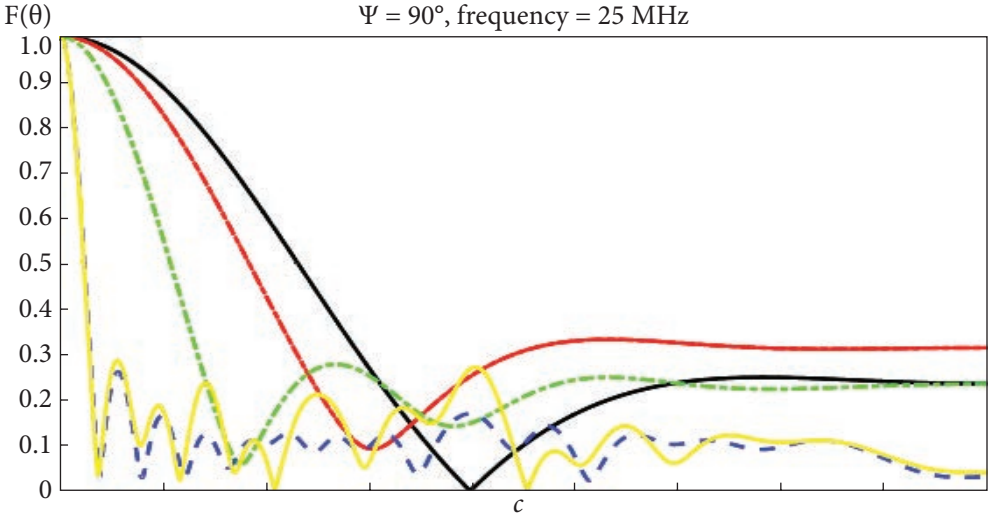

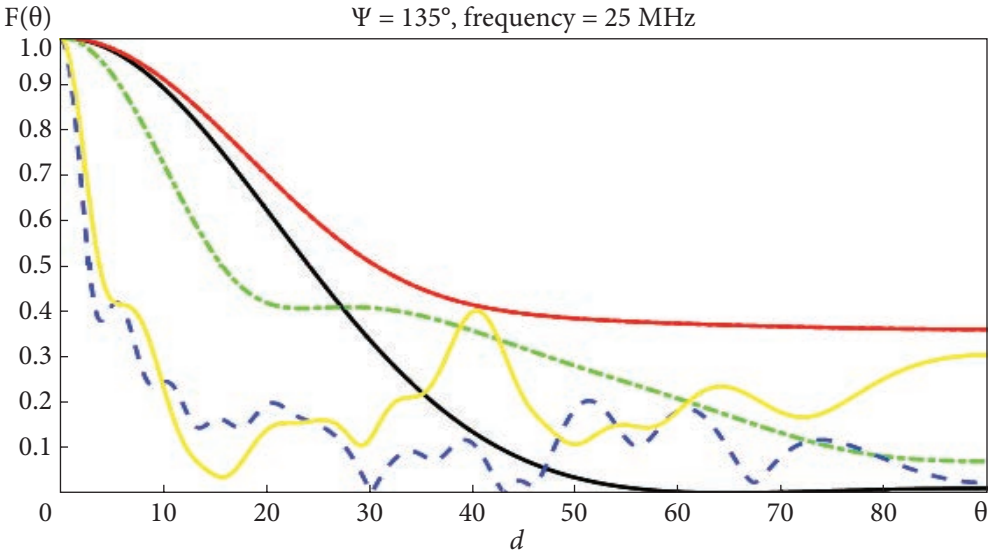

End of Fig. 5.7

Table 5.2. **A brief comparison of the characteristics of the GURT subarray and non-equidistant AAs developed based on Latin squares and their nested matrix**

Comparison parameters	GURT (5×5)	$(X, Y)_{L3}$	$(X, Y)_{L4}$	$(X, Y)_{L9}$	$(X, Y)_{Lr3*3}$
MBW, °	67.8867	57.3193	32.9639	7.2360	7.4181
SLL, dB	–19.6258	–10.4945	–12.6955	–18.7148	–18.8833
The number of antenna elements	25	9	16	81	81
Effective covering area, d^2	25	36	100	2025	2025
Calculation time, seconds	2.824519	2.427971	2.503327	6.861223	6.928961

The following points should be noted from the above simulation results:

1) AAs, constructed by using Latin squares, share common properties with equidistant dense arrays and the AAs constructed using magic squares. However, they have a unique advantage: lower levels of side lobes and complete coverage of their spatial frequencies. This is a critically important aspect that meets the requirements of radio astronomy.

2) Each column (or row) of the Latin square is an incremental arithmetic series of continuous natural numbers, which are linear. Using a non-linear construction method, the AA synthesized with the Latin square has geometric characteristics (a fixed geometric profile). As the order of the matrix increases, the geometric features (contour/profile) become more apparent and resemble a "Radial form" with center in the upper left corner on the XOY plane.

3) In particular, compared to the traditional uniform GURT subarray (5×5) of 25 elements, the AA, constructed using a Latin square of 4^{th} order (16 elements in total) based on the traditional algorithm (1.8), can simultaneously reduce the width of the main beam and lower the level of the side lobe. See Table 5.2 and Fig. 5.7 for details.

5.4. AA design by using the new Latin square, taking CDS as elements

This section focuses on AAs constructed by using the new Latin square, which takes cyclic difference sets (CDSs) as its elements.

CDS — A (ν, k, λ) is a subset $\mathbf{D} = \{d_1, d_2, ..., d_k\}$ of integers modulo v such that each $\{1,2, ..., \nu - 1\}$ can be represented as the difference $(d_i - d_j)$ modulo ν exactly λ times in various ways [29]. Some CDSs that will be used below are shown in the Table 5.3 and a more comprehensive introduction to CDS can be found in Chapter 3.

It is worth mentioning that to date, CDS have been widely used in many areas of research, such as applied mathematics and engineering practice. Their unique properties and satisfactory characteristics have been highly praised. The use of CDS in the construction of AAs has also achieved excellent results. For a

Table 5.3. **Some Cyclic Difference Sets (CDSs)**

Name	ν	k	λ	n	$\mathbf{D} = \{d_1, \ldots, d_k\}$
CDS3	7	3	1	2	1, 2, 4
CDS4	13	4	1	3	0, 1, 3, 9
CDS9s	19	9	4	5	1, 4, 5, 6, 7, 9, 11, 16, 17
CDS9m	37	9	2	7	1, 7, 9, 10, 12, 16, 26, 33, 34
CDS9b	73	9	1	8	0, 1, 12, 20, 26, 30, 33, 35, 57

one-dimensional (linear) AA, CDS's inherent characteristics enable the creation of excellent AAs with uniform spatial frequency and full coverage directly from the CDS elements. This approach was pioneered by Leeper in the 1970s [14, 15]. Later, from the late 1980s, L.E. Kopilovich and L.G. Sodin continued their improvement and attempted to construct two-dimensional AAs using CDSs [18—21].

However, using a one-dimensional set to construct a two-dimensional AAs often presents challenges, as it cannot ensure complete coverage of spatial frequency while minimizing redundancy. The utilization of CDSs within Latin squares for AA construction represents a significant advancement, building upon prior research and findings in this field.

One effective way to construct a new Latin square is through permutation group theory, which generates square matrices with specific symmetries via permutation operations. CDS as elements of a Latin square can be considered as carefully designed permutations that ensure that each row and column contains all n elements without repetition. It is worth mentioning that CDS is also a key concept in coding theory. A CDS is a specific set of integers where the difference between any two elements, taken modulo a positive integer, is unique. This property is highly valuable in signal processing and array design, helping reduce interference and enhance signal quality. For instance, in a CDS with N elements, selecting appropriate parameters allows the construction of a set with $N(N-1)$ distinct nonzero differences. This enables the formation of $N(N-1)$ independent beam directions in a two-dimensional antenna array, significantly enhancing beam-forming capabilities. By designing cyclic difference sets appropriately, the radiation pattern of an antenna array can be optimized to strengthen desired signals and suppress interference.

Moreover, CDSs operate naturally in finite fields, offering mathematical advantages for antenna design. They enable the construction of sequences with specific cross-correlation properties, which are crucial for minimizing interference and distinguishing signals from different directions, thereby improving radio system performance. By integrating the new Latin square with CDSs, antenna array design can achieve higher efficiency and performance. The structured difference properties of CDSs can guide element placement in antenna arrays, generating radiation patterns with low cross-correlation. This integration enhances signal clarity, reduces interference, and improves transmission efficiency in communication systems.

The core concept involves substituting natural numbers with CDSs as elements in Latin squares to enhance the coverage area of the resulting AA and optimize RP performance, ensuring maximum spatial frequency coverage. Examples of Latin square matrices of the 3rd, 4th, and 9th orders utilizing CDSs as elements are denoted as L_{CDS3}, L_{CDS4}, L_{CD9m}, and L_{CDS9b}, respectively. Next, we use the traditional synthesis method described in the formula (1.8) to generate the corresponding AAs and calculate their RPs.

$$L_{\mathrm{CDS3}}=\begin{bmatrix}1&2&4\\4&1&2\\2&4&1\end{bmatrix}, \tag{5.10}$$

$$L_{\mathrm{CDS4}}=\begin{bmatrix}1&2&4&10\\10&1&2&4\\4&10&1&2\\2&4&10&1\end{bmatrix}, \tag{5.11}$$

$$L_{\mathrm{CDS9s}}=\begin{bmatrix}1&4&5&6&7&9&11&16&17\\17&1&4&5&6&7&9&11&16\\16&17&1&4&5&6&7&9&11\\11&16&17&1&4&5&6&7&9\\9&11&16&17&1&4&5&6&7\\7&9&11&16&17&1&4&5&6\\6&7&9&11&16&17&1&4&5\\5&6&7&9&11&16&17&1&4\\4&5&6&7&9&11&16&17&1\end{bmatrix}, \tag{5.12}$$

$$L_{\mathrm{CDS9m}}=\begin{bmatrix}1&7&9&10&12&16&26&33&34\\34&1&7&9&10&12&16&26&33\\33&34&1&7&9&10&12&16&26\\26&33&34&1&7&9&10&12&16\\16&26&33&34&1&7&9&10&12\\12&16&26&33&34&1&7&9&10\\10&12&16&26&33&34&1&7&9\\9&10&12&16&26&33&34&1&7\\7&9&10&12&16&26&33&34&1\end{bmatrix}, \tag{5.13}$$

$$L_{\mathrm{CDS9b}}=\begin{bmatrix}1&2&13&21&27&31&34&36&58\\58&1&2&13&21&27&31&34&36\\36&58&1&2&13&21&27&31&34\\34&36&58&1&2&13&21&27&31\\31&34&36&58&1&2&13&21&27\\27&31&34&36&58&1&2&13&21\\21&27&31&34&36&58&1&2&13\\13&21&27&31&34&36&58&1&2\\2&13&21&27&31&34&36&58&1\end{bmatrix}, \tag{5.14}$$

where L_{CDS4} and L_{CDS9b} are the Latin squares of the 4th and 9th order, taking {CDS4 + 1} and {CDS9b + 1} as elements, since the element 0 actually does not contribute to the generation of the AA coordinate matrix. And for other CDSs containing 0 elements, the same processing method is used, that is, using {CDS + 1} as an element of the Latin square.

The location of GURT subarray (5×5) and the AAs developed based on new Latin squares of the 3rd order ($(X, Y)_{Lcds3}$), 4th order ($(X, Y)_{Lcds4}$), and 9th order ($(X, Y)_{Lcds9s}$, $(X, Y)_{Lcds9m}$, $(X, Y)_{Lcds9b}$) is shown in Fig. 5.8.

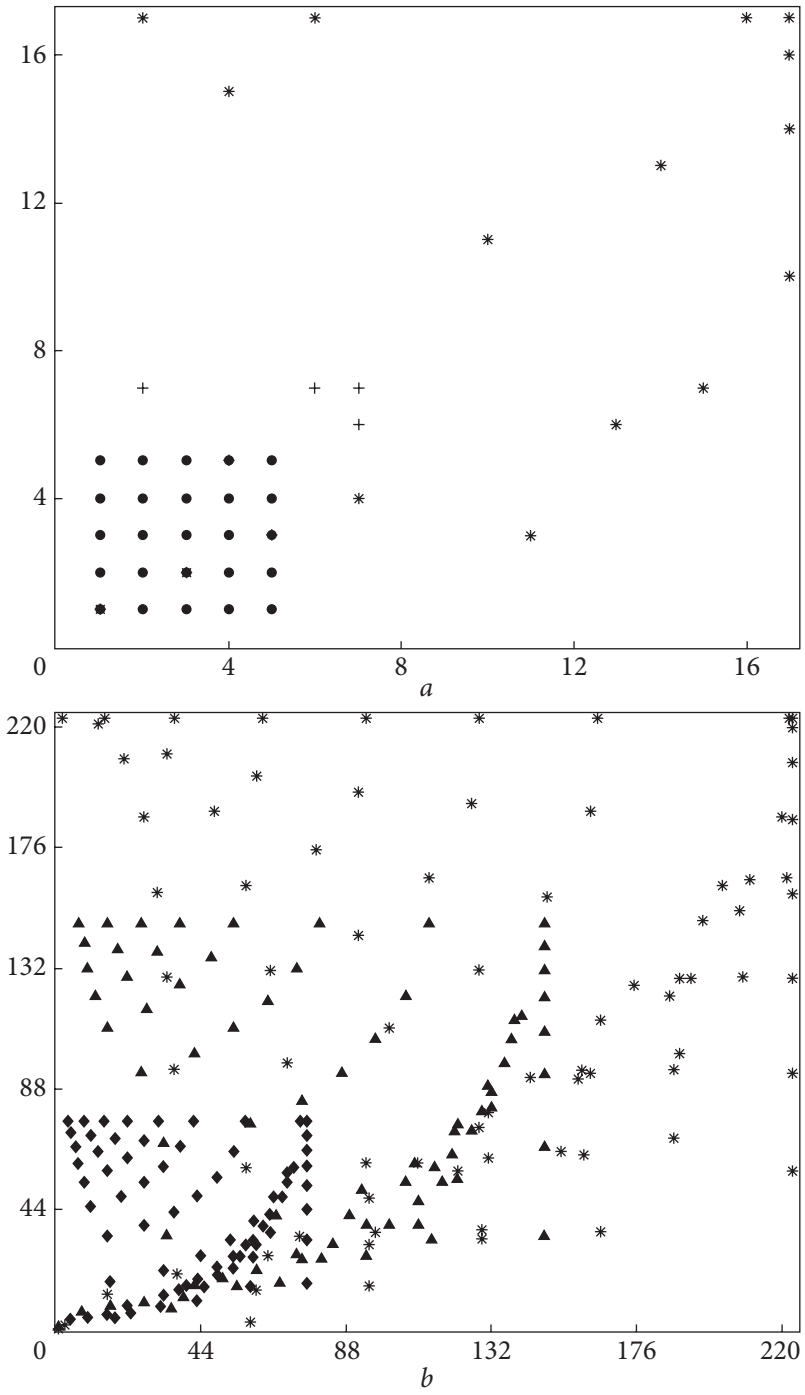

Fig. 5.8. Location of coordinates of AAs: *a* — • — GURT subarray (5×5), + — $(X, Y)_{\text{Lcds3}}$, ✳ — $(X, Y)_{\text{Lcds4}}$, *b* — ◆ — $(X, Y)_{\text{Lcds9s}}$, ▲ — $(X, Y)_{\text{Lcds9m}}$, ✳ — $(X, Y)_{\text{Lcds9b}}$

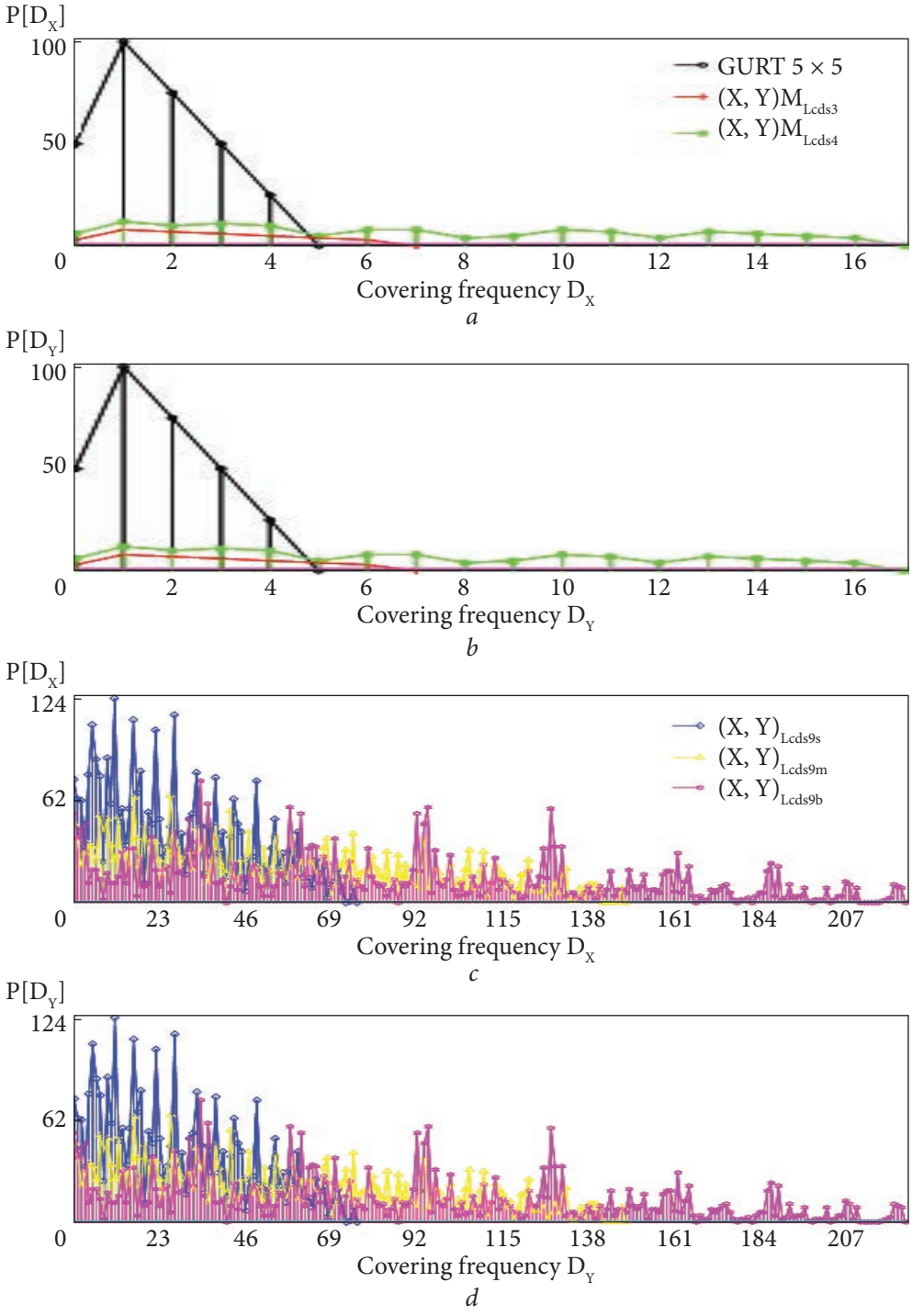

Fig. 5.9. Spatial frequencies covered by AAs: GURT subarray (5×5), $(X, Y)_{Lcds3}$, $(X, Y)_{Lcds4}$, $(X, Y)_{Lcds9s}$, $(X, Y)_{Lcds9m}$, and $(X, Y)_{Lcds9b}$, along the X (*a*, *c*) and Y (*b*, *d*) axes

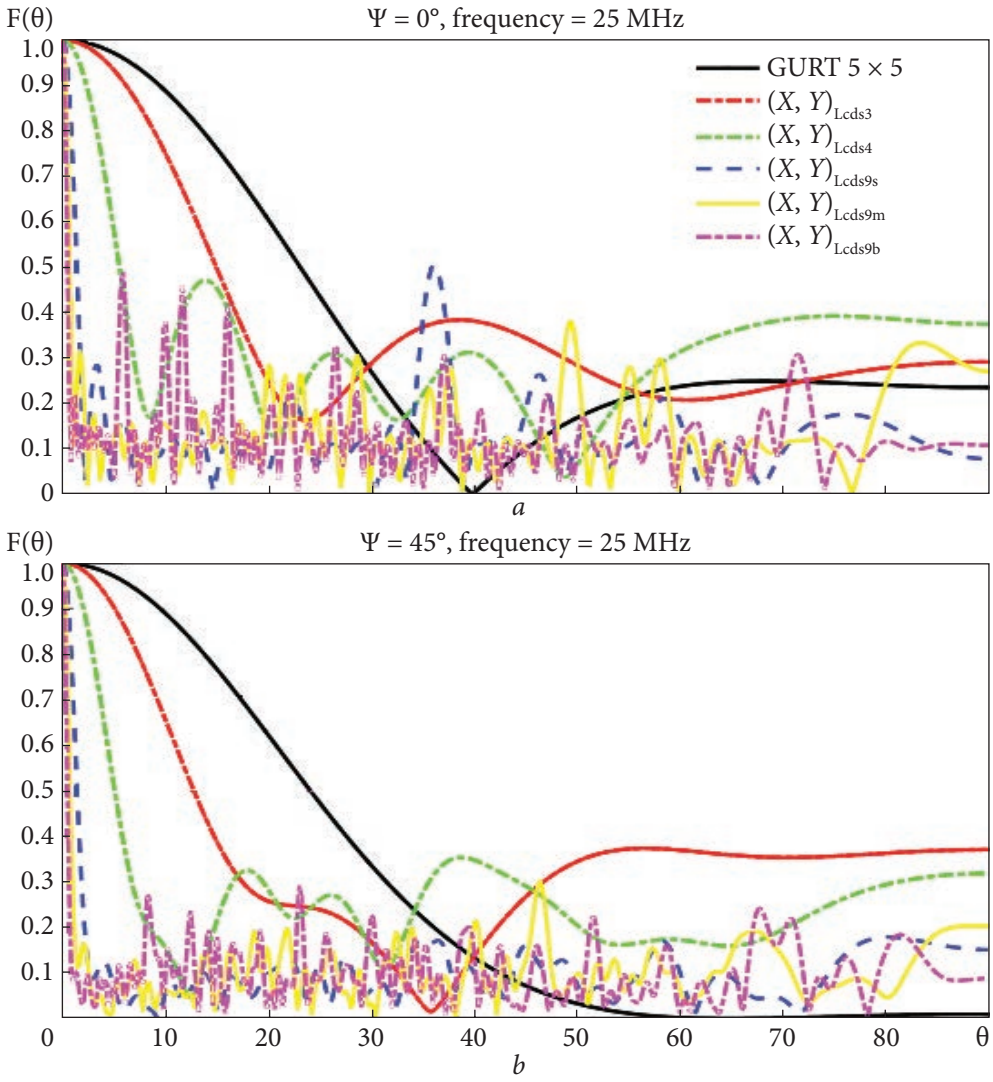

The spatial frequencies covered by GURT subarray (5 × 5) and the AAs developed based on new Latin squares (taking CDS as elements) of the 3rd order ($(X, Y)_{Lcds3}$), 4th order ($(X, Y)_{Lcds4}$), 9th order ($(X, Y)_{Lcds9s}$, $(X, Y)_{Lcds9m}$, $(X, Y)_{Lcds9b}$) are shown in Fig. 5.9

Fig. 5.10 presents the simulation results of the normalized RPs of these AAs at a frequency of 25 MHz. Table 5.4 displays the corresponding RP parameters and design calculation times for these AAs.

From the simulation results above, several observations are evident:

1) Since a CDS of the same order has several variants, determined by different moduli, the spatial frequency redundancy varies accordingly. Thus, the

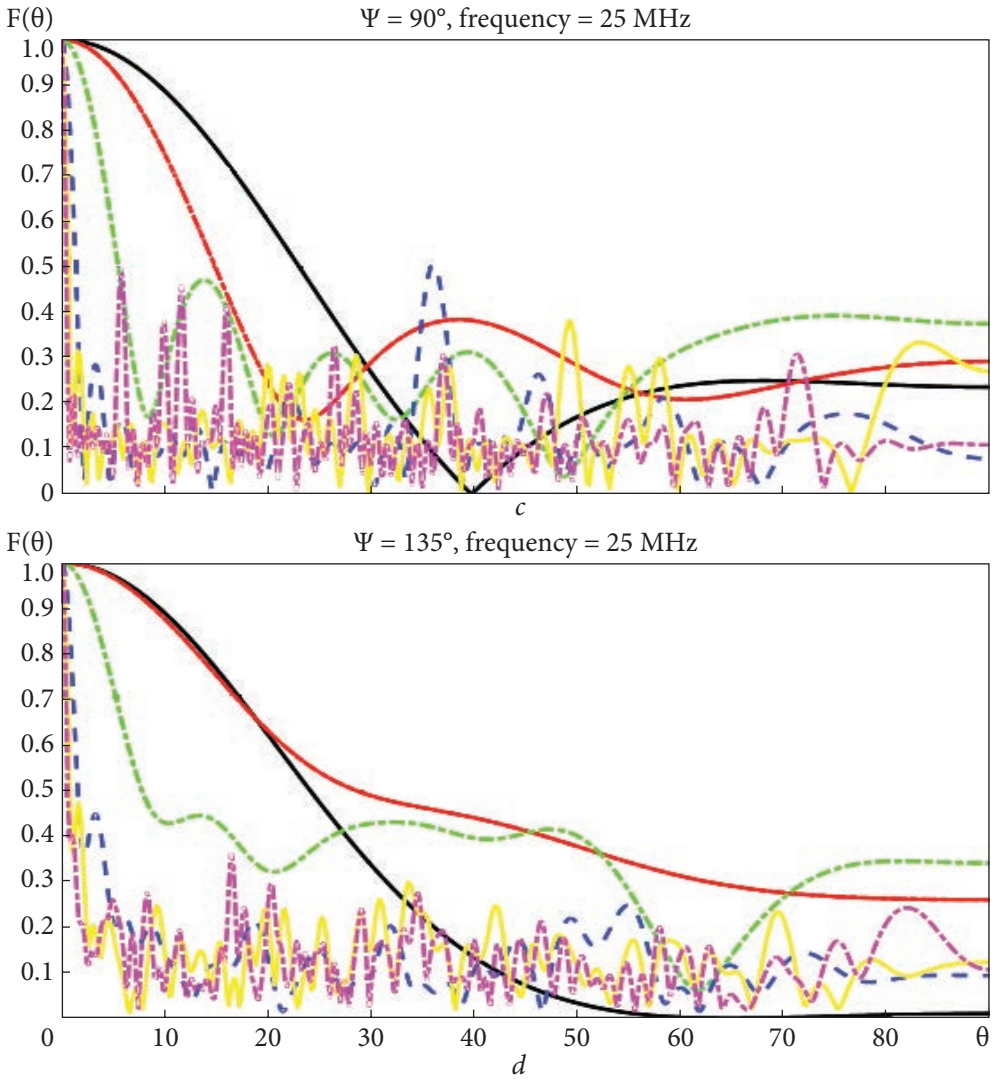

Fig. 5.10. Cross-section of the normalized RP in different planes Ψ (*a* — Ψ = 0°, *b* — Ψ = 45°, *c* — Ψ = 90°, *d* — Ψ = 135°) corresponding to the frequency of 25 MHz for the GURT subarray 5 × 5 sublattice and AAs developed based on new Latin squares (taking CDS as elements) of the 3rd ($(X, Y)_{Lcds3}$), 4th ($(X, Y)_{Lcds4}$), and 9th ($(X, Y)_{Lcds9s}$, ($(X, Y)_{Lcds9m}$, ($(X, Y)_{Lcds9b}$)) orders

new Latin square matrix taking CDM as elements also exhibits multiple variants, resulting in diverse spatial distributions and RP characteristics of the generated AA.

2) Compared to the original Latin square matrix with natural numbers as elements, the new Latin square matrix using CDS as elements demonstrates

Table 5.4. **A brief comparison of the characteristics of the GURT subarray and non-equidistant AAs developed based on new Latin squares (taking CDS as elements)**

Comparison parameters	GURT (5×5)	$(X, Y)_{\text{Lcds3}}$	$(X, Y)_{\text{Lcds4}}$	$(X, Y)_{\text{Lcds9s}}$	$(X, Y)_{\text{Lcds9m}}$	$(X, Y)_{\text{Lcds9b}}$
MBW, °	67.8867	47.2004	17.0439	4.1843	2.1988	1.3992
SLL, dB	–19.6258	–9.9276	–11.8085	–18.5061	–18.7253	–18.8069
The number of antenna elements	25	9	16	81	81	81
Effective covering area, d^2	25	49	289	5776	21904	49729
Calculation time, seconds	3.039379	1.963207	2.373630	7.270354	7.191380	7.460928

superior properties and versatility in AA synthesis. It ensures full/almost-full coverage of spatial frequencies over a larger area, reduces the width of the main RP beam, and minimizes degradation in the level of side lobes of the RP.

3) Similar to the Latin squares with consecutive natural numbers as elements, when using new Latin squares (taking CDS as elements) to synthesize AA by the traditional formula (1.8), the synthesized AA is distributed in a fan-shaped region in the upper left corner of the XOY plane and does not fill the entire plane. Therefore, it is necessary to explore new synthesis methods to ensure that the resulting AR fills the space as uniformly as possible.

5.5. AA design by using the unit triangular matrix and Latin square triangular matrices

In linear algebra, a **triangular matrix** is a special square matrix where all elements below (or above) the main diagonal are zero [30, 31]. If all elements on the main diagonal (either above or below) of a triangular matrix are unity, the matrix is referred to as unitriangular. **Unitriangular matrices** are a subset of triangular matrices, and all unitriangular matrices are also unipotent. This section considers the possibility of synthesis of AA using lower **triangular** matrices, which behave as follows:

$$UniTriO(n) = \begin{bmatrix} 1 & 0 & 0 & \cdots & 0 & 0 \\ 1 & 1 & 0 & \cdots & 0 & 0 \\ 1 & 1 & 1 & \cdots & 0 & 0 \\ \vdots & \vdots & \vdots & \ddots & \vdots & \vdots \\ 1 & 1 & 1 & \cdots & 1 & 0 \\ 1 & 1 & 1 & \cdots & 1 & 1 \end{bmatrix} = \text{tril}\left[Ones(n)\right], \tag{5.15}$$

$$UniTriL(n)=\begin{bmatrix} 1 & 0 & 0 & \cdots & 0 & 0 \\ n & 1 & 0 & \cdots & 0 & 0 \\ n-1 & n & 1 & \cdots & 0 & 0 \\ \vdots & \vdots & \vdots & \ddots & \vdots & \vdots \\ 3 & 4 & 5 & \cdots & 1 & 0 \\ 2 & 5 & 4 & \cdots & n & 1 \end{bmatrix}=\mathrm{tril}\left[L_n\right], \tag{5.16}$$

where *Ones*(n) means an $n \times n$ matrix of units or a matrix where each element is equal to one [31]. The matrix (5.16) is derived by setting zero elements above the diagonal of the Latin square (5.5).

Given the operation rules governing matrices, there are significant opportunities for further improvement. If we express relation (1.8) in matrix form, then:

$$X=\begin{bmatrix} S_{1,1} & S_{1,2} & S_{1,3} & \cdots & S_{1,n-1} & S_{1,n} \\ S_{2,1} & S_{2,2} & S_{2,3} & \cdots & S_{2,n-1} & S_{2,n} \\ S_{3,1} & S_{3,2} & S_{3,3} & \cdots & S_{3,n-1} & S_{3,n} \\ \vdots & \vdots & \vdots & \ddots & \vdots & \vdots \\ S_{n-1,1} & S_{n-1,2} & S_{n-1,3} & \cdots & S_{n-1,n-1} & S_{n-1,n} \\ S_{n,1} & S_{n,2} & S_{n,3} & \cdots & S_{n,n-1} & S_{n,n} \end{bmatrix} \cdot \begin{bmatrix} 1 & 1 & 1 & \ldots & 1 & 1 \\ 0 & 1 & 1 & \ldots & 1 & 1 \\ 0 & 0 & 1 & \ldots & 1 & 1 \\ \vdots & \vdots & \vdots & \ddots & \vdots & \vdots \\ 0 & 0 & 0 & \ldots & 1 & 1 \\ 0 & 0 & 0 & \ldots & 0 & 1 \end{bmatrix} = S \cdot UniTriO^T, \tag{5.17}$$

$$Y=\begin{bmatrix} 1 & 0 & 0 & \ldots & 0 & 0 \\ 1 & 1 & 0 & \ldots & 0 & 0 \\ 1 & 1 & 1 & \ldots & 0 & 0 \\ \vdots & \vdots & \vdots & \ddots & \vdots & \vdots \\ 1 & 1 & 1 & \ldots & 1 & 0 \\ 1 & 1 & 1 & \ldots & 1 & 1 \end{bmatrix} \cdot \begin{bmatrix} S_{1,1} & S_{1,2} & S_{1,3} & \cdots & S_{1,n-1} & S_{1,n} \\ S_{2,1} & S_{2,2} & S_{2,3} & \cdots & S_{2,n-1} & S_{2,n} \\ S_{3,1} & S_{3,2} & S_{3,3} & \cdots & S_{3,n-1} & S_{3,n} \\ \vdots & \vdots & \vdots & \ddots & \vdots & \vdots \\ S_{n-1,1} & S_{n-1,2} & S_{n-1,3} & \cdots & S_{n-1,n-1} & S_{n-1,n} \\ S_{n,1} & S_{n,2} & S_{n,3} & \cdots & S_{n,n-1} & S_{n,n} \end{bmatrix} = UniTriO \cdot S, \tag{5.18}$$

where X, Y, S, and *UniTriO* are n^{th} order square matrices. Among them, X, Y, and S represent the abscissa matrix, the ordinate matrix, and the common matrix forming the magic/Latin square used, respectively. *UniTriO* is the lower unitriangular matrix of the matrix of units, and the operator "T" means the transposition of the matrix.

To further suppress interference, reduce energy losses, increase efficiency, and minimize redundancy in AA synthesis using the Latin square, the matrix in expressions (5.17) and (5.18) is replaced. This aims to achieve full coverage of spatial frequencies over a larger space/area with the same number of antenna elements.

$$X_{\text{Tri}}=L_n \cdot UniTriL_n^T=\begin{bmatrix} 1 & 2 & 3 & \ldots & n-1 & n \\ n & 1 & 2 & \ldots & n-2 & n-1 \\ n-1 & n & 1 & \ldots & n-3 & n-2 \\ \vdots & \vdots & \vdots & \ddots & \vdots & \vdots \\ 3 & 4 & 5 & \ldots & 1 & 2 \\ 2 & 3 & 4 & \ldots & n & 1 \end{bmatrix} \cdot \begin{bmatrix} 1 & n & n-1 & \ldots & 3 & 2 \\ 0 & 1 & n & \ldots & 4 & 3 \\ 0 & 0 & 1 & \ldots & 5 & 4 \\ \vdots & \vdots & \vdots & \ddots & \vdots & \vdots \\ 0 & 0 & 0 & \ldots & 1 & n \\ 0 & 0 & 0 & \ldots & 0 & 1 \end{bmatrix}, \tag{5.19}$$

$$Y_{\text{Tri}}=UniTriL_n \cdot L_n=\begin{bmatrix} 1 & 0 & 0 & \ldots & 0 & 0 \\ n & 1 & 0 & \ldots & 0 & 0 \\ n-1 & n & 1 & \ldots & 0 & 0 \\ \vdots & \vdots & \vdots & \ddots & \vdots & \vdots \\ 3 & 4 & 5 & \ldots & 1 & 0 \\ 2 & 3 & 4 & \ldots & n & 1 \end{bmatrix} \cdot \begin{bmatrix} 1 & 2 & 3 & \ldots & n-1 & n \\ n & 1 & 2 & \ldots & n-2 & n-1 \\ n-1 & n & 1 & \ldots & n-3 & n-2 \\ \vdots & \vdots & \vdots & \ddots & \vdots & \vdots \\ 3 & 4 & 5 & \ldots & 1 & 2 \\ 2 & 3 & 4 & \ldots & n & 1 \end{bmatrix}, \tag{5.20}$$

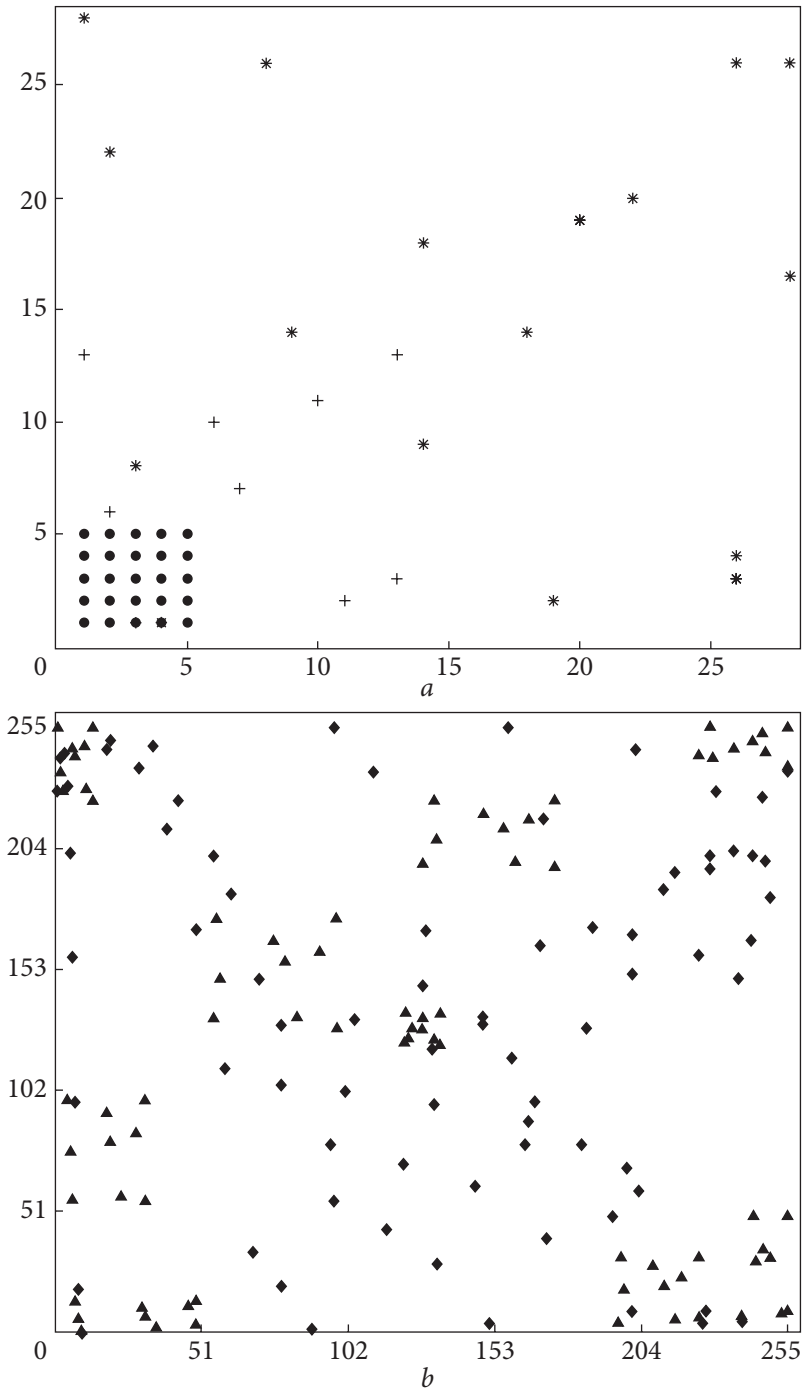

Fig. 5.11. Location of coordinates of AAs: • — GURT subarray (5×5), + — $(X_{Tri}, Y_{Tri})_{L3}$, ✳ — $X_{Tri}, Y_{Tri})_{L4}$, ◆ — $(X_{Tri}, Y_{Tri})_{L9}$, and ▲ — $(X_{Tri}, Y_{Tri})_{Lr3*3}$

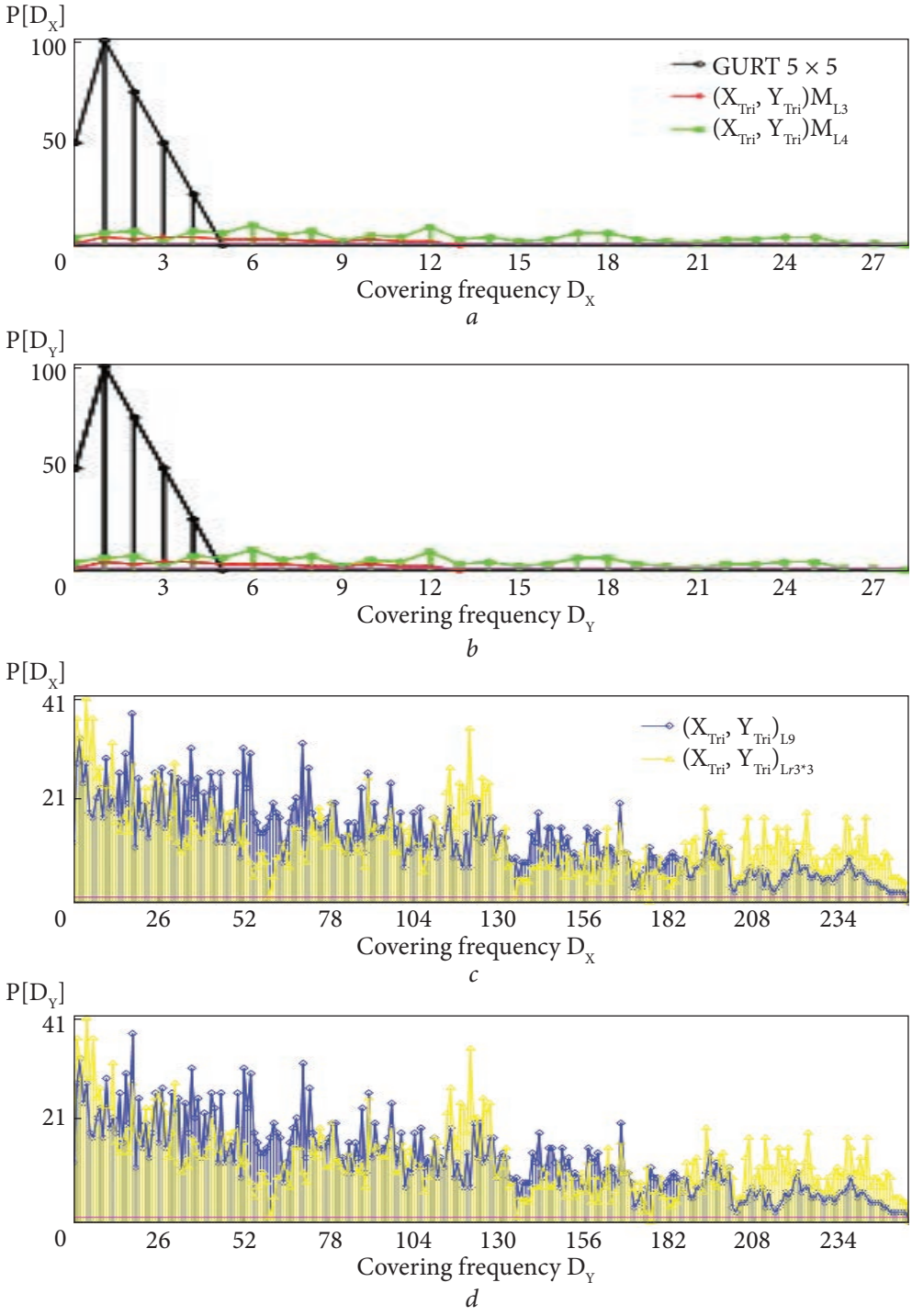

Fig. 5.12. Spatial frequencies covered by AAs: GURT subarray (5×5), $(X_{Tri}, Y_{Tri})_{L3}$, $(X_{Tri}, Y_{Tri})_{L4}$, $(X_{Tri}, Y_{Tri})_{L9}$, and $X_{Tri}, Y_{Tri})_{Lr3*3}$ along the X (*a*, *c*) and Y (*b*, *d*) axes

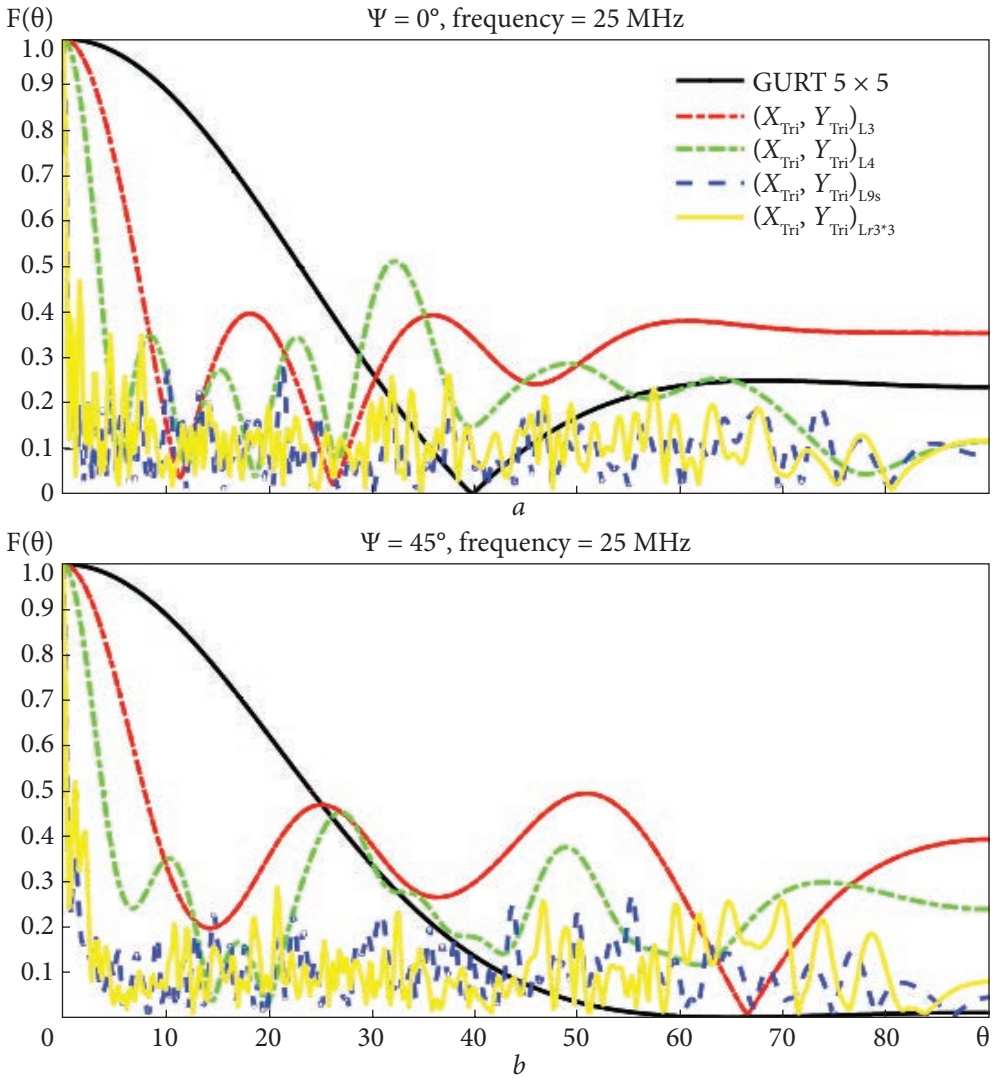

where n represents the order of square matrices X_{Tri}, Y_{Tri}, denoting the abscissa matrix and the ordinate matrix, respectively, obtained through a novel method utilizing triangular matrices.

Here, we specifically emphasize the integration of the new method with Latin square matrices, using L_3, L_4, L_9, and L_{r3*3} as examples for illustration. The AA constructed using this new method is distinguished by the subscript "Tri," contrasting with AA synthesized based on the traditional method formula (1.8).

The spatial configurations of the AA designs based on Latin square matrices, using the new triangular matrix method, along with the GURT subarray (5×5), are depicted in Fig. 5.11. Corresponding spatial frequencies along the

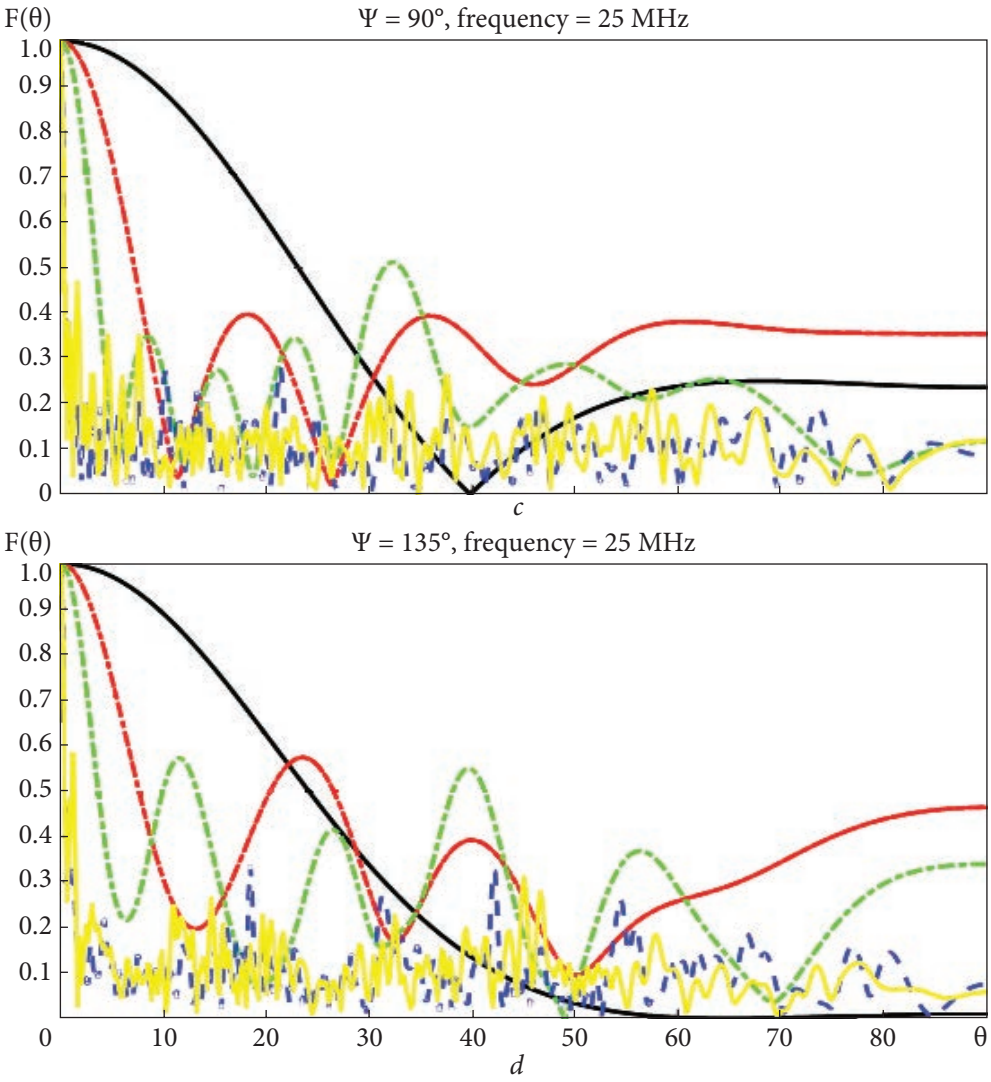

Fig. 5.13. Cross-section of the normalized RP in different planes Ψ (*a* — Ψ = 0°, *b* — Ψ = 45°, *c* — Ψ = 90°, *d* — Ψ =135°) corresponding to the frequency of 25 MHz for the GURT subarray 5×5 sublattice and AAs developed based on a new synthesis method (using triangular matrix), the Latin squares of the 3rd ($(X_{Tri}, Y_{Tri})_{L3}$), 4th ($(X_{Tri}, Y_{Tri})_{L4}$), 9th ($(X_{Tri}, Y_{Tri})_{L9}$) orders, and the nested Latin square matrix of the 3rd order ($(X_{Tri}, Y_{Tri})_{Lr3*3}$)

abscissa and ordinate are illustrated in Fig. 5.12. Simulation results for the cross-section of normalized RP at 25 MHz frequency are presented in Fig. 5.13. RP parameters and calculation times for these AAs are detailed in Table 5.5.

The location of the GURT subarray (5×5) and the AAs developed based on a synthesis method (triangular Latin matrix) and Latin squares of the 3rd order

Table 5.5. **A brief comparison of the characteristics of the GURT subarray and non-equidistant AAs developed based on Latin squares and a new synthesis method**

Comparison parameters	GURT (5 × 5)	$(X_{Tri}, Y_{Tri})_{L3}$	$(X_{Tri}, Y_{Tri})_{L4}$	$(X_{Tri}, Y_{Tri})_{L9}$	$(X_{Tri}, Y_{Tri})_{Lr3*3}$
MBW, °	67.8867	21.6813	10.4697	1.3992	1.3992
SLL, dB	–19.6258	–9.8433	–11.9922	–18.7964	–18.6177
The number of antenna elements	25	9	16	81	81
Effective covering area, d^2	25	169	784	65025	65025
Calculation time, seconds	2.462642	1.940133	2.251281	7.007086	6.812028

($(X_{Tri}, Y_{Tri})_{L3}$), 4th order ($(X_{Tri}, Y_{Tri})_{L4}$), 9th order ($(X_{Tri}, Y_{Tri})_{L9}$ and the nested matrix of the Latin square of the 3rd order ($(X_{Tri}, Y_{Tri})_{Lr3*3}$) is shown in Fig. 5.11.

The spatial frequencies covered by the GURT subarray (5 × 5) and the AAs developed based on a new method and Latin squares 3rd ($(X_{Tri}, Y_{Tri})_{L3}$), 4th ($(X_{Tri}, Y_{Tri})_{L4}$), 9th ($(X_{Tri}, Y_{Tri})_{L9}$), and the nested matrix of the Latin square of the 3rd order ($(X_{Tri}, Y_{Tri})_{Lr3*3}$) are shown in Fig. 5.12.

From the simulation results above, it is not difficult to see the following points:

1) The new method (using triangular matrices) effectively extends the coverage area of AAs synthesized based on Latin squares. It achieves this by narrowing the main beam while maintaining a practically acceptable side lobe level compared to AAs generated using the traditional method, as shown in formula (1.8).

2) The AAs synthesized by the new method and Latin squares maintain complete coverage of spatial frequencies. The distribution of AA elements on the spatial plane is non-linear and relatively uniform, which results in minimal productivity differences with changes in the angle Ψ.

3) AAs synthesized by the new method and Latin squares demonstrate scalability: as the matrix order increases, the number of antenna elements also increases. This optimization of the AA structure ensures continuous coverage of spatial frequencies. However, it's important to note that this scalability comes at the cost of increased economic investment and thermal noise, which represent the primary drawback.

4) The new synthesis method still offers opportunities for further enhancement and innovation. One promising idea involves exploring alternative matrices to optimize and improve AA synthesis. The goal is to ensure that AAs synthesized with a specific number of elements achieve comprehensive and uniform coverage of large spatial frequencies.

5.6. Comprehensive analysis of AA design methods by using various mathematical concepts

To more comprehensively analyze the above methods and improve the research methods, here we formulate specific requirements for comparison. Let's determine the number of elements of the AA, which is equal to 25, using the following methods: the magic square of the 5th order M_5, the Latin square of the 5th order L_5, the new Latin square of the 5th order taking CDS elements L_{CDS5}, and the upper triangular matrix of the Latin square of the 5th order $UniTriL_5$. The results are as follows:

$$M_5 = \begin{bmatrix} 17 & 24 & 1 & 9 & 15 \\ 23 & 5 & 7 & 14 & 16 \\ 4 & 6 & 13 & 20 & 22 \\ 10 & 12 & 19 & 21 & 3 \\ 11 & 18 & 25 & 2 & 9 \end{bmatrix}, \tag{5.21}$$

$$L_5 = \begin{bmatrix} 1 & 2 & 3 & 4 & 5 \\ 5 & 1 & 2 & 3 & 4 \\ 4 & 5 & 1 & 2 & 3 \\ 3 & 4 & 5 & 1 & 2 \\ 2 & 3 & 4 & 5 & 1 \end{bmatrix}, \tag{5.22}$$

$$M_{\text{cds5}} = \begin{bmatrix} 3 & 6 & 7 & 12 & 14 \\ 14 & 3 & 6 & 7 & 12 \\ 12 & 14 & 3 & 6 & 7 \\ 7 & 12 & 14 & 3 & 6 \\ 6 & 7 & 12 & 14 & 3 \end{bmatrix}, \tag{5.23}$$

$$UniTriL_5 = \begin{bmatrix} 1 & 0 & 0 & 0 & 0 \\ 5 & 1 & 0 & 0 & 0 \\ 4 & 5 & 1 & 0 & 0 \\ 3 & 4 & 5 & 1 & 0 \\ 2 & 3 & 4 & 5 & 1 \end{bmatrix}. \tag{5.24}$$

The new AA synthesis method uses the formulas (5.19) and (5.20) to calculate the X and Y coordinate matrices, respectively. The spatial configuration of the designed AAs, including AAs based on the matrices M_5, L_5, and L_{CDS5} according to the old method (1.8), AAs based on L_5 and $UniTriL_5$ according to the new synthesis method, as well as the GURT subarray (5×5), is shown in Fig. 5.14.

The corresponding spatial covering frequencies along the abscissa and ordinate axes are displayed in Fig. 5.15. The simulation results of the normalized RP at a frequency of 25 MHz are illustrated in Fig. 5.16. The relevant RP parameters and the calculation times of these antenna arrays are presented in Table 5.6.

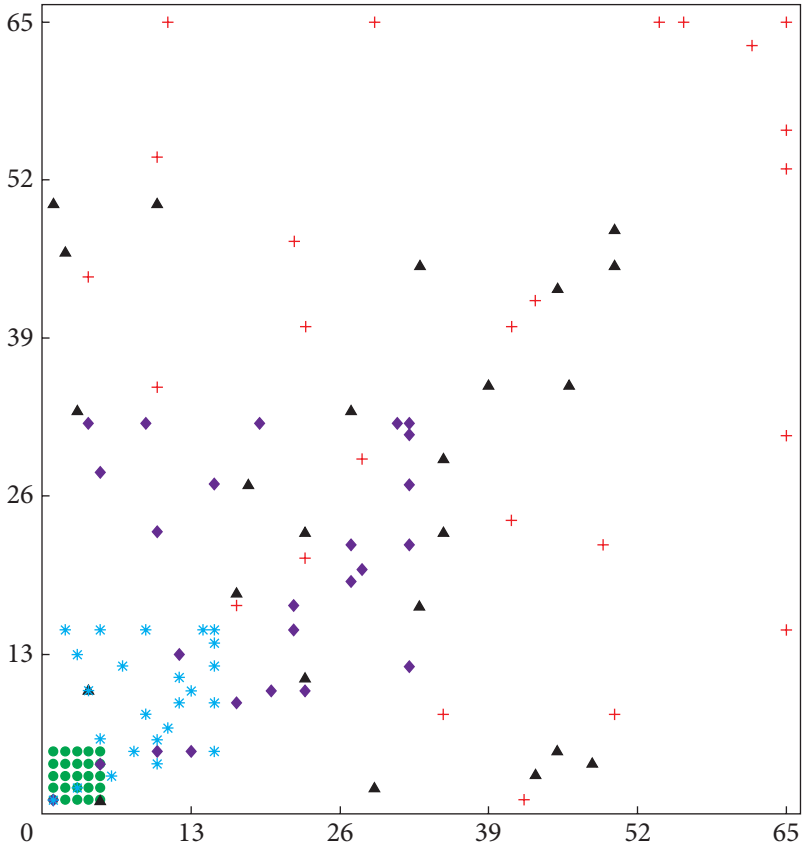

Fig. 5.14. Location of coordinates of AAs: • — GURT subarray (5×5), + — $(X, Y)_{M5}$, ✳ — $(X, Y)_{L5}$, ◆ — $(X, Y)_{Lcds5}$, and ▲ — $(X_{Tri}, Y_{Tri})_{L5}$

The spatial frequencies covered by the GURT subarray (5×5) and the AAs developed based on the magic square of the 5th order ($(X, Y)_{M5}$), the Latin square of the 5th order ($(X, Y)_{L5}$), the new Latin square (taking CDS as elements) of the 5th order ($(X, Y)_{Lcds5}$) and the new synthesis method (using triangular matrix) for fifth-order Latin square ($(X_{Tri}, Y_{Tri})_{L5}$), are shown in Fig. 5.15.

Based on the above results of the simulation, a comprehensive comparative analysis is presented as follows:

1) When a specific number of AA elements is used, the width of the main beam and the average level of the side lobes of the RP are crucial conditions for the optimal design of the AA. Considering the law of conservation of energy, these conditions cannot be optimized simultaneously. Reducing the width of the main beam must be accompanied by an increase (deterioration) in the level of the side lobes. Nevertheless, it is possible to balance these two conditions by adjusting and changing the position of the AA elements (i.e., optimizing the AA

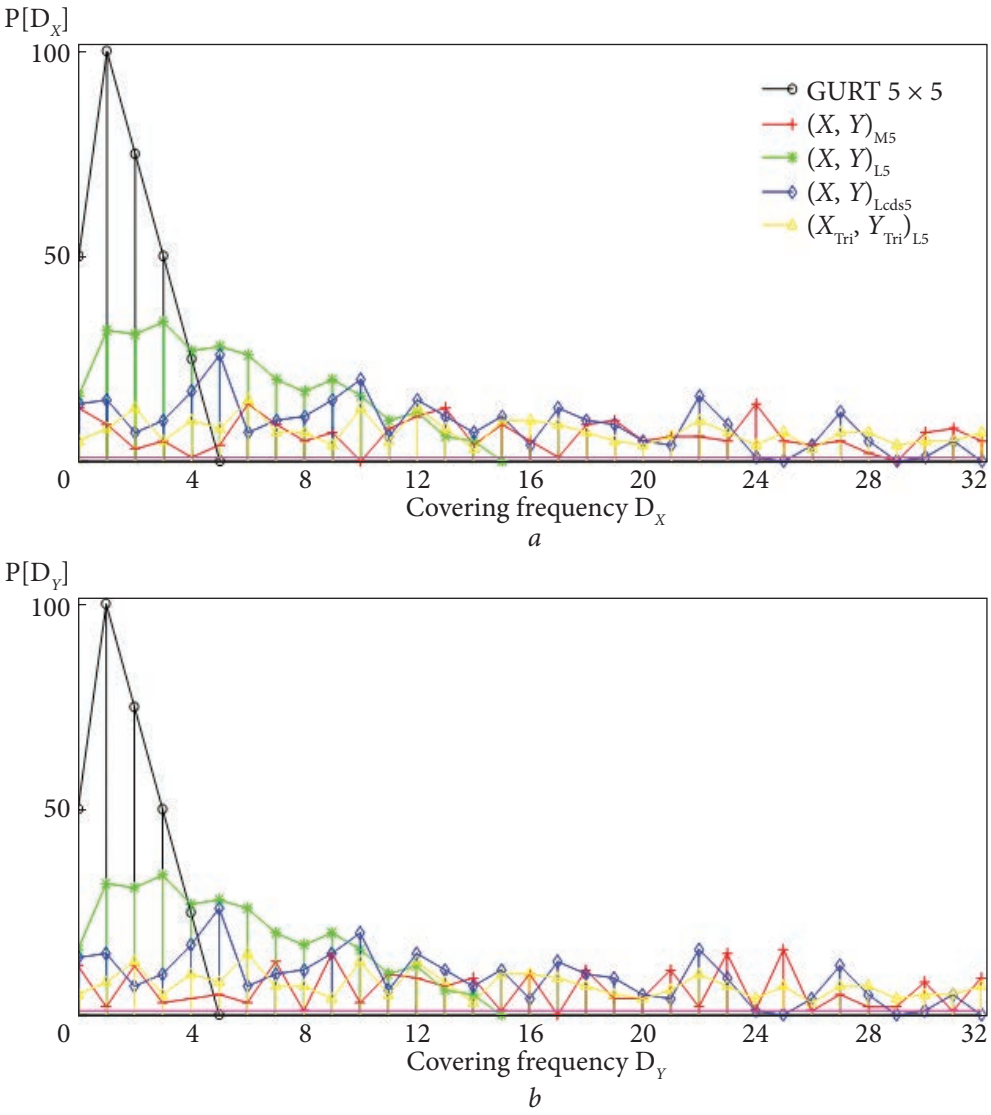

Fig. 5.15. Spatial frequencies covered by AAs: GURT subarray (5 × 5), $(X, Y)_{M5}$, $(X, Y)_{L5}$, $(X, Y)_{Lcds5}$, and $(X_{Tri}, Y_{Tri})_{L5}$, along the X (*a*) and Y (*b*) axes

design). This optimization ensures that the obtained AA's RP maintains good side lobe levels without significant degradation while achieving the narrowest possible width of the main beam.

2) AAs synthesized using magic squares and new Latin square matrices taking CDS as elements cannot completely cover the entire range of spatial frequencies. Consequently, the corresponding side lobes of the RP of the obtained AAs are slightly "dirty."

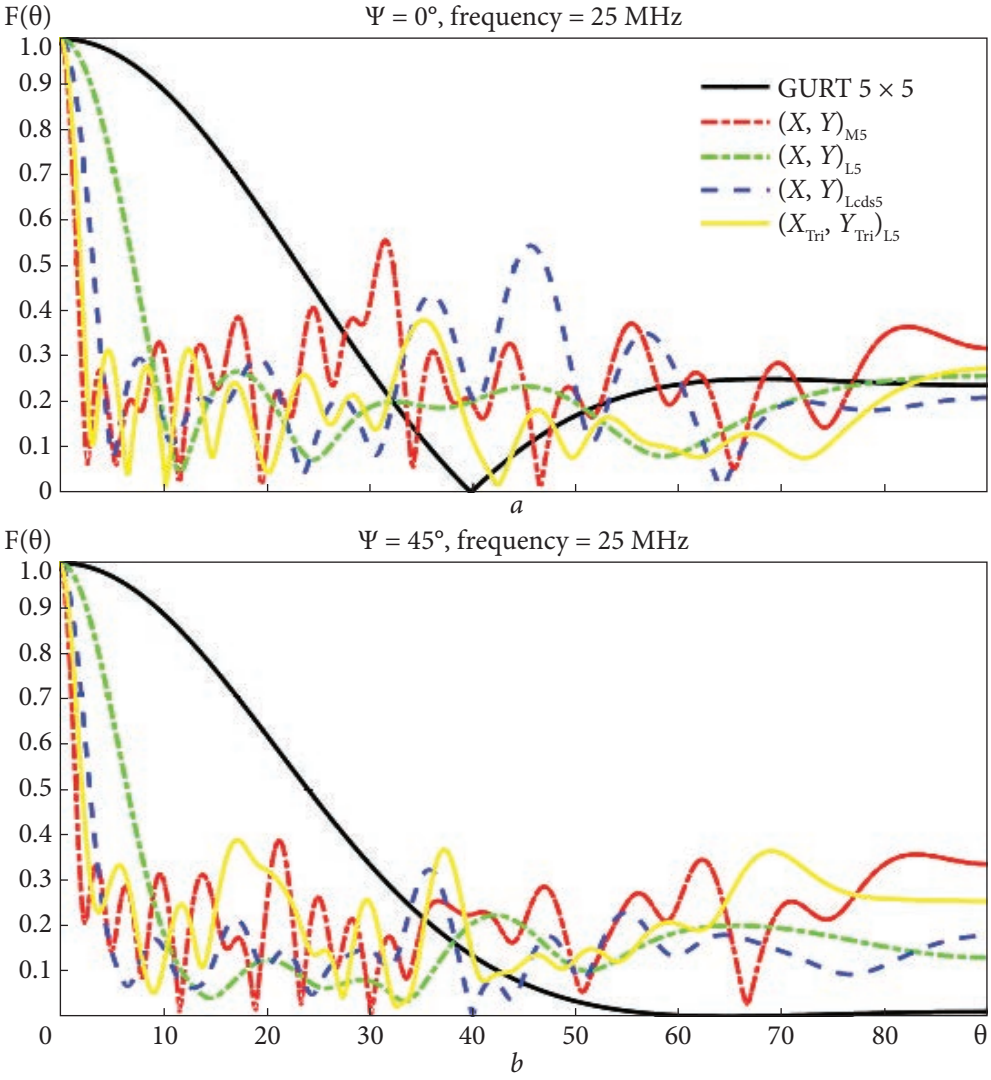

Table 5.6. **A brief comparison of the characteristics of the GURT subarray and non-equidistant AAs, which were developed based on old and new matrix synthesis methods**

Comparison parameters	GURT (5×5)	$(X, Y)_{M5}$	$(X, Y)_{L5}$	$(X, Y)_{Lcds5}$	$(X_{Tri}, Y_{Tri})_{L5}$
MBW, °	67.8867	4.8595	21.6280	7.7957	6.1966
SLL, dB	–19.6258	–13.9877	–14.1335	–14.0626	–14.0258
The number of antenna elements	25	25	25	25	25
Effective covering area, d^2	25	4225	225	1764	2500
Calculation time, seconds	3.145462	2.905225	2.780467	2.852933	2.972460

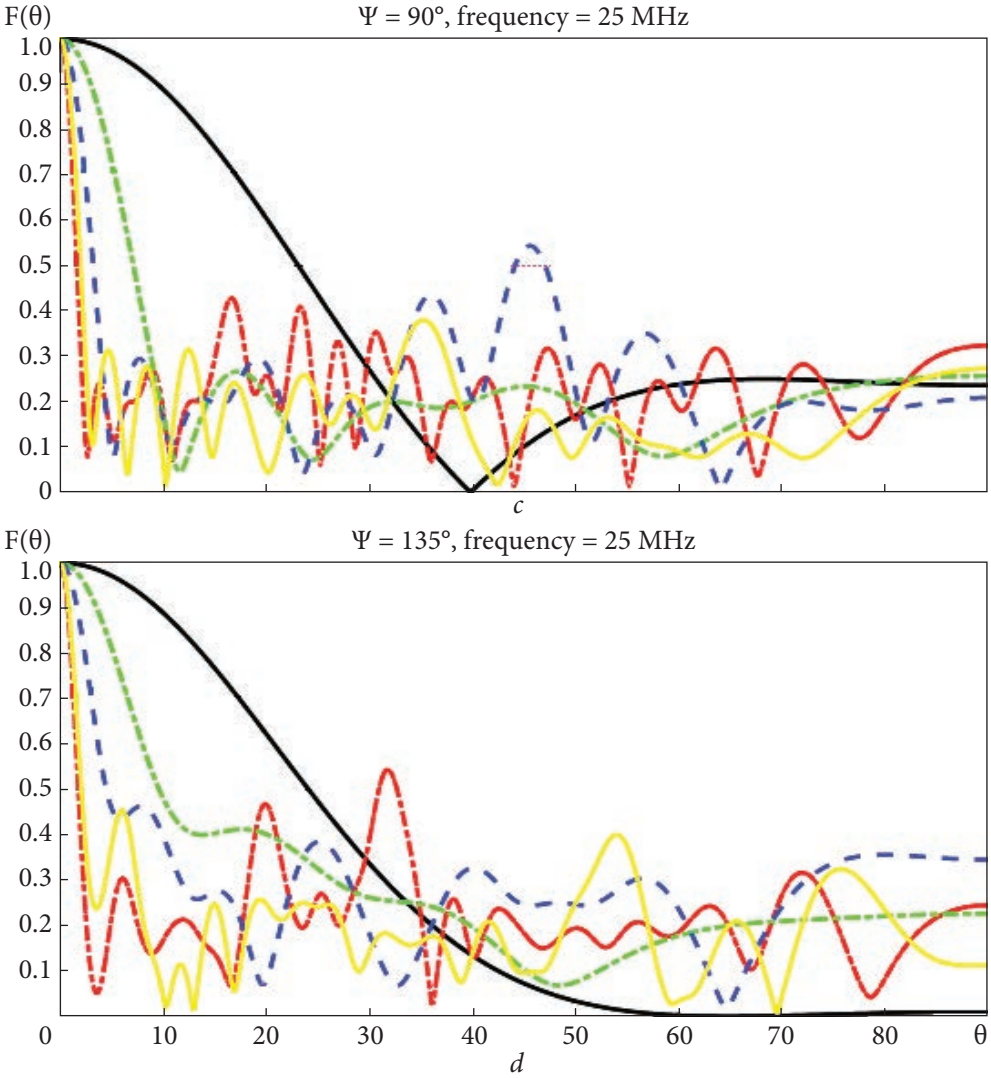

Fig. 5.16. Cross-section of the normalized RP in different planes Ψ (*a* — Ψ = 0°, *b* — Ψ = 45°, *c* — Ψ = 90°, *d* — Ψ = 135°) corresponding to the frequency of 25 MHz for the GURT subarray 5 × 5 sublattice and AAs developed based on the magic square of the 5th order $(X, Y)_{M5}$), the Latin square of the 5th order $(X, Y)_{L5}$), the new Latin square (taking CDS as elements) of the 5th order $((X, Y)_{Lcds5})$ and the new synthesis method (using triangular matrix) for 5th order Latin square $((X_{Tri}, Y_{Tri})_{L5})$

3) Compared to the magic square, the spatial frequency of the AA synthesized using the Latin square matrix is fully aligned along the *X* and *Y* axes and also has better spatial symmetry.

4) The Latin square matrix with continuous natural numbers as elements can provide full spatial frequency coverage. Furthermore, using its lower triangular matrix for AA synthesis can expand the effective area and further distri-

bute the AA elements on a wider scale while ensuring full spatial frequency coverage. This arrangement makes the width of the main RP beam of the AA narrower, and due to the "appropriate" position of the AA elements, the side lobe levels of the RP can also be maintained without deterioration.

5.7. Conclusion

The considered new approaches to the construction of non-equidistant sparse AAs, based on the use of mathematical constructions such as magic squares, Latin squares (including new Latin squares taking CDSs as elements), and triangular matrices, have made it possible to obtain a number of unique advantages over traditional AA design methods. This innovative approach enhances both the simplicity and efficiency of the design process.

Key attributes of this method include its scalability, non-linear problem-solving capabilities, and the ability to incorporate multidimensional constraints. By transforming complex non-linear optimization problems into simpler, linear matrix operations, this method provides a robust framework for a sparse AA design procedure that can be expanded and adapted as needed.

Particularly, compared to equidistant AAs (such as the GURT subarray), the superiority and usability of the sparse AA, constructed based on the matrix new method, are proven to a certain extent. Its combination of simplicity, efficiency, scalability, and adaptability makes it a powerful tool for meeting current and future AA design challenges. By transforming complex non-linear problems into manageable matrix modules and matrix operations, this approach not only improves design results but also broadens the accessibility and variety of complex AA design techniques.

CONCLUSIONS

The monograph addresses general issues related to the synthesis and design of non-quidistant sparse antenna arrays (AAs), highlighting their advantages, key parameters, and methods for synthesizing arrays. It introduces an algorithm for calculating the coordinates of elements in various two-dimensional non-equidistant (sparse planar) AAs using special matrix squares such as the Latin square, magic square, triangular square, unit matrix, etc. The radiation patterns (RPs), spatial covering frequencies, main RP beam width, and RP sidelobe levels of AAs, constructed using various special squares/matrices, are evaluated.

The main results obtained are as follows:

1) For the first time, the construction of non-equidistant AAs based on Latin squares is proposed. The AA coordinates are calculated using the same algorithm as for AAs based on magic squares, utilizing the values of the Latin square elements. This algorithm uses the generator matrix values to form an interferometer with neighboring elements. The study of directional patterns and sidelobe levels indicates that the synthesized AAs provide full spatial frequency coverage within the component placement area, albeit with significant redundancy. While this redundancy does not affect the main lobe width, it can reduce the fill and redundancy factors significantly, albeit with an increase in the average sidelobe level. The possibility of synthesizing large AAs using nested Latin squares is demonstrated, and properties of the lattices obtained using additive and multiplicative displacement and rotation parameters are explored. The results suggest that mutual rotation of individual layers within a synthetic lattice can enhance its properties. This method offers new opportunities for creating non-equidistant AAs with low fill and redundancy factors and acceptable sidelobe levels, outperforming currently used two-dimensional lattices based on cyclic difference sets (CDS). Additionally, combining a magic square with an additive shift of elements to the Latin square yields op-

timal properties, forming new Latin squares through rotation (transposition) operations.

2) A novel method of using a new CDS Latin square matrix (taking CDS as elements) for constructing sparse AAs is introduced. The AA's coordinates are calculated similarly to those in magic-square-based AAs. The values of the generative matrix serve as a basis for an interferometer/AA formed by neighboring elements. The resulting AAs almost completely cover the spatial frequency of the effective area with minimal redundancy. The RP (especially, the sidelobe levels and main beam width) of non-equidistant AAs is analyzed, demonstrating that the AAs based on Latin squares taking CDS as elements have superior characteristics compared to those created by L.E. Kopilovich and those based on nested Latin squares using magic squares as submatrices. This method opens new possibilities for creating non-equidistant AAs with small filling and redundancy factors with acceptable RP sidelobe levels, surpassing previous Kopilovich-CDS AAs, which are designed based solely on CDSs. The algorithm allows for flexible adjustment of design parameters (v, k, λ), meeting practical needs more effectively. This synthesis method is applicable in low-frequency radio telescopes.

3) A new direct and efficient method for generating sparse AAs based on Latin squares and their triangular matrices is proposed. This method ensures full spatial frequency coverage, reduces AA's redundancy, and minimizes the number of AA's elements without excessively compromising sidelobe control. The synthesized array features a very narrow RP main beam and low sidelobe levels, making it multifunctional and adaptable for various applications. Such two-dimensional non-equidistant AAs with low redundancy are suitable for radar, communication, radio astronomy, radiotherapy, remote sensing, automotive, biomedical imaging, navigation, and other fields. When the number of AA's elements synthesized using this method is sufficiently large, the array maintains a fixed geometric form, exhibiting consistent properties when the number of antenna elements is scaled.

4) Utilizing the Latin square and its triangular matrix for AA design, compared to uniform AAs at an operating frequency of 25 MHz, achieves nearly complete spatial frequency coverage within the effective area (where antenna components are located) with a low fill factor. This significantly reduces sidelobes and improves spatial frequency coverage without additional components, achieving full spatial frequency coverage.

In particular, based on new methods of constructing a two-dimensional non-equidistant (sparse planar) AA using mathematical constructions such as magic squares and Latin squares (including new Latin squares taking CDS as elements), many unique properties can be obtained, including:

1) ***Simplicity and Efficiency***. The novel approach to constructing two-dimensional non-equidistant (sparse planar) AAs using mathematical con-

structs such as magic squares and Latin squares, including new Latin squares taking CDS as elements, offers significant advantages. It circumvents the multidimensional complexity and non-linearity typical of traditional AA optimization methods by leveraging fundamental mathematical concepts such as matrix multiplication, nesting, and element generation. This results in a straightforward and efficient method for developing sparse AAs.

2) ***Regularity and Scalability***. The mathematical foundations used (magic squares, Latin squares, CDS, triangular matrices) facilitate scalability with increasing matrix order. By systematically increasing the matrix order, the synthesized AAs can achieve considerable size while maintaining regularity and predictability in their design.

3) ***Non-linearity and Multidimensionality.*** The approach to AA design through these mathematical constructs represents a nonlinear method employing linear forms (matrices). Although matrices are conventionally used for solving linear equations, here they play a crucial role in generating and evolving AA coordinate matrices of varying sizes. This approach supports multidimensional constraints, where different matrices can encode various constraints affecting the obtained AA coordinate matrix through matrix multiplication.

4) ***New Perspective and Future Directions.*** This method introduces a new perspective for AA design, distinct from traditional approaches, and offers promising directions for future research. It establishes a clear foundation with transparent levels of complexity. By expressing nonlinear challenges in a simplified linear form using matrices, the method exhibits robust scalability and adaptability. Future advancements may involve integrating, modifying, or substituting additional mathematical concepts to further optimizing AA design. As the number and complexity of designed AAs grow, comprehensive studies on the characteristics and geometric properties of sparse AAs can establish a robust knowledge base for systematic AA classification.

REFERENCES

1. Rocca, P., Oliveri, G., Mailloux, R.J., Massa, A. (2016). Unconventional phased array architectures and design methodologies. *A Review, Proc. of the IEEE*. Vol. 104, No. 3. p. 544—560. https://doi.org/10.1109/JPROC.2015.2512389
2. Ishimaru, A. (1962). Theory of unequally-spaced arrays. *IRE Transactions on Antennas and Propagation*. Vol. 10. No. 6. p. 691—702. https://doi.org/10.1109/TAP.1962.1137952
3. Jain, R., Mani, G.S. (2012). Solving "antenna array thinning problem" using genetic algorithm. *Applied Computational Intelligence and Soft Computing*. Vol. 2012. Article ID 946398. 14 p. https://doi.org/10.1155/2012/946398
4. Haupt, R.L. (1994). Thinned arrays using genetic algorithms. *IEEE Transactions on Antennas and Propagation.* Vol. 42. No. 7. p. 993—999. https://doi.org/10.1109/8.299602
5. Mahanti, G.K., Pathak, N., Mahanti, P.K. (2007). Synthesis of thinned linear antenna arrays with fixed sidelobe level using real-coded genetic algorithm. *Progress in Electromagnetics Research*. Vol. 75. p. 319—328. http://dx.doi.org/10.2528/PIER07061304
6. Zhang, L., Jiao, Y.C., Chen, B., Li, H. (2012). Orthogonal genetic algorithm for planar thinned array designs. *International Journal of Antennas and Propagation.* Vol. 2012. Article ID 319037. 7 p. https://doi.org/10.1155/ 2012/319037
7. Goudos, S.K., Sahalos, J.N. (2016). Design of large thinned arrays using different biogeography-based optimization migration models. *International Journal of Antennas and Propagation.* Vol. 2016. Article ID 5359298. 11 p. https://doi.org/10.1155/2016/5359298
8. Oliveri, G., Manica, L., Massa, A. (2010). ADS-based guidelines for thinned planar arrays. *IEEE Transactions on Antennas and Propagation*. Vol. 58. No. 6. p. 1935—1948. https://doi.org/10.1109/TAP.2010.2046858
9. Jiang, Q., Chen, J.X., Liu, D. (2015). Binary inheritance learning particle swarm optimisation and its application in thinned antenna array synthesis with the minimum sidelobe level. *IET Microwaves, Antennas & Propagation*. Vol. 9. No. 13. p. 1386—1391. https://doi.org/10.1049/iet-map.2015.0071

10. Quevedo-Teruel, O., Rajo-Iglesias, E. (2006). Ant colony optimization in thinned array synthesis with minimum sidelobe level. *IEEE Antennas and Wireless Propagation Letters*. Vol. 5. p. 349—352. https://doi.org/10.1109/ LAWP.2006.880693
11. Keizer, W.P.M.N. (2008). Linear array thinning using iterative FFT techniques. *IEEE Transactions on Antennas and Propagation.* Vol. 56. No. 8. p. 2757—2760. https://doi.org/10.1109/TAP.2008.927580
12. Keizer, W.P.M.N. (2009). Large planar array thinning using iterative FFT techniques. *IEEE Transactions on Antennas and Propagation*. Vol. 57. No. 10. p. 3359—3362. https://doi.org/10.1109/TAP.2009.2029382
13. Wang, X.K., Jiao, Y.C., Tan, Y.Y. (2012). Gradual thinning synthesis for linear array based on iterative Fourier techniques. *Progress in Electromagnetics Research*. Vol. 123. p. 299—320. http://dx.doi.org/10.2528/ PIER11100903
14. Wang, X.K., Wang, G.B. (2018). A Hybrid Method Based on the Iterative Fourier Transform andthe Differential Evolution for Pattern Synthesis of SparseLinear Arrays. *International Journal of Antennas and Propagation*. Vol. 2018. Article ID 6309192. p. 1—7. https://doi.org/10.1155/2018/6309192
15. Patent USA. No 4071848. Thinned aperiodic antenna arrays with improved peak side lobe level control / D.C. Leeper. 31/01/1978. https://patentimages. storage.googleapis. com/30/73/fa/25b9b72c3d3e8a/US4071848.pdf
16. Leeper, D.G. (1999). Isophoric arrays-massively thinned phased arrays with well-controlled sidelobes. *IEEE Transactions on Antennas and Propagation*. Vol. 47, No. 12. p. 1825—1835. https://doi.org/10.1109/8.817659
17. Sodin, L.G. (2005). Some problems of the theory of phased antenna arrays, topical for radio astronomy. *Radiophysics and Radio Astronomy*. Vol. 10 (Special Release). p. 128—142. http://dspace.nbuv.gov.ua/bitstream/handle/123456789/103841/08-Sodin.pdf?sequence=1
18. Kopilovich, L.E., Sodin, L.G. (2001). *Multielement System Design in Astronomy and Radio Science*. Dordrecht : Springer Netherlands, 183 p. https://doi.org/10.1007/978-94-015-9751-7
19. Kopilovich, L.E., Sodin, L.G. (1989). Linear non-equidistant array antennas based on difference sets. *Radio Engineering and Electronics*. Vol. 34. No. 10. p. 2059—2066. https://doi.org/10.1007/978-94-015-9751-7_6
20. Kopilovich, L.E., Sodin, L.G. (1994). Synthesis of non-equidistant array antennas based on the theory of difference sets. *Radio Engineering and Electronics*. Vol. 39. No. 3. p. 380—389.
21. Kopilovich, L.E., Sodin, L.G. (1992). Sectionalized nonequidistant linear array antennas based on difference sets. *Radio Engineering and Electronics*. Vol. 37. No. 12. p. 2155—2160.
22. Kravchenko, V.F., Lutsenko, V.I., Lutsenko, I.V., et al. (2017). Non-equidistant two-dimensional antenna arrays based on "magic" squares. *Journal of Measurement Science and Instrumentation*. Vol. 8. No. 3. p. 244—253. https://doi.org/10.3969/j.issn.1674-8042.2017.03.006
23. Kravchenko, V.F., Lutsenko, V.I., Luo, Y,. et al. (2019). Non-equidistant two-dimensional antenna arrays based on Latin squares. *Journal of Measurement Science and*

Instrumentation. Vol. 10. No. 1. p. 38—48. https://doi.org/10.3969/j.issn.1674-8042.2019.01.006
24. Luo, Y., Guo, Q., Lutsenko, V.I., Zheng, Y. (2019). Nonequidistant Two-Dimensional Antenna Arrays Based on the Structure of Latin Squares Taking Cyclic Difference Sets as Elements. *European Microwave Conference in Central Europe, EuMCE-2019*: Conf. Proc. (Prague, Czech Republic, 13—15 May 2019). Prague, p. 421—424. https://ieeexplore.ieee.org/document/ 8874813/references#references
25. Colbourn, C.J., Dinitz, J.H. (Eds.). (2006). *Handbook of Combinatorial Designs*. Chapman and Hall /CRC, 1016 p. https://doi.org/10.1201/ 9781420010541
26. Axler, S. (2014). *Linear Algebra Done Right*. Cham: Springer International Publishing, 340 p. https://doi.org/10.1007/978-3-319-11080-6
27. Konovalenko, A.A., Yerin, S.M., Bubnov, I.M., et al. (2016). Astrophysical studies using small-sized low-frequency new-generation radio telescopes. *Radiophysics and Radio Astronomy*. Vol. 21. No.2. p. 83—131. https://doi.org/10.15407/rpra21.02.083
28. Konovalenko, A.A. (2017). Progress in low-frequency radio astronomy and I.S. Shklovskii's contribution to its development. *Astron. Rep*. Vol. 61. p. 317—323. https://doi.org/10.1134/S1063772917040102
29. Baumert, L.D. (1971). *Cyclic Difference Sets (Lecture Notes in Mathematics, 182)*. Berlin: Springer-Verlag, 172 p.
30. Bernstein, D.S. (2009). *Matrix Mathematics: Theory, Facts, and Formulas* (2nd ed.). Princeton: Princeton University Press, 1184 p.
31. Horn, R.A., Johnson, C.R. (2013). *Matrix Analysis* (2nd ed.). Cambridge: Cambridge University Press, 643 p.
32. Shifrin, Ya.S. (1971). *Issues of the statistical theory of antennas*. M.: Rad. radio, 383 p.
33. Kopilovych, L.E. (2012). Redundant changes of antennas on the two-dimensional aperture of the interferometer, which provide full coverage of the central regions in the plane of spatial frequencies. *Radiophysics and Radioastronomy*. Vol. 17. No. 2. p. 1176—182.
34. Colbourn, C.J., Dinitz, J.H. (Eds.). (2007). *Handbook of Combinatorial Designs* (2nd ed.). Boca Raton: Chapman & Hall/CRC, 1016 p.
35. Björner, A.A, Stanley, R.P. (2010). *Combinatorial Miscellany*. Geneva: L'Enseignement Mathématique, 164 p.
36. Dénes, J., Keedwell, A.D. (1974). *Latin Squares and their Applications*. New York-London: Academic Press, 547 p.
37. Fujimotom, K. (2001). *Mobile Antenna Systems Handbook* (3rd ed.). Norwood: Artech House, 680 p.
38. Lorente, D., Limbach, M., Gabler, B. (2019). L-Band Antenna Array for Next Generation DLR Airborne SAR Sensor. *12th German Microwave Conference (GeMiC-2019)*: Conf. Proc. (Stuttgart, Germany, 25—27 March 2019). Stuttgart, p. 182—185. https://doi.org/10.23919/ GEMIC.2019.8698151
39. Arnauti, El-G., Saalmann, O., Brenner, A.R. (2017). Ultra-high resolution airborne experiments with a new Ka-band SAR sensor. *European Radar Conference (EURAD-2017)*: Conf. Proc. (Nuremberg, Germany, 11-13 October 2017). Germany, p. 409—412. https://doi.org/10.23919/ EURAD.2017.8249234

40. Kraus, T., Krieger, G., Bachmann, M., et al. (2021). Formation Considerations for Distributed Satellite SAR Systems. *13th European Conference on Synthetic Aperture Radar. (EUSAR-2021)*: Conf. Proc. (Germany, 29 March—01 April 2021, online). Germany, p. 1—6. https://ieeexplore.ieee.org/ document/9472632
41. Fang, T., Deng, Y., Liang, D., et al. (2020). Multichannel Sliding Spotlight SAR Imaging: First Result of GF-3 Satellite. *IEEE Transactions on Geoscience and Remote Sensing.* Vol. 60. p. 1925—1928. https://doi.org/10.1109/TGRS. 2021.3068208
42. Li, Q., Feng, L., Zheng, S., et al. (2022). Research on Sliding spotlight imaging algorithm. *3rd China International SAR Symposium. (CISS-2022)*: Conf. Proc. (Shanghai, China, 02—04 November 2022). Shanghai, p. 1—5. https://doi.org/10.1109/ CISS57580.2022.9971246
43. Kendra, J.R., Bloy, G.J., Hughes, J. (2021). Rotary-Motion-Extended Array Synthesis (R-MXAS): Simultaneous Sparsity and Sensitivity in a Synthetic Aperture Imaging Radiometer. *IEEE International Geoscience and Remote Sensing Symposium. (IGARSS-2021)*: Conf. Proc. (Brussels, Belgium, 11—16 July 2021). Brussels, p. 7696-7699. https://doi.org/10.1109/ IGARSS47720.2021.9554144
44. Chen, S. (2017). An Efficient Method for Investigating and Optimizing Near Field Characteristics of Planar Antenna Arrays. *Wireless Personal Communications: An International Journal.* Vol. 95 (2). p. 223—232. https://doi.org/10.1007/s11277-016-3888-2
45. Bogosanovic, M., Williamsoni, A.G. (2005). Antenna Array with Beam Focused in Near Field Zone. *Electronics Letters*. Vol. 39. p. 704—705. https://doi.org/10.1049/ el:20030479
46. Wang, X., Zhong, Y., Wang, Y. (2015). An Improved Antenna Array Pattern Synthesis Method Using Fast Fourier Transform. *International Journal of Antennas and Propagation.* Vol. 2015 (Special Issue). Article ID 316962. p. 1—9. https://doi.org/ 10.1155/2015/316962
47. Wang, D., Shen, Z., Su, X., et al. (2021). Gm-Compensated 46-101 GHz Broadband Power Amplifier for High-Resolution FMCW Radars. *IEEE International Symposium on Circuits and Systems (ISCAS-2021)*: Conf. Poc. (Daegu, South Korea, 22—28 May 2021). Daegu, p. 1—5. https://doi.org/10.1109/ ISCAS51556.2021.9401773
48. Morrison, R.L., Phelps, E.B. (2019). Radio Astronomy Techniques for Multistatic Radar Imaging and Localization of Space Objects. *2019 International Applied Computational Electromagnetics Society Symposium (ACES-2019)*: Conf. Proc. (Miami, FL, USA, 14—19 April 2019). Miami, p. 1—2. https://ieeexplore.ieee.org/document/8713030
49. Carter, W.H. (1999). On Refocusing a Radio Telescope to Image Sources in the Near Field of the Antenna Array. *IEEE Transactions on Antennas and Propagation*. Vol. 37 (3). p. 314—319. https://doi.org/10.1109/8.18727
50. Chen, S.-P. (2014). Improved Near Field Focusing of Antenna Arrays with Novel Weighting Coefficients. *2014 IEEE 6th International Symposium on Wireless Vehicular Communications (WiVeC 2014)*: Conf. Proc. (Vancouver, BC, Canada, 14—15 September 2014). Vancouver, p. 1—4. https://doi.org/10.1109/WIVEC.2014.6953228
51. Schüngel, M., Dietrich, S., Ginthör, D., et al. (2020). Analysis of Time Synchronization for Converged Wired and Wireless Networks. *2020 25th IEEE International Conference on Emerging Technologies and Factory Automation (ETFA)*: Conf. Proc. (Vienna,

Austria, 08—11 September 2020). Vienna, p. 198—205. https://doi.org/10.1109/ETFA46521.2020. 9212068
52. Ebadi, S., Gatti, R. V., Marcaccioli, L., et al. (2009). Near Field Focusing in Large Reflector Array Antennas Using 1-bit Digital Phase Shifters. 2009 European Microwave Conference (EuMC-2009): Conf. Proc. (Rome, Italy, 29 September—01 October 2009). Rome, p. 1029—1032. https://doi.org/10.23919/ EUMC.2009.5296377
53. Mailloux, R.J. (2005). *Phased Array Antenna Handbook* (2nd ed.). Norwood: Artech House Inc., 515 p.
54. Goldstein, R.M., Zebker, H.A. (1987). Interferometric radar measurement of ocean surface currents. *Nature*. Vol. 328, No. 6132. p. 707—709. https://doi.org/10.1038/328707a0
55. Piquenard, A. (1974). *Radio Wave Propagation*. New York: Wiley, 343 p. https://doi.org/10.1007/978-1-349-01394-4
56. Mazda, F. (1993). *Telecommunications Engineer's Reference Book* (1st ed.). Oxford: Butterworth-Heinemann, 1142 p. https://doi.org/10.1016/C2013-0-06529-2
57. Collin, R.E. (1969). *Antenna Theory, Part 1* (R.E. Collin, F.J. Zucker Eds.). New York: McGraw-Hill Book Company, 676 p. ISBN 10: 0070117993
58. Fang, D.G. (2010). *Antenna Theory and Microstrip Antennas*. Boca Raton: CRC Press, 311 p. https://doi.org/10.1201/b10302
59. Balanis, C.A. (1997). *Antenna Theory Analysis and Design*. Hoboken: John Wiley, 1095 p.
60. Hartley, R.V.L. (1923). Relations of carrier and side-bands in radio transmission. *Proceedings of the Institute of Radio Engineers*. Vol. 2, No. 2. p. 90—112. https://doi.org/10.1109/JRPROC.1923.219862
61. Shu, F., Qin, Y., Liu, T., et al. (2018). Low-Complexity and High-Resolution DOA Estimation for Hybrid Analog and Digital Massive MIMO Receive Array. *IEEE Transactions on Communications*. Vol. 66, No. 6. p. 2487—2501 https://doi.org/10.1109/TCOMM.2018.2805803
62. Couch, Leon W. (2001). *Digital and analog communication systems* (7th ed.). Englewood Cliffs: Prentice-Hall Inc., 758 p.
63. Hui, W., Chen, Z., Zheng, S. (2017). Preliminary Research of Low-RCS Moving Target Detection Based on Ka-Band Video SAR. *IEEE Geoscience and Remote Sensing Letters*. Vol. 14, No. 6. p. 1—5. https://doi.org/10.1109/ LGRS.2017.2679755
64. Tommasini, R., Löwenthal, F., Balmer, J., et al. (1998). Iterative method for phase-amplitude retrieval and its application to the problem of beam-shaping and apodization. *Opt. Commun*. Vol. 153, No. 4—6. p. 339—346. https://doi.org/10.1016/S0030-4018(98)00246-6
65. Hao, Z.-C., He, M., Hong, W. (2016). Design of a millimeter-wave high angle selectivity shaped-beam conformal array antenna using hybrid genetic/space mapping method. *IEEE Antennas Wireless Propag. Lett*. Vol. 15. p. 1208—1212. https://doi.org/10.1109/LAWP.2015.2501403
66. Josefsson, L. (2006). *Conformal Array Antenna Theory and Design*. Hoboken: Wiley-IEEE Press, 488 p. https://doi.org/10.1002/047178012X
67. Bhattacharyya, A.K. (2006). *Phased Array Antennas: Floquet Analysis, Synthesis, BFNs and Active Array Systems*. Hoboken: Wiley-Interscience, 528 p.

68. Chatterjee, D. (2006). Numerical Modeling of Conformal Phased Arrays on Tactical Systems. *2006 IEEE Military Communications conference (MILCOM-2006): Conf. Proc. (Washington, USA, 23—25 October 2006)* Washington, p. 1—7. https://doi.org/10.1109/MILCOM.2006.302359
69. Li, H., Jiang, Y., Ding, Y., et al. (2018). Low-sidelobe pattern synthesis for sparse conformal arrays based on PSO-SOCP Optimization. *IEEE Access*. Vol. 6. p. 77429—77439. https://doi.org/10.1109/ACCESS.2018.2883042
70. Lee, S.W. (1982). A Review of GTD Calculation of Mutual Admittance of Slot Conformal Array. *Electromagnetics*. Vol. 2, No. 2. p. 85—127. https://doi.org/10.1080/02726348208915159
71. Ertürk, V.B., Bakir, O., Rojas, R.G., et al. (2006). Scan Blindness Phenomenon in Conformal Finite Phased Arrays of Printed Dipoles. *IEEE Trans. Antennas and Propagat.* Vol. 54, No. 6. p. 1699—1708. https://doi.org/10.1109/ TAP.2006.875482
72. Shapira, J., Felsen, L.B., Hessel, A. (1974). Ray Analysis of Conformal Antenna Arrays. *IEEE Trans. Antennas. Propagat*. Vol. 22, No. 1. p. 49—63. https://doi.org/10.1109/TAP.1974.1140710
73. Macon, C.A., Trott, K.D., Kempel, L.C. (2003). A Practical Approach to Modeling Doubly Curved Conformal Microstrip Antennas. *Progress in Electromagnetics Research (PIER)*. Vol. 40. p. 295—314. http://dx.doi.org/10.2528/ PIER02122903
74. Balanis, C.A. (2016). *Antenna theory: analysis and design* (3rd ed.). New Jersey: John Wiley & Sons, 1072 p.
75. Jakes, W.C. (1974). *Microwave mobile communications* (1st ed.). New Jersey: John Wiley & Sons, 645 p.
76. Panduro, M.A., Covarrubias, D.H., Brizuela, C.A., et al. (1992). A multi-objective approach in the linear antenna array design. *AEU-Int J Electron Commun*. 2005. Vol. 59. No. 4. p. 205—212 https://doi.org/10.1016/j.aeue.2004.11.017
77. Haykin, S., Reilly, J. P., Kezys, V. (1992). Some aspects of array signal processing. *IEE Proceedings F - Radar and Signal Processing.* Vol. 139, No. 1. p. 1—26. https://doi.org/10.1049/ip-f-2.1992.0001
78. Munk, B.A. (2003). *Finite Antenna Arrays and FSS*. NY, USA: IEEE-Wiley Press, 357 p. https://doi.org/10.1002/0471457531
79. Bhattacharya, A.K. (2006). *Phased Array Antennas: Floquet Analysis, Synthesis, BFNs and Active Array Synthesis*. NY, USA: Wiley-Interscience, 528 p.
80. Lo, Y.T., Lee, S.W. (1998). *Antenna Handbook: Theory, Applications and Design*. NY, USA: Van Nostrand Reinhold Co., 1131 p. https://doi.org/10.1007/ 978-1-4615-6459-1
81. Ertürk, V.B., Rojas, R.G. (2003). Efficient Analysis of Input Impedance and Mutual Coupling of Microstrip Antennas on Large Cylinders. *IEEE Trans. Antennas and Propagat.* Vol. 51. No. 4. p. 739—749. https://doi.org/10.1109/ TAP.2003.811060
82. Chapman, S.J., Lawry, J.M.H., Ockendon, J.R., et al. (1999). On The Theory of Complex Rays. *SIAM Review*. Vol. 41. No. 3. p. 417—509. https://doi.org/10.1137/S0036144599352058
83. Almagboul, M.A., Shu, F., Qian, Y., et al. (2019). Atom search optimization algorithm based hybrid antenna array receive beamforming to control sidelobe level and steering the null. *AEU-Int J Electron Commun*. Vol. 111. Article ID 152854. 15 p. https://doi.org/10.1016/j.aeue.2019. 152854

84. Zhang, J., Mao, X., Zhang, M., et al. (2023). Synthesis of thinned planar arrays based on precoded subarray structures. *IEEE Antennas and Wireless Propagation Letters*. Vol. 22. No. 1. p. 44—8. https://doi.org/10.1109/ LAWP.2022.3201382
85. Kibaroglu, K., Sayginer, M., Rebeiz, G.M. (2018). A scalable 64-element 28 ghz phased-array transceiver with 50 dbm eirp and 8-12 gbps 5g link at 300 meters without any calibration. *2018 IEEE/MTT-S International Microwave Symposium — IMS (IMS-2018)*: Conf. Proc. (Philadelphia, PA, USA, 10—15 June 2018). Philadelphia, p. 496—8. https://doi.org/10.1109/ MWSYM.2018.8439404
86. Maher, T., Cheng, D. (1963). Random removal of radiators from large linear arrays. *IEEE Trans Antennas and Propagation*. Vol. 11. No. 2. p. 106—112. https://doi.org/10.1109/TAP. 1963.1138000
87. Lo, Y. (1964). A mathematical theory of antenna arrays with randomly spaced elements. *IEEE Trans Antennas and Propagation*. Vol. 12, No. 3. p. 257—268. https://doi.org/10.1109/TAP.1964.1138220
88. Urvinder, S., Munish, R. (2014). Design of thinned concentric circular antenna arrays using firefly algorithm. *IET Microw. Antennas. Propag*. Vol. 8. No. 12. p. 894—900. https://doi.org/10.1049/iet-map.2013.0695
89. Aksoy, E., Afacan, E. (2009). Planar antenna pattern nulling using differential evolution algorithm. *AEU-Int J Electron. Commun*. Vol. 63. No. 2. p. 116—122. https://doi.org/10.1016/j.aeue.2007.11.006
90. Ghosh, P., Das, S. (2011). Synthesis of thinned planar concentric circular antenna arrays — A differential evolutionary approach. *Prog. Electromagn. Res. B*. Vol. 29. p. 63—82. http://dx.doi.org/10.2528/PIERB11020204
91. Vankayalapati, S., Pappula, L., Ghosh, D. (2023). Element thinning using discrete cat swarm optimization for 5G/6G applications. *Prog. Electromagn. Res. B*. Vol. 101. p. 119—135. https://doi.org/10.2528/PIERB23051702
92. Pradhan, P.M., Panda, G. (2012). Connectivity constrained wireless sensor deployment using multiobjective evolutionary algorithms and fuzzy decision making. *Ad. Hoc. Networks*. Vol. 10. No. 6. p. 1134—1145. https://doi.org/10.1016/ j.adhoc.2012.03.001
93. Zhang, J., Mao, X., Zhang, M., et al. (2023). Synthesis of thinned planar arrays based on precoded subarray structures. *IEEE Antennas Wirel. Propag. Lett*. Vol. 22. No. 1. p. 44—48. https://doi.org/10.1109/LAWP.2022.3201382
94. Durmus, A. (2020). The optimal synthesis of thinned concentric circular antenna arrays using slime mold algorithm. *Electromagnetics*. Vol. 40. No. 8. p. 541-553. https://doi.org/10.1080/02726343.2020.1838044
95. Monzingo, R.A., Haupt, R., Miller, T. (2011). *Introduction to Adaptive Arrays* (2nd ed.). Raleigh: SciTechPublishing, Inc., 559 p. https://doi.org/10.1049/ SBEW046E
96. Trees, H.L.V. (2004). *Optimum Array Processing: Part IV of Detection, Estimation, and Modulation Theory*. Virginia: John Wiley & Sons, 1471 p.
97. Naidu, P.S. (2009). *Sensor Array Signal Processing* (2nd ed.). London: CRC Press, 558 p.
98. Massa, A., Rocca, P., Oliveri, G. (2015). Compressive Sensing in Electromagnetics — A Review. *IEEE Antennas and Propagation Magazine*. Vol. 57. No. 1. p. 224—38. https://doi.org/10.1109/MAP.2015.2397092

99. Berry, M.V. (1989). Uniform Asymptotic Smoothing of Stokes' Discontinuities. *Proc. R. Soc. Lond. A*. Vol. 422. p. 7—21. https://doi.org/10.1098/ rspa.1989.0018
100. Thors, B., Rojas, R.G. (2003). Uniform Asymptotic Solution for the Radiation from a Magnetic Current Source on a Large Dielectric Coated Circular Cylinder: Non-Paraxial Region. *Radio Science*. Vol. 38. No. 5. 12 p. https://doi.org/10.1029/2002RS002782
101. Togköz, C., Pathak, P.H., Marhefka, R.J. (2005). An Asymptotic Solution for the Surface Magnetic Field Within the Paraxial Region of a Circular Cylinder with a Impedance Boundary Condition. IEEE Trans. Antennas Propagat. Vol. 53. No. 4. p. 1435—1443. https://doi.org/10.1109/TAP.2005. 844461
102. Togköz, C., Marhefka, R.J. (2006). A UTD Based Asymptotic Solution for the Surface Magnetic Field on a Source Excited Circular Cylinder with an Impedance Boundary Condition. IEEE Trans. Antennas Propagat. Vol. 54. No. 6. p. 1750–1757. https://doi.org/10.1109/TAP.2006.875490
103. Elliot, R.S. (2003). *Antenna Theory and Design* (rev. ed.). NY, USA: IEEE-Wiley Press (Classic Reissue), 625 p.
104. Ridwan, M., Abdo, M., Jorswieck, E. (2011). Design of non-uniform antenna arrays using genetic algorithm. *13th International Conference on Advanced Communication Technology (ICACT2011)*: Conf. Proc. (Gangwon, South Korea, 13-16 February 2011). Gangwon, p. 422—427. https://ieeexplore.ieee.org/xpl/conhome/5740523/proceeding
105. Simon, R.S., Aragon-Zavala, A. (2007). *Antennas and Propagation for Wireless Communication Systems* (2nd ed.). London: John Wiley & Sons., 546 p.
106. Marr, J.M., Snell, R.L., Kurtz, S.E. (2016). *Fundamentals of radio astronomy: Observational methods*. Boca Raton: CRC Press Publ., 350 p.
107. Condon, J.J., Ransom S.M. (2016). *Essential Radio Astronomy*. Princeton: Princeton University Press Publ., 376 p.
108. Mogyla, A.A., Mytsenko, I.M., Voytovich, O.A., et al. (2019). Building a passive-active radio-meteorological measuring system based on dual-frequency radar. *Telecommunications and Radio Engineering*. Vol. 78. No. 15. p. 1355—1367. https://doi.org/10.1615/TelecomRadEng.v78.i15.50
109. Coleman, C.J., Watson, R.A., Yardley, H. (2008). A practical bistatic passive radar system for use with DAB and DRM illuminators. *2008 IEEE Radar Conference*: Conf. Proc. (Rome, Italy, 26-30 May 2008). Rome, p. 1—6.
110. Brzozowski, M., Pakowski, M., Jakielaszek, Z., et al. (2021). Challenges of preparation and realization of combined field tests of passive and active radar sensors on an example APART-GAS 2019 trials. *2021 IEEE 8th International Workshop on Metrology for AeroSpace (MetroAeroSpace)*: Conf. Proc. (Naples, Italy, 23-25 June 2021). Naples, p. 188—192. https://doi.org/10.1109/MetroAeroSpace51421.2021.9511746
111. Fränken, D., Liegl, A. (2022). Integration of Multi-Band Passive and Multi-Functional Active Radar Data. *IEEE Radar Conference. (RadarConf22)*: Conf. Proc. (New York City, NY, USA, 21-25 March 2022). NY, p. 1—6. https://doi.org/10.1109/RadarConf2248738.2022.9764215
112. Pavlikov, V., Volosyuk, V., Zhyla, S., et al. (2021). Active-Passive Radar for Radar Imaging from Aerospace Carriers. *IEEE 19th International Conference on Smart Tech-*

nologies (EUROCON): Conf. Proc. (Lviv, Ukraine, 06—08 July 2021). Lviv, p. 18—24. https://doi.org/10.1109/EUROCON52738. 2021.9535619
113. Andriychuk, M. (2021). Asymptotic regularisationof the solution to theproblemof electromagneticfield scattering froma set of small impedanceparticles. *IET Microw. Antennas Propag*. Vol. 15. No. 10. p. 1330—1346. https://doi.org/10.1049/ mia2.12171
114. Bird, T.S. (1985). Accurate Asymptotic Solution for the Surface Field Due to Apertures in a Conducting Cylinder. *IEEE Trans. Antennas and Propagat*. Vol. 33. p. 1108—1117. https://doi.org/10.1109/TAP.1985.1143497
115. Bahrami, H., Porter, E., Santorelli, A., et al. (2015). Flexible sixteen antenna array for microwave brest cancer detection. *IEEE Transactions on Biomedical Engineering*. Vol. 62. No. 10. p. 2516—2525. https://doi.org/10.1109/ TBME.2015.2434956
116. Volosyuk, V., Zhyla, S., Pavlikov ,V., et al. (2021). Mathematical description of imaging processes in ultra-wideband active aperture synthesis systems using stochastic sounding signals. *Radioelectronic and Computer Systems*. No. 4. p. 166—182. https://doi.org/10.32620/reks.2021.4.14
117. Patwari, A., Gudheti, R.R. (2020). Novel MRA-Based Sparse MIMO and SIMO Antenna Arrays for Automotive Radar Applications. *Progress In Electromagnetics Research B*. Vol. 86. p. 103—119. https://doi.org/ 10.2528/PIERB19121602
118. Schooneveld, V.C. (1987). *Image Formation from Coherence Functions in Astronomy*. Berlin: Springer Publ., 340 p. https://doi.org/10.1007/978-94-009-9449-2
119. Carozzi, T.D., Woan, G. (2021). A generalized measurement equation and van Cittert-Zernike theorem for wide-field radio astronomical interferometry. *Monthly Notices of the Royal Astronomical Society*. Vol. 395. No. 3. p. 1558—1568. https://doi.org/10.1111/j.1365-2966.2009.14642.x
120. Cappellen, W.A., Ardenne, A. (2017). Development of mid-frequency aperture arrays for radio astronomy. *IEEE Radio and Antenna Days of the Indian Ocean (RADIO-2017)*: Conf. Proc. (Cape Town, South Africa, 25-28 September 2017). Cape Town, p. 1—2. https://doi.org/10.23919/RADIO.2017.8242214
121. Hall, P.J., Benthem, P., Sutinjo, A.T. (2016). Aperture array verification system 1: Overview of a square kilometre array prototype. *International Conference on Electromagnetics in Advanced Applications (ICEAA-2016)*: Conf. Proc. (Cairns, QLD, Australia, 19—23 September 2016). Cairns, p. 345—348. https://doi.org/10.1109/ ICEAA. 2016.7731394
122. International Commission on Non-Ionizing Radiation Protection (ICNIRP). (2009). *Exposure to high frequency electromagnetic fields, biological effects and health consequences (100kHz — 300GHz)*. Germany, 358 p. http://www.emf.ethz.ch/archive/ var/ICNIRP_effekte_RFReview.pdf
123. Stutzman, W.L., Thiele, G.A. (2012). *Antenna theory and design* (3rd ed.). New York: Wiley, 848 p.
124. Lutsenko, I.V., Popov, I.V., Lutsenko, I.V. (2008). Bistatic Radars with Illumination by Ionospheric Signals of High-Frequency Communication Stations. *Telecommunications and Radio Engineering*. Vol. 67. No. 4. p. 285—292. https://doi.org/10.1615/ TelecomRadEng.v67.i4.10
125. Lutsenko V. I., Lutsenko I. V., Popov I. V. (2008). Illumination of air environment using radiation of SW broadcasting stations. *The 5th European Radar Conference*:

Conf. Proc. (Amsterdam, Netherlands, 30—31 October 2008). Amsterdam, p. 396—399. https://ieeexplore.ieee.org/stamp/ stamp.jsp?tp=&arnumber=4760885
126. Lutsenko, V.I., Lutsenko, I.V., Popov, I.V. (2015). Illumination of the Air Environment Using Radiation of HF Broadcast Stations. *Radiophysics and Quantum Electronics*. Vol. 58. No. 1. p. 9—18. https://doi.org/10.1007/ s11141-015-9576-3
127. Anderson, T.S., McCarthy, M.P., Holzworth, R.H. (2020). Detection of VLF attenuation in the Earth-ionosphere waveguide caused by X-class solar flares using a global lightning location network. *Space Weather*. Vol. 18. Article ID e2019SW002408. 9 p. https://doi.org/10.1029/2019SW002408
128. Georges, T.M. (1967). Evidence for the influence of atmospheric waves on ionospheric motions. *Journal of Geophysical Research*. Vol. 72. No. 1. p. 422—425. https://doi.org/10.1029/JZ072i001p00422
129. Hussar, P.E., Smith-Rowland, E.M. (2002). An Asymptotic Solution for Boundary Layer Fields Near a Convex Impedance Surface. *Journal of Electromagnetic Waves and Applications*. Vol. 16. No. 2. p. 185—208.
130. Federal Communications Commission (FCC). (2016). *FCC. Title 47: Telecommunication, Electronic Code of Federal Regulations*. https://www.ecfr.gov/current/title-47
131. Chatterjee, D. (2005). Paraxial and Source Region Behavior of a Class of Asymptotic and Rigorous (MoM) Solutions in the High-Frequency Planar Limit. *IEEE Antennas and Wireless Propagation Letters*. Vol. 4. p. 71—74. https://doi.org/10.1109/LAWP.2005.844140
132. Chatterjee, D. (2005). Paraxial Region Comparison of Creeping Wave Formulations for Axial and Circumferential Magnetic Current Elements on a PEC Circular Cylinder. *IEEE Antennas and Propagation Symposium Digest*: Conf. Proc. (Washington, DC, 3—8 July 2005). Washington, Vol. 3B. p. 147—150. https://doi.org/10.1109/APS.2005.1552456
133. IEEE. (2014). *American National Standard Dictionary of Electromagnetic Compatibility (EMC) including Electromagnetic Environmental Effects (E3). ANSI C63.14-2014 (Revision of ANSI C63.14-2009)*. p. 1—76, https://doi.org/10.1109/IEEESTD.2014.6974973
134. Volosyuk, V. & Zhyla, S. (2022). Statistical Theory of Optimal Stochastic Signals Processing in Multichannel Aerospace Imaging Radar Systems. *Computation*. Vol 10. Special Issue. Article ID 224. 16 p. https://doi.org/10.3390/computation10120224
135. ITU. (1990). Feasibility of Frequency Sharing between Radio Astronomy and other Services (Report 696-2). *CCIR: Doc. of the XVIIth Plenary Assembly*. Düsseldorf, Annex to Vol. II. p. 568-584.
136. ITU. (1966). *Documents of the XIth Plenary Assembly (Report 224-1).* CCIR: ITU, Geneva, Vol. IV. p. 537—548.
137. Barnbaum, C.A., Bradley R.F. (1998). A new approach to interference excision in Radio Astronomy: real-time adaptive cancellation. *Astron. J*. Vol. 116. p. 2598—2614. https://doi.org/10.1086/300604
138. Ellingson, S.W., Cazemier, W. (2003). Efficient multibeam synthesis with interference nulling for large arrays. *IEEE Trans. Ant. Prop*. Vol. 51. No. 3. p. 503—511. https://doi.org/10.1109/TAP.2003.809840

139. Fomalont, E.B., Windhorst, R., Kristian, J.A., et al. (1991). The micro-jansky radio source population at 5 GHz. *Astron. J.* Vol. 102. p. 1258—1277. https://doi.org/10.1086/115952
140. Kraus, J.D. (1986). *Radio Astronomy* (2nd ed.). New York: Cygnus-Quasar Books, 719 p.
141. Greenhill, L.J., Kondratko ,P.T., Lovell, J.E.J., et al. (2003). The Discovery of H2O Maser Emission in Seven Active Galactic Nuclei and at High Velocities in the Circinus Galaxy. *Astrophys. J. (Letters)*. Vol. 582. No. 1. p. 11-14. https://doi.org/10.1086/367602
142. Thompson, A.R. (1982). The response of a radio-astronomy synthesis array to interfering signals. *IEEE Trans. Ant. Prop.* Vol. 30, No 3. p. 450—456. https://doi.org/10.1109/TAP.1982.1142799
143. Wootten, A., Thompson, A.R. (2009). The Atacama Large Millimeter/Submillimeter Array. *Proceedings of the IEEE*. Vol. 97. No. 8. p. 1463—1471. https://doi.org/10.1109/JPROC.2009.2020572
144. Walter, F., Decarli, R., Carilli, C., et al. (2012). The intense starburst HDF 850.1 in a galaxy overdensity at z ≈ 5.2 in the Hubble Deep Field. *Nature*. Vol. 486. p. 233—238. https://doi.org/10.1038/nature11073
145. Kallunki, J., Bezrukovs, V., Madkour, W., (2022). et al. Importance of Spectrum Management in Radio Astronomy. *Latvian Journal of Physics and Technical Sciences*. Vol. 59. No. S3. p. 30—38. https://doi.org/10.2478/lpts-2022-0022
146. Burke, B.F., Graham-Smith, F. (2019). *An introduction to radio astronomy* (4th ed.). Cambridge:CambridgeUniversityPress,516 p.https://doi.org/10.1017/9781316987506
147. Ewen, H.I., Purcell, E.M. (1951). Observations of a line in the galactic radio spectrum. *Nature*. Vol. 168. p. 356. https://doi.org/10.1038/168356a0
148. Wei, L., Wijnholds, S.J., Hurley, P. (2017). Robust recovery for aperture synthesis imaging. *IEEE International Conference on Image Processing (ICIP-2017)*: Conf. Proc. (Beijing, China, 17—20 September 2017). Beijing, p. 3570—3574. https://doi.org/10.1109/ICIP.2017.8296947
149. Fu, P., Hu, F., Hu, H., et al. (2020). A Wavenumber Domain Imaging Algorithm for Synthetic Aperture Interferometric Radiometry in Near-Field. *IEEE International Geoscience and Remote Sensing Symposium. (IGARSS-2020)*: Conf. Proc. (September 26—October 2 2020, Virtual Symposium). p. 6511—6514. https://doi.org/10.1109/IGARSS39084.2020.9323395
150. Philippe, B., Reynaert, P. (2020). A Quadrature Phase Detector in 28 nm CMOS for Differential mm-Wave Sensing Applications Using Dielectric Waveguides. *IEEE 44th European Solid State Circuits Conference (ESSCIRC 2018)*: Conf. Proc. (Dresden, Germany, 03—06 September 2018). Dresden, p. 114—117. https://doi.org/10.1109/ESSCIRC.2018.8494306
151. Robinson, J., Rahmat-Samii, Y. (2004). Particle Swarm Optimization in Electromagnetics. *IEEE Transactions on Antennas and Propagation*. Vol. 52. No.2. p. 397—407. https://doi.org/10.1109/TAP.2004.823969
152. Liu, Y., Nie, Z., Liu, Q.-H. (2008). Reducing the number of elements in a linear antenna array by the matrix pencil method. *IEEE Trans. Antennas Propag*. Vol. 56. No. 9. p. 2955—2962. https://doi.org/10.1109/ TAP.2008.928801

153. Bucci, O., Perna, S., Pinchera, D. (2012). Advances in the deterministic synthesis of uniform amplitude pencil beam concentric ring arrays. *IEEE Trans. Antennas Propag.* Vol. 60. No. 7. p. 3504—3509. https://doi.org/ 10.1109/TAP.2012.2196945
154. Kay, S., Saha, S. (2002). Design of sparse linear arrays by Monte Carlo importance sampling. *IEEE J. Ocean. Eng.* Vol. 27. No. 4. p. 790—799. https://doi.org/10.1109/JOE.2002.804325
155. Cui, J., Legenkiy, M., Khrychov, V. (2020). Diffraction properties of azimuthally symmetric gratings in a hollow circular dielectric waveguide. *Results in Physics.* Vol. 18. p. 103204—103204. https://doi.org/10.1016/ j.rinp.2020.103204
156. Legenkyi, M., Khrychov, V. (2019). Pulsed antenna based on a non-homogeneous conical line. *Bulletin of Kharkiv National University named after V. N. Karazin. Series "Radio Physics and Electronics"*. Issue 31. p. 59—65. https://doi.org/10.26565/2311-0872-2019-31-06
157. Legenkiy, M., Khrychov, V. (2021). Numerical modeling of electromagnetic scattering from complex shape object with coating. *Frequenz*. Vol. 76. No. 1—2. p. 75—82. https://doi.org/10.1515/freq-2021-0062
158. Akhmedov, R., Dumin, O., Katrich, V. (2018). Impulse radiation of antenna with circular aperture. *Telecommunications and Radio Engineering*. Vol. 77. Iss. 20. p. 1767—1784. https://doi.org/10.1615/ TelecomRadEng.v77.i20.10
159. Dumin, O., Akhmedov, R., Cherkasov, D. (2018). Pulsed radiation of an antenna with a circular aperture in the near zone. *Bulletin of Kharkiv National University named after V. N. Karazin. Series "Radio Physics and Electronics"*. Issue 28. p. 30—33. https://periodicals.karazin.ua/radiophysics/article/view/12591
160. Berdnik, S.L., Katrich, V.A., Nesterenko, M.V., et al. (2020). Yagi-Uda Combined Radiating Structures of Centimeter and Millimeter Wave Band. *Progress in Electromagnetics Research M*. Vol. 93. p. 89—97. http://dx.doi.org/10.2528/PIERM20041506
161. Pogarsky, S.A., Mayboroda, D.V. (2023). A broadband patch antenna based on a planar unclosed annular radiator. *Radio Physics and Radio Astronomy*. Vol. 28. No. 2. p. 158—165. https://doi.org/10.15407/rpra28.02.158
162. Kaliberda, M.E., Pogarsky, S.A., Sierhieieva, A.A. (2023). Integral equations in the H-polarized wave scattering from metasurface formed by finite multilayer graphene strip grating inside grounded dielectric slab. *Opt. Quant. Electron.* Vol 55. Article ID 1050. 18 p. https://doi.org/10.1007/s11082-023-05288-5
163. Mayboroda, D., Pogarsky, S. (2021). Microstrip monopole antenna with complicated topology. *Lecture Notes in Networks and Systems*. Vol. 152. p. 394—403. https://doi.org/10.1007/978-3-030-58359-0_22
164. Qi, L., Kaliuzhnyi, M., Shen, Z., et al. (2023). Chirp Rates Estimation for Multiple LFM Signals by DPT-SVD. *Circuits, Systems and Signal Processing.* Vol. 42. No. 5. p. 2804-2827. https://doi.org/10.1007/s00034-022-02225-x
165. Guo, Q., Kaliuzhnyi, M., Liu, J. (2022). YOLOX-SAR: High-precision Object Detection System Based on Visible and Infrared Sensors for SAR Remote Sensing. *IEEE Sensors Journal*. Vol 22. No. 17. p. 17243—17253. https://doi.org/10.1109/JSEN.2022.3186889

166. Kaliuzhnyi, M. (2021). Generalizing the sampling theorem for a frequency-time domain to sample signals under the conditions of a priori uncertainty. *Eastern-European Journal of Enterprise Technologies*. Vol. 3. No. 9 (111). p. 6—15. https://doi.org/10.15587/1729-4061.2021.235844
167. Volosyuk, V., Zhyla, S. (2022). Statistical Theory of Optimal Functionally Deterministic Signals Processing in Multichannel Aerospace Imaging Radar Systems. *Computation*. Vol. 10. Special Issue. Article ID 213. 20 p. https://doi.org/10.3390/computation10120213
168. Volosyuk, V., Zhyla, S., Pavlikov, V. (2021). Optimal Radar Cross Section Estimation in Synthetic Aperture Radar with Planar Antenna Array. *Radioelectronic and Computer Systems*. Vol. 1. p. 50—59. https://doi.org/10.32620/ REKS.2021.1.04

LIST OF ABBREVIATIONS AND ACRONYMS

AA — antenna array
AM — amplitude modulation
AFT — adaptive Fourier transform
CDS — cyclic difference sets
IRE — Institute of Radiophysics and Electronics
KhNU — V.N. Karazin Kharkiv National University
MBW — main beam width of the AA RP
RP — radiation pattern
RS — radar stations
SLL — the average level of the side lobes of the AA RP
SAA — sparse antenna array
UAA — uniformed antenna array
WFT — windowed Fourier transform
Δw_0 — MBW
$\Delta w_{0.707}$ — the half-power width of the main beam of the AA RP
m — SLL
α — the AA filling factor
β — the AA redundancy coefficient
N_0 — the number of lattice elements
v — the number of nodes of equidistant grids in which they can be located

У монографії представлені інноваційні методи конструювання двовимірних нееквідистантних антенних решіток (АР), особливо призначених для радіотелескопів, що працюють у діапазоні 8—80 МГц. Запропоновано прямі та прості техніки, з акцентом на конфігураціях, заснованих на латинських квадратах та їхніх трикутних матрицях. Ці методи забезпечують повне покриття просторових частот із високим ступенем розрідження та мінімальним бічним випромінюванням. Основні внески включають перше використання латинського квадрата в конструкції АР, піонерне поєднання циркулярних диференціальних наборів і латинських квадратів для планарних розріджених решіток, а також інтеграцію латинських квадратів і їхніх нижніх трикутних матриць у планарному розрідженому масиві. Запропонована матрична методика є ефективнішою та прямішою за традиційні ітераційні та оптимізаційні підходи на основі видалення елементів.

Для науковців і фахівців, які займаються розробкою методів і технологій дистанційного зондування за допомогою випромінювання наземних і космічних радіотехнічних систем. Вона буде корисною студентам і викладачам у галузі радіофізики, адже пропонує комплексний підхід до конструювання АР, що може сприяти як академічним дослідженням, так і практичним застосуванням у радіоастрономії.

Наукове видання

НАЦІОНАЛЬНА АКАДЕМІЯ НАУК УКРАЇНИ
ІНСТИТУТ РАДІОФІЗИКИ ТА ЕЛЕКТРОНІКИ
ім. О.Я. УСИКОВА НАН УКРАЇНИ

ЛО Іян, ЛУЦЕНКО Владислав Іванович,
ШУЛЬГА Сергій Миколайович

СИНТЕЗ ДВОМІРНИХ НЕЕКВІДИСТАНТНИХ АНТЕННИХ РЕШІТОК З ВИКОРИСТАННЯМ СПЕЦІАЛЬНИХ МАТРИЦЬ

Англійською мовою

Редактор *О.В. Нікітченко*

Художнє оформлення *Є.О. Ільницького*
Технічний редактор *Т.М. Шендерович*
Виготовлення ілюстрацій *О.В. Нікітченка*
Комп'ютерна верстка *В.Г. Веденської*

Підписано до друку 16.10.2025. Формат 70 × 100/16. Гарн. Minion pro.
Ум. друк. арк. 10,56. Обл.-вид. арк. 10,40. Тираж 100 прим. Зам. № 7822

Видавець і виготовлювач
Видавничий дім «Академперіодика» НАН України
вул. Терещенківська, 4, Київ, 01024, Україна

Свідоцтво про внесення до Державного реєстру суб'єктів
видавничої справи серії ДК № 544 від 27.07.2001

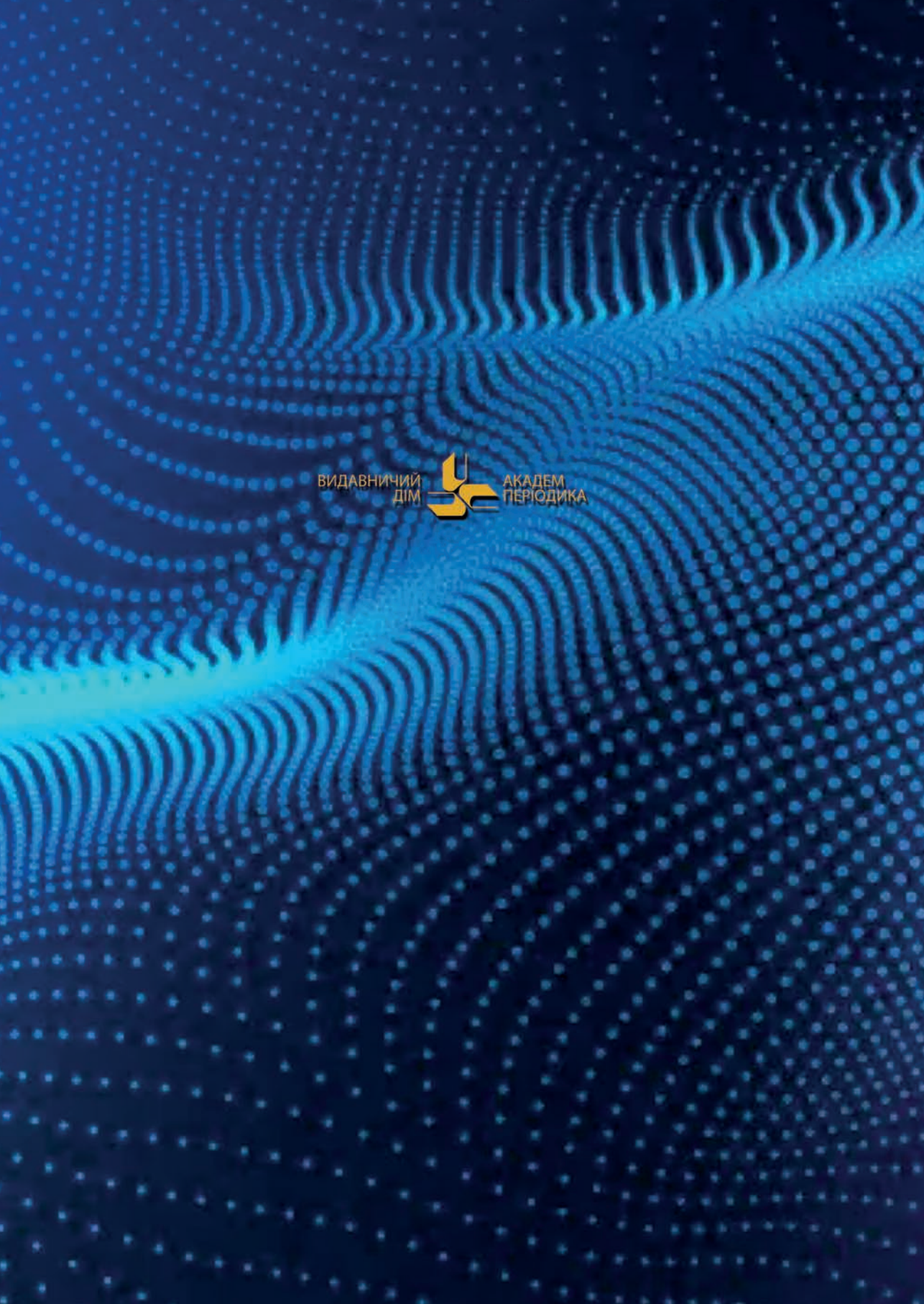
ВИДАВНИЧИЙ ДІМ
АКАДЕМ ПЕРІОДИКА